

Modification of Lithium-Rich Manganese Oxide Materials: Coating, Doping and Single Crystallization

Hui Li,*^[a] Huijuan Zhang,^[a] Ying Liang,^[b] Rong Chen,^[a] and Yuliang Cao*^[c]

The increasing demand for portable electronics, electric vehicles and energy storage devices has spurred enormous research efforts to develop high-energy-density advanced lithium-ion batteries (LIBs). Lithium-rich manganese oxide (LRMO) is considered as one of the most promising cathode materials because of its high specific discharge capacity ($> 250 \text{ mAh g}^{-1}$), low cost, and environmental friendliness, all of which are expected to propel the commercialization of lithium-ion batteries. However, practical applications of LRMO are still limited by low coulombic efficiency, significant capacity and voltage decay, slow reaction kinetics, and poor rate performance.

This review focus on recent advancements in the modification methods of LRMO materials, systematically summarizing surface coating with different physical properties (e.g., oxides, metal phosphates, metal fluorides, carbon, conductive polymers, lithium compound coatings, etc.), ion doping with different doping sites (Li sites, TM sites, O sites, etc.), and single crystal structures. Finally, the current states and issues, key challenges of the modification of LRMO are discussed, and the perspectives on the future development trend base on the viewpoint of the commercialization of LRMO are also provided.

1. Introduction

In the past three decades, lithium-ion battery (LIB) cathode materials that have been commercialized on a large scale mainly include layered LiCoO_2 (LCO), layered multicomponent $\text{LiNi}_{1-x-y}\text{Co}_x\text{Mn}_y\text{O}_2$ (NCM) and $\text{LiNi}_{1-x-y}\text{Co}_x\text{Al}_y\text{O}_2$ (NCA), olivine type LiFePO_4 (LFP), and spinel structure LiMn_2O_4 (LMO) and so on.^[1] However, the energy density of the full cells with these positive electrode matching Si/C anode is hard to reach 350 Wh kg^{-1} , which cannot meet the rapidly growing demand for higher energy density batteries.^[2]

Lithium-rich manganese oxide ($x \text{ Li}_2\text{MnO}_3 \cdot (1-x) \text{ LiTMO}_2$, $0 < x < 1$, TM=Ni, Co, Mn and other transition metals and their combinations, LRMO) is regarded as one of the most promising cathode materials due to its high specific discharge capacity of more than 250 mAh g^{-1} , low cost, and environmental friendliness.^[3] The high capacity of LRMO can be attributed to the combination of cationic and anionic redox, which differs from traditional layered oxide electrodes. The initial charging process of LRMO includes a short voltage ramp below 4.5 V corresponds to the extraction of Li^+ from the LiMO_2 phase, while TM is oxidized (Co^{3+} to Co^{4+} , Ni^{2+} to Ni^{4+}) as the voltage increases to $\approx 4.5 \text{ V}$ corresponds to delithiation of the Li_2MnO_3 phase. As the charging voltages further increases to $> 4.5 \text{ V}$, O^{2-}

also be oxidized to participate in the charge compensation process, resulting in the escape of oxygen from the material. However, the above complex reaction mechanism bring difficulties to the large-scale commercialization of LRMO, more specifically, (1) the low initial coulombic efficiency (ICE) caused by the irreversible oxidation-reduction reaction of anionic oxygen during the first cycle of charging;^[4] (2) the different electronic conductivity of the Li_2MnO_3 phase lead to the poor rate performance; (3) voltage/capacity fading due to the irreversible oxygen loss and transition metal migration.^[5]

To address these problems, great efforts have been devoted for improving the structural stability of LRMO, such as surface modification, ion doping, structure regulation.^[2,6] These methods can effectively improve the cycling stability and voltage decay of LRMO cathode, as well as the ICE. Previous reviews on LRMOs mostly focus on progress and challenges, and rarely systematically mentioned and compared the advantages of different coating, doping and single crystal modification methods. In this review, the reaction mechanism, electrochemical characteristics, main challenges and modification strategies of LRMO electrodes during charge and discharge are summarized. And we systematically introduce the research progress on the modification methods of LRMO cathodes through surface coating, ion doping and single crystallization (Figure 1). By comparing the advantages and disadvantages of each modification method, we summarize the current challenges in improving the electrochemical properties of LRMO cathode materials and look forward to the future research directions for the modification of LRMO cathode materials.

[a] H. Li, H. Zhang, R. Chen
State Key Laboratory of New Textile Materials & Advanced Processing Technologies, Wuhan Textile University, Wuhan, 430200, China
E-mail: lih@whu.edu.cn

[b] Y. Liang
Hubei Key Laboratory of Low Dimensional Optoelectronic Material and Devices, Hubei University of Arts and Science, Xiangyang, 441053, China

[c] Y. Cao
Hubei Key Lab of Electrochemical Power Sources, College of Chemistry & Molecular Science, Wuhan University, Wuhan, 430072, China
E-mail: ylcao@whu.edu.cn

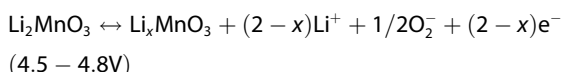
2. Problems and Origins of LRMO Materials

The electrochemical properties of LRMO materials are related to the electrochemical behavior of LiTMO_2 and Li_2MnO_3 . The

LiTMO_2 layered phase provides capacity at low voltages (< 4.5 V), while the Li_2MnO_3 Li-rich phase contributes capacity at high voltages (> 4.5 V).^[11] According to the chemical equation, the reversible charge storage mechanism of LiTMO_2 and the irreversible electrochemical process can be expressed by the following formula.^[12]



or



2.1. Capacity Loss in the Initial Cycle

Due to the unique charging and discharging mechanisms of LRMO materials, the ICE of most LRMO electrodes is less than 85%, which does not meet the commercial requirements. As mentioned earlier, during the first charging process, the Li_2MnO_3 component is activated and the oxygen release has a long charging platform at about 4.5 V, which makes the LRMO

material have a high specific capacity. At this stage, however, the removal of Li^+ ions from Li_2MnO_3 is inevitably accompanied by oxygen evolution. Additionally, some TM ions migrate to the Li layer after the excess Li^+ ions are removed, leading to phase transition on the surface of the material.^[13] As a result, it becomes more difficult for Li^+ ions to reinsert into MnO_2 during discharge, resulting in irreversible capacity loss and low ICE.^[11] Furthermore, the unnecessary consumption of Li^+ ions caused by side reactions between the cathode material and the liquid electrolyte, and the formation of the solid electrolyte interface (SEI) film, also reduces ICE.^[14] The valency of Mn in LRMO materials remains mostly at +4 during the electrochemical process. To maintain the charge balance of the structure, the anion (i.e. oxygen ion) in the material provides electrons (unhybridized O 2p) to participate in the oxidation reaction. The oxygen redox process can be divided into two parts: the reversible part inside the particle and the irreversible part on the surface (mainly the Li_2MnO_3 component). The deactivation theory suggests that the simultaneous deactivation of Li^+ and O^{2-} in the lattice produces Li_2O , which not only reduces the reversible Li^+ , but also further inhibits the transport of Li^+ ions due to the accumulation of Li_2O on the electrode surface. The surface oxygen portion is over-oxidized and lost in the form of O_2 , CO_2 , and CO during the initial charging-discharge cycle.^[15] It is evident that surface unstable oxygen plays a crucial role in irreversible initial capacity loss. Therefore, reducing surface



Hui Li received her Ph.D. (2020) in chemistry from Wuhan University, and then worked as a postdoctoral fellow at College of Chemistry and Molecular Sciences in Wuhan University, and now works as an associate professor of state key laboratory of new textile materials & advanced processing technologies in Wuhan Textile University. Her research interests mainly focus on electrochemical energy-storage materials and technologies.



Huijuan Zhang started her Master's degree in chemical science at Wuhan Textile University in 2022. At present, her main research direction is the modification of lithium-rich manganese oxide materials.



Prof. Ying Liang received her Ph. D degree from Central China Normal University in 2008. Currently, she is working at the Institute of functional materials, Hubei University of Arts and Science. Her research interest is focused on new energy storage materials. She has participated in the national natural science foundation and other scientific research projects.



Prof. Rong Chen received his Ph.D. in 2006 from the University of Hong Kong. Following a 2-years research associate appointment working at the University of Hong Kong. He is now a professor in State Key Laboratory of New Textile Materials & Advanced Processing Technologies of Wuhan Textile University. His current research interest involves the development of novel functional nanomaterials with controllable sizes, unusual morphologies and interesting architectures.



Prof. Yuliang Cao received his Ph.D. degree in 2003 from Wuhan University, and then he worked as a visiting scholar in Pacific Northwest National Laboratory from 2009 to 2011. He is now a professor in the college of chemistry and molecular sciences, Wuhan University. His research interests focus on developing advanced energy storage materials (e.g., carbonous materials, alloy nano-composite anodes, transition metal oxide cathodes, phosphate framework materials, and novel safety electrolytes) for lithium/sodium ion batteries.

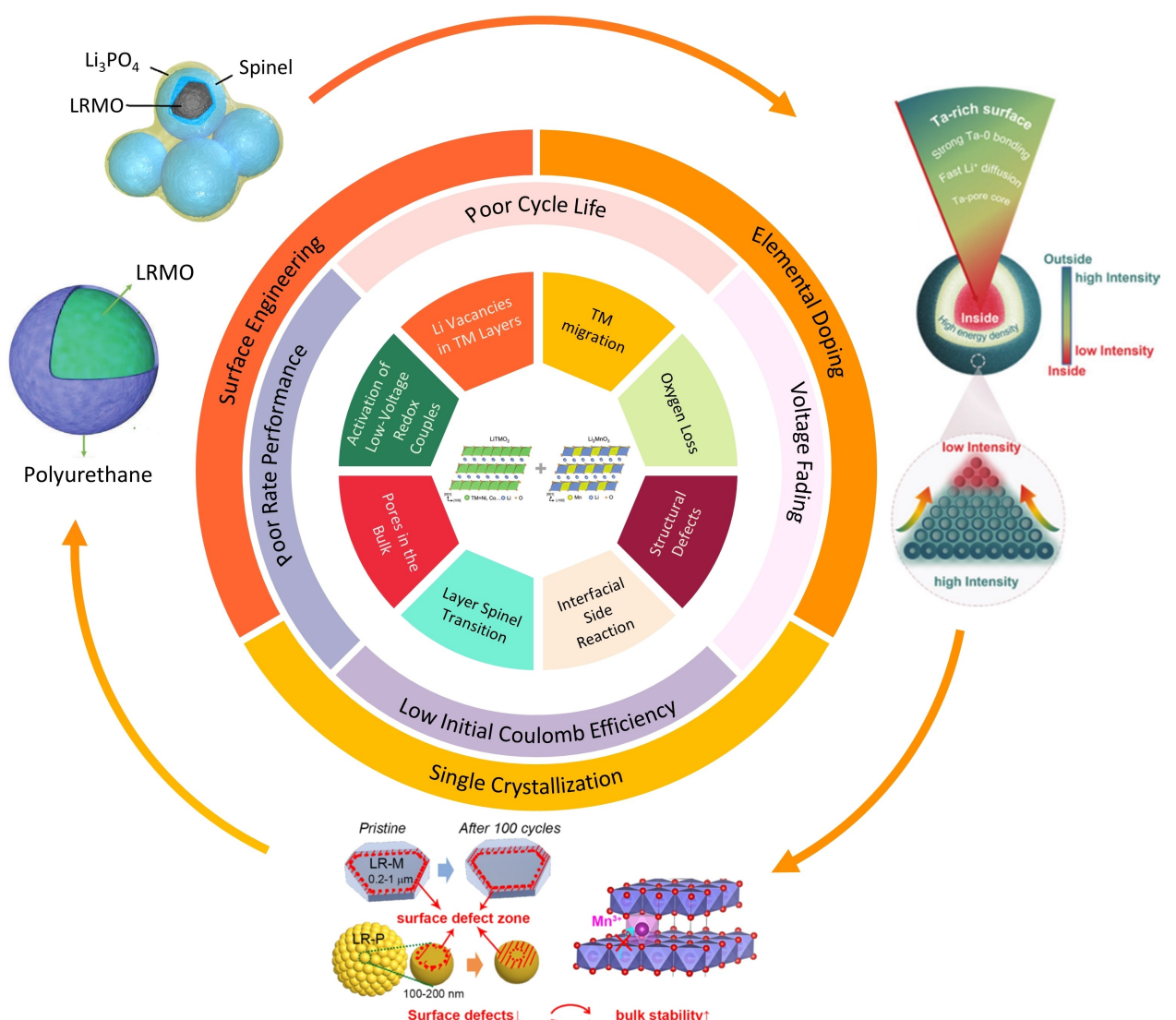


Figure 1. Schematic illustration of various challenges and corresponding strategies of LRMOs. Reproduced with permission.^[7] Copyright 2022, Elsevier. Reproduced with permission.^[8] Copyright 2024, Wiley-VCH. Reproduced with permission.^[9] Copyright 2021, Elsevier. Reproduced with permission.^[10] Copyright 2023, Wiley-VCH.

unstable or stable oxygen by surface modification such as constructing surface oxygen vacancy, surface coatings, and ionic doping is an effective approach to improve the ICE.

2.2. Poor Rate Performance

There are many reasons for the poor rate performance of LRMO materials. Among them, the Li_2MnO_3 component is considered to be the key influencing factor restricting the rate performance of LRMO material.^[16] This is due to the low electronic conductivity and the diffusion coefficient of Li^+ of Li_2MnO_3 , as well as the poorer reaction kinetics of Mn compared to Ni and Co. The TM layer of Li_2MnO_3 is occupied by excessive Li ions, which hinders the transport of electrons in LRMO and the diffusion of Li^+ . Through the primary principle of molecular dynamics calculation, Gao et al. found almost no Li^+ diffusion in

the Li_2MnO_3 under 2500 K within the simulation time of 10 ps.^[17] The irreversible phase transition from the lamellar phase Li_2MnO_3 to the spinel phase LiMn_2O_4 and the resulting defects hinder the diffusion of lithium ions.^[18] Yu et al. used the XAS technique to determine the reaction kinetics of each element. The results showed that the reaction kinetics of Mn sites from Li_2MnO_3 were slower than that of Ni and Co sites. The main reason may be caused by oxygen redox reaction, resulting in Mn migration and oxygen release. Therefore, an effective strategy to improve the rate performance of LRMO is to optimize the performance of Li_2MnO_3 , such as composition optimization, Mn lattice stabilization, and doping.^[16]

In LRMO material, the addition of Ni and Co can contribute to the emergence of lithium.^[19] However, the presence of Ni and Co accelerates the side reaction between the active material and the electrolyte, consuming the active material and promoting the formation of more SEI on the surface of the

cathode particles.^[20] The resulting passivation layer is one of the main reasons for the increased interfacial charge transfer resistance.^[21] In addition, Co and Ni in LRMO materials can activate lattice oxygen to a certain extent, and their TM–O bonds are weak compared to Mn–O.^[22] It can reduce the formation of OVs, thereby promoting the formation of dimeric oxygen and oxygen, accelerates the irreversible phase transition, which is unfavorable to the electrochemical performance of LRMO.^[23] Unlike the three-dimensional ion diffusion channels in spinel structures, Li⁺ migration in LRMO materials is anisotropic. The Li⁺ in the positive electrode of LRMO is only removed/inserted in the two-dimensional plane of the (010) (or (100)) lattice plane, which also limits the ionic conductivity of the material.^[24]

Therefore, considering the internal and external modifications of the LRMO material, improving the dynamic properties is key to enhancing the rate performance of the LRMO material. One way is to obtain a shorter Li⁺ diffusion length, a larger contact area, and more active sites by reducing the grain size of the primary particles. The other method is surface modification, which is used to prevent the dissolution of TM ions into the electrolyte and inhibit the formation of surface passivation layers, thereby ensuring the surface stability and internal structural integrity of the positive electrode material to improve the rate performance.^[25]

2.3. Voltage/Capacity Fading

As the LRMO material cannot completely and continuously maintain the integrity and order of the layered structure at a higher charging voltage, the average voltage of LRMO material always shows continuous attenuation during cycling. Researchers suggest that the voltage fading during charging and discharging is mainly related to the release of oxygen from LRMO, the migration of TM ions, and the phase transition.^[15,26] These problems are not isolated from each other, but are intrinsically linked.

In the LRMO material, oxygen ions occupy the 6c site, and oxygen ions play a framework role in supporting cations. Therefore, the reversibility of oxygen during the reaction will directly determine the stability of the material structure. The mechanisms of irreversible loss of oxygen could be explained by O–O dimer theory, that is, the oxygen that loses one electron tends to form a covalent bond with each other, forming an O–O dimer.^[27] The O–O dimer on the surface of the material has high activity, which will lead to the nucleophilic reaction between the O–O dimer and the electrolyte to generate CO₂.^[28] After the release of oxygen, oxygen vacancies are generated, which weakens the bond energy of the TM–O bond, making it easier for TM to migrate to the Li site and undergo a phase transition. During the long-term cycle, the release of oxygen also causes the average valence state of TM ions to decrease continuously. The main reason is that the reduction of highly active oxygen leads to the activation of Mn³⁺/Mn⁴⁺ and Co²⁺/Co³⁺ redox-reduction pairs, which in-

creases the Fermi level and decreases the average voltage (Figure 2a).^[15,29]

Yan et al. found that TMⁿ⁺ (such as Ni and Co) preferentially migrated and segregated on the surface of LRMO materials during the synthesis process.^[18b] The migration of TMⁿ⁺ and the deintercalation of Li on the surface of LRMO materials will form a surface reconstruction layer (SRL). This SRL is considered to be a dynamic barrier for lithium ion diffusion, which will cause high voltage polarization and lead to rapid capacity decay of LRMO materials.^[30] The TM migration and oxygen loss at high voltage will lead to the rearrangement of Co 3d and Mn 3d electron orbitals, which in turn inhibits Co^{2+/3+} redox in subsequent cycles and triggers Mn^{3+/4+} redox (Figure 2b).^[31] In addition, the migration of TM ions will lead to the mixed arrangement of Li⁺/Ni²⁺ (TM). The migration of TM ions to the Li layer will block the Li⁺ diffusion channel, resulting in poor lithium ion diffusion kinetics, and also reduce the Ni diffusion kinetics, resulting in a certain amount of capacity loss and phase transition during the cycle.

The main reason for the voltage decay of LRMO materials is that the structure changes from layered to spinel phase, and the phase transition will inevitably involve the migration of Li⁺ and TMⁿ⁺. Therefore, Mohanty et al. used density functional theory (DFT) calculations to illustrate the process by which ion migration leads to material phase transitions (Figure 2c).^[32] As the charging voltage continues to rise, some TMⁿ⁺ will be removed from the original octahedron and then enter the lithium vacancy. The migration of TMⁿ⁺ means that LRMO has undergone a transition from layered to spinel, and the spinel structure cannot provide a good migration channel, which eventually leads to voltage attenuation. In order to solve these problems, many strategies have been proposed, including surface engineering, element doping, structure and morphology design, and remarkable results have been achieved.

Based on the above analysis, we then systematically assess the effect of different modification methods of LRMO cathodes through surface coating, ion doping, and single crystallization.

3. Surface Coating

Surface coating, as the most widely modification method for LIB cathode materials, is also suitable for LRMO cathode materials.^[33] Firstly, the coating layer can physically isolate the surface of LRMO material and electrolyte, further inhibiting the interface side reaction and HF erosion in the electrolyte, and suppress the dissolution of transition metal ion. Secondly, the coating layer chemically bonds with the surface of the active material particles, changing the surface chemical properties of the bulk. Finally, the the coating layer can also prevent the exposure of reactive oxygen species generated at high voltage, alleviating the severe side reactions.

Herein, the reported surface coating of LRMO cathode materials can be divided into the following categories: oxide, metal phosphate, metal fluoride, carbon, conductive polymer and lithium compound coatings. Table 1 summarizes the effect of surface coating on the electrochemical performance of LRMO.

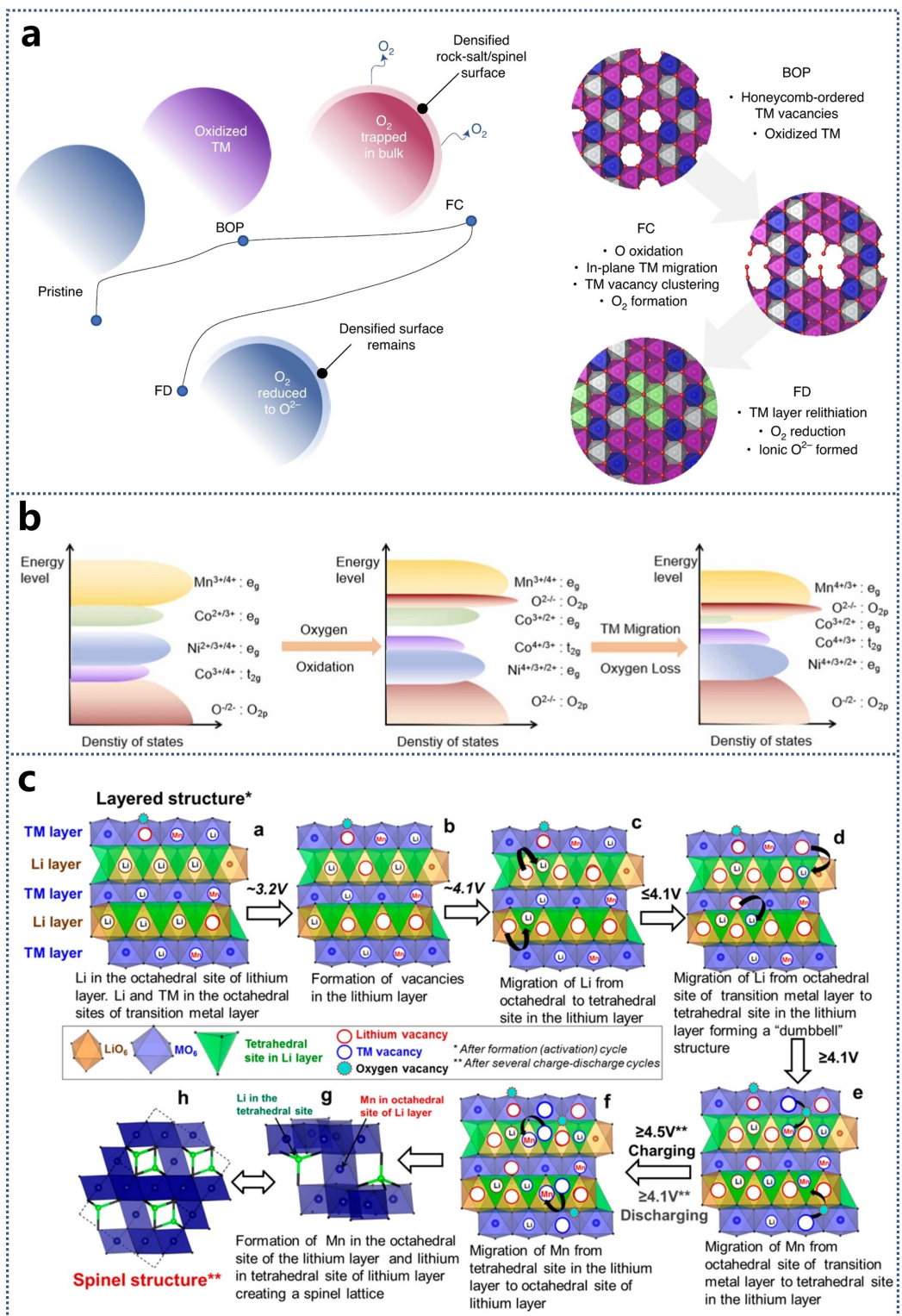


Figure 2. (a) Mechanism of the 1st cycle voltage hysteresis (BOP: the beginning of plateau; FC: full charge; FD: full discharge): Macro-scale changes to the cathode particles and atomic-scale changes to ordering within the TM layer. Reproduced with permission.^[15] Copyright 2020, The Author(s). (b) The TM migration and oxygen loss at high voltages result in rearrangement of Co 3 d and Mn 3 d electronic orbitals, and then suppresses the Co^{2+/3+} redox and triggers the Mn^{3+/4+} redox in the subsequent cycles. Reproduced with permission.^[31] Copyright 2024, Elsevier. (c) Phase transition process of LRMO cathode materials. Reproduced with permission.^[32] Copyright 2014, American Chemical Society.

Table 1. Effects of different surface coatings on the electrochemical performance of LRMOS (1 C = 250 mA g⁻¹).

Coating materials	Cathode materials	Initial discharge capacity/ (mAh g ⁻¹)	Initial coulombic efficiency (%)	Capacity retention	Rate capacity/ (mAh g ⁻¹)	Ref.
Oxides	Al ₂ O ₃	Li _{1.2} Ni _{0.18} Co _{0.03} Mn _{0.58} O ₂	282.04 (0.1 C)	85.2	97.6%, 90 cycles, 1 C	– [34b]
	Nanolayers Al ₂ O ₃	Li _{1.2} Mn _{0.55} Ni _{0.15} Co _{0.1} O ₂	254.4 (0.12 C)	–	85.87%, 500 cycles, 1.2 C	– [34a]
	MgO	Li _{1.2} Mn _{0.54} Ni _{0.13} Co _{0.13} O ₂	260.8 (0.08 C)	78	96.4%, 100 cycles, 0.8 C	– [35]
	SnO ₂	Li _{1.2} Mn _{0.54} Ni _{0.13} Co _{0.13} O ₂	264.6 (0.12 C)	–	89.9%, 200 cycles, 1.2 C	– [38]
	MnO ₂	Li _{1.2} Mn _{0.567} Ni _{0.167} Co _{0.066} O ₂	299 (0.08 C)	88	93%, 50 cycles, 0.08 C	157 (4 C) [56a]
	MnO ₂	Li _{1.2} Ni _{0.18} Co _{0.04} Mn _{0.58} O ₂	294.4 (0.08 C)	95.4	82.6%, 100 cycles, 0.4 C	82.1 (8 C) [56b]
	MoO ₃	Li _{1.2} Mn _{0.54} Ni _{0.13} Co _{0.13} O ₂	288.7 (0.1 C)	89.6	85.3%, 100 cycles, 0.8 C	177.8 (3.2 C) [54]
	ZrO ₂	Li _{1.2} Mn _{0.54} Ni _{0.13} Co _{0.13} O ₂	308.5 (0.1 C)	95.38	68.68%, 170 cycles, 0.2 C	– [46]
	In ₂ O ₃	Li _{1.2} Mn _{0.54} Ni _{0.13} Co _{0.13} O ₂	261.1 (0.1 C)	72.5	80%, 200 cycles, 1 C	109.1 (5 C) [37]
	SiO ₂	Li _{1.2} Ni _{0.2} Mn _{0.6} O ₂	238.3 (0.08 C)	73.8	103.7%, 50 cycles, 0.16 C	128.4 (8 C) [36b]
	TiO ₂	Li _{1.2} Mn _{0.54} Ni _{0.13} Co _{0.13} O ₂	276.5 (0.1 C)	80.8	87.8%, 200 cycles, 2 C	78.1 (5 C) [137]
	TiO ₂	Li _{1.2} Mn _{0.54} Ni _{0.13} Co _{0.13} O ₂	254.6 (0.24 C)	82.4	79.6%, 100 cycles, 1.2 C	130.3 (6 C) [49]
	ZnO	Li _{1.2} Mn _{0.54} Ni _{0.13} Co _{0.13} O ₂	267 (0.08 C)	80.7	–	135.1 (3.2 C) [43]
	CeO ₂	Li[Li _{0.17} Ni _{0.2} Co _{0.05} Mn _{0.58}]O ₂	290.5 (0.12 C)	83.4	90.8%, 80 cycles, 1 C	192 (2 C) [44e]
	CeO ₂	Li _{1.2} Mn _{0.54} Ni _{0.13} Co _{0.13} O ₂	260 (0.88 C)	–	80.35%, 150 cycles, 0.88 C	– [44b]
	V ₂ O ₅	Li _{1.2} Mn _{0.54} Ni _{0.13} Co _{0.13} O ₂	279.5 (0.1 C)	87.8	96.3%, 50 cycles, 0.1 C	113.6 (5 C) [57]
	Y ₂ O ₃	Li _{1.4} Mn _{0.61} Ni _{0.18} Co _{0.18} Al _{0.03} O _{2.4}	280.3 (0.1 C)	82.3	89.1%, 200 cycles, 0.5 C	122.4 (5 C) [51a]
	WO ₃	Li _{1.2} Ni _{0.2} Mn _{0.6} O ₂	252.2 (0.1 C)	84.97	97%, 100 cycles, 2.08 C	115 (6 C) [42]
	Er ₂ O ₃	Li _{1.2} Mn _{0.54} Ni _{0.13} Co _{0.13} O ₂	277 (0.08 C)	87.8	101%, 300 cycles, 0.8 C	– [50]
	Sm ₂ O ₃	Li [Li _{0.2} Mn _{0.56} Ni _{0.16} Co _{0.08}]O ₂	287.7 (0.08 C)	86	91.5%, 80 cycles, 0.8 C	153.2 (8 C) [47]
	Pr ₆ O ₁₁	Li[Li _{0.17} Ni _{0.17} Co _{0.10} Mn _{0.56}]O ₂	277.9 (0.05 C)	93.63	91.2%, 50 cycles, 0.05 C	196.2 (1 C) [45]
	La ₂ O ₃	Li _{1.2} Mn _{0.54} Ni _{0.13} Co _{0.13} O ₂	276.9 (0.1 C)	–	71%, 100 cycles, 0.1 C	90.2, (5 C) [53]
	Ce _{0.8} Sn _{0.2} O _{2-a}	Li _{1.2} Mn _{0.54} Ni _{0.13} Co _{0.13} O ₂	315.1 (0.05 C)	92.77	81.2%, 100 cycles, 0.1 C	181.1 (5 C) [70]
	Mg ₂ TiO ₄	Li _{1.2} Mn _{0.54} Ni _{0.13} Co _{0.13} O ₂	271 (0.1 C)	84.6	81%, 700 cycles, 2 C	– [63]
Phosphates	AlPO ₄	Li _{1.2} Mn _{0.54} Ni _{0.13} Co _{0.13} O ₂	–	–	89%, 35 cycles, 0.12 C	162.7 (4.8 C) [71a]
	AlPO ₄	Li[Li _{0.2} Fe _{0.1} Ni _{0.15} Mn _{0.55}]O ₂	267.2 (0.2 C)	78.9	74.4%, 50 cycles, 0.1 C	175.3 (1 C) [71b]
	FePO ₄	Li _{1.2} Mn _{0.54} Ni _{0.13} Co _{0.13} O ₂	271.7 (0.05 C)	85.1	95%, 100 cycles, 0.5 C	167.9 (2 C) [71c]
	SmPO ₄	Li _{1.2} Mn _{0.54} Ni _{0.13} Co _{0.13} O ₂	281.8 (0.12 C)	82.5	88.4%, 100 cycles, 1 C	– [74a]
	CePO ₄	Li _{1.2} Mn _{0.54} Ni _{0.13} Co _{0.13} O ₂	281 (0.1 C)	92.19	83.75%, 80 cycles, 0.1 C	110 (10 C) [71d]
	PrPO ₄	Li _{1.2} Mn _{0.54} Ni _{0.13} Co _{0.13} O ₂	286.9 (0.1 C)	90	89.3%, 100 cycles, 0.5 C	– [74b]
	LaPO ₄	Li _{1.2} Mn _{0.54} Ni _{0.13} Co _{0.13} O ₂	283.4 (0.1 C)	89.3	83.2%, 200 cycles, 1 C	146.2 (10 C) [71e]
Fluorides	AlF ₃	Li _{1.2} Mn _{0.54} Ni _{0.13} Co _{0.13} O ₂	283.3 (0.12 C)	88.3	84.4%, 200 cycles, 1.2 C	– [76d]

Table 1. continued

Coating materials	Cathode materials	Initial discharge capacity/ (mAh g ⁻¹)	Initial coulombic efficiency (%)	Capacity retention	Rate capacity/ (mAh g ⁻¹)	Ref.	
LiF/FeF ₃	Li _{1.2} Mn _{0.54} Ni _{0.13} Co _{0.13} O ₂	291.8 (0.08 C)	–	89.14%, 60 cycles, 0.08 C	129 (16 C)	[84]	
CaF ₂	Li _{1.2} Mn _{0.54} Ni _{0.13} Co _{0.13} O ₂	262.7 (0.1 C)	99.2	90.2%, 100 cycles, 0.1 C	152.1 (3 C)	[78]	
CeF ₃	Li _{1.2} Mn _{0.54} Ni _{0.13} Co _{0.13} O ₂	222.8 (0.1 C)	80	91.7%, 50 cycles, 0.1 C	103.1 (5 C)	[80]	
MgF ₂	Li(Li _{0.2} Ni _{0.17} Co _{0.07} Mn _{0.56})O ₂	220 (0.1 C)	76	86%, 50 cycles, 0.1 C	130 (2 C)	[77c]	
CoF ₂	Li _{1.2} Ni _{0.2} Mn _{0.6} O ₂	259.1 (0.1 C)	84.4	93.0%, 100 cycles, 0.1 C	167.5 (5 C)	[79]	
SmF ₃	Li1.2Mn0.52Co0.08Ni0.2O2	245.7 (0.1 C)	74.6	84.5%, 150 cycles, 2 C	132.3 (5 C)	[83]	
LaF ₃	Li _{1.2} Mn _{0.54} Ni _{0.13} Co _{0.13} O ₂	256.1 (0.08 C)	–	86.7%, 100 cycles, 0.4 C	111.5 (8 C)	[81b]	
Carbon	Carbon	Li _{1.5} Ni _{0.23} Co _{0.08} Mn _{0.54} O ₂	≈ 250 (0.12 C)	–	94%, 300 cycles, 2 C	–	[90]
	Carbon	Li _{1.2} Mn _{0.54} Ni _{0.13} Co _{0.13} O ₂	263 (0.2 C)	96.7	92%, 100 cycles, 0.2 C	100 (10 C)	[86e]
	Graphene	Li _{1.2} Mn _{0.54} Ni _{0.13} Co _{0.13} O ₂	290 (0.05 C)	74	90%, 100 cycles, 0.5 C	120 (3 C)	[87a]
	Graphene	Li _{1.2} Mn _{0.54} Ni _{0.13} Co _{0.13} O ₂	313 (0.05 C)	> 100	75.7%, 50 cycles, 0.2 C	125 (10 C)	[88]
	Graphene quantum dot	Li _{1.2} Mn _{0.54} Ni _{0.13} Co _{0.13} O ₂	252.6 (0.2 C)	65.7	86.5%, 150 cycles, 1 C	113.2 (5 C)	[87b]
Polymers	Polyimide	Li _{1.2} Mn _{0.54} Ni _{0.13} Co _{0.13} O ₂	269.8 (0.08 C)	–	90.6%, 50 cycles, 0.08 C	191.5 (2 C)	[92e]
	Polyaniline	Li _{1.5} Ni _{0.2} Co _{0.2} Mn _{0.6} O ₂	302.9 (0.1 C)	83.5	92.4%, 200 cycles, 0.5 C	146.2 (10 C)	[92a]
	PEDOT:PSS	Li _{1.2} Ni _{0.2} Mn _{0.6} O ₂	286.5 (0.1 C)	77.85	51.6%, 100 cycles, 1 C	135.2 (2 C)	[92d]
	Polyurethane	Li _{1.2} Mn _{0.54} Ni _{0.13} Co _{0.13} O ₂	297.9 (0.1 C)	88.6	80.0%, 300 cycles, 1 C	138.3 (7 C)	[8]
	Polyacrylonitrile	Li _{1.2} Mn _{0.54} Ni _{0.13} Co _{0.13} O ₂	291.1 (0.1 C)	83.1	73.7%, 275 cycles, 0.5 C	–	[92f]
Lithium-ion conductive	Li ₃ PO ₄	Li _{1.2} Ni _{0.2} Mn _{0.6} O ₂	257 (0.1 C)	92	85.49%, 100 cycles, 1 C	–	[110]
	Li ₃ PO ₄	Li _{1.2} Mn _{0.54} Ni _{0.13} Co _{0.13} O ₂	226.1 (0.1 C)	75.78	78%, 100 cycles, 0.2 C	118 (5 C)	[111b]
	LiF	Li _{1.2} Mn _{0.54} Ni _{0.13} Co _{0.13} O ₂	242.4 (0.05 C)	80	95%, 100 cycles, 1 C	–	[75]
	Li ₂ TiO ₃	Li _{1.08} Mn _{0.54} Co _{0.13} Ni _{0.13} O ₂	276.5 (0.1 C)	86.3	99.7%, 125 cycles, 0.2 C	–	[98b]
	LiAlF ₄	Li _{1.2} Ni _{0.2} Mn _{0.6} O ₂	246 (0.1 C)	81.2	90.9%, 3000 cycles, 5 C	133 (5 C)	[100]
	Li _{0.5} La _{0.5} TiO ₃	Li _{1.2} Mn _{0.54} Ni _{0.13} Co _{0.13} O ₂	261.6 (0.12 C)	86.4	≈ 85%, 100 cycles, 0.12 C	150 (6 C)	[103]
	Li _{0.75} La _{0.42} TiO ₃	Li _{1.2} Mn _{0.6} Ni _{0.2} O ₂	256 (0.08 C)	74	95.4%, 30 cycles, 0.08 C	114.14 (4 C)	[108]
	La ₂ Li _{0.5} TiCo _{0.5} O ₄	Li _{1.2} Mn _{0.54} Ni _{0.13} Co _{0.13} O ₂	269.1 (0.1 C)	81.2	82.6%, 200 cycles, 2 C	136.7 (5 C)	[66]
	Li ₄ V ₂ Mn(PO ₄) ₄	Li _{1.2} Mn _{0.54} Ni _{0.13} Co _{0.13} O ₂	300 (0.05 C)	84.2	78.1%, 200 cycles, 1 C	157.5 (2 C)	[114e]
	LiCoPO ₄	0.4Li ₂ MnO ₃ –0.6LiNi _{1/3} Co _{1/3} Mn _{1/3} O ₂	≈ 250 (0.08 C)	94	82%, 100 cycles, 1 C	135 (9.6 C)	[114b]
	LiErO ₂	Li _{1.2} Mn _{0.54} Ni _{0.13} Co _{0.13} O ₂	269.1 (0.05 C)	81.4	79.8%, 150 cycles, 1 C	162.1 (5 C)	[99]
	Li ₂ ZrO ₃	Li _{1.2} Mn _{0.54} Ni _{0.13} Co _{0.13} O ₂	275.7 (0.1 C)	–	70.9%, 200 cycles, 1 C	125.2 (5 C)	[96b]
	Li _{0.5} Mn _{0.5} O	Li _{1.2} Mn _{0.6} Ni _{0.2} O ₂	≈ 250 (0.1 C)	80.3	80.7%, 200 cycles, 1 C	131 (10 C)	[107]
	LiNbO ₃	0.5Li ₂ MnO ₃ –0.5LiNi _{1/3} Co _{1/3} Mn _{1/3} O ₂	280.5 (0.1 C)	63.3	82.05%, 100 cycles, 0.5 C	104.18 (5 C)	[138]
	LiAlO ₂	Li _{1.2} Mn _{0.54} Ni _{0.26} O ₂	245 (0.1 C)	82.28	81.84%, 300 cycles, 1 C	–	[94]

Table 1. continued

Coating materials	Cathode materials	Initial discharge capacity/ (mAh g ⁻¹)	Initial coulombic efficiency (%)	Capacity retention	Rate capacity/ (mAh g ⁻¹)	Ref.
Lithium active material	$\text{Li}_{0.25}\text{La}_3\text{Zr}_2\text{Al}_{0.25}\text{O}_{12}$	282.4 (0.1 C)	85.6	95.7 %, 300 cycles, 0.8 C	136.9 (4 C)	[102]
	$\text{La}_{0.8}\text{Sr}_{0.2}\text{MnO}_{3-y}$	243.5 (0.104 C)	80	94 %, 200 cycles, 5 C	144 (5 C)	[67]
	LiMn_2O_4	283 (0.1 C)	94	91 %, 200 cycles, 1 C	–	[116a]
Lithium active material	$\text{Li}_4\text{Mn}_5\text{O}_{12}$	296.3 (0.1 C)	85.8	97.4 %, 300 cycles, 1 C	183.6 (3 C)	[116b]
	LiFePO_4	282.8 (0.1 C)	81	98.1 %, 120 cycles, 0.1 C	125.3 (5 C)	[114a]

3.1. Oxides

The oxide coating layer undergoes a reaction with HF in the electrolyte, leading to the formation of metal fluorides. This reaction serves to remove HF and subsequently enhances the structural stability of the electrode. Nevertheless, an excessive amount of oxides can impede the transport rate of Li^+ ions and the electronic conductivity of LRMO. Consequently, this leads to an elevation in the resistance of electron and ion transport at the coating interface. Numerous non-transition metal oxides have been employed as coating layers to stabilize the surface of LRMO, such as Al_2O_3 ,^[34] MgO ,^[35] SiO_2 ,^[36] In_2O_3 ,^[37] SnO_2 ,^[38] and other binary or multi-metal oxides. Among these oxides, Al_2O_3 is the most widely used one owing to its low cost and easy deposition,^[39] as well as the high stability under high temperatures.^[40] The reported Al_2O_3 layer coating methods include dry prilling coating (DPC) (Figure 3a),^[34a] wet chemical synthesis (Figure 3b,c).^[34b,c] For example, Wu et al. prepared a thin layer of Al_2O_3 on the surface of LRMO cathode (Figure 3c),^[41] the Al_2O_3 -coated LRMO cathode showed much better cycling stability than the pristine electrode. The prepared Al_2O_3 layer can keep the LRMO surface stable, and the surface spinel-like phase generated between the cathode material and Al_2O_3 can facilitate the three-dimensional (3D) diffusion of lithium ions. Zhao et al. found SiO_2 coating exhibited a superior absorption of hydrofluoric acid (HF) in the electrolyte, providing a scavenging effect for HF and decreasing the side reactions of LRMO with the electrolyte.^[36] Shi et al. prepared MgO-coated LRMO via melting impregnation method followed by a solid-state reaction. The thin MgO coating layer can reduce the charge transfer resistance of the active material during cycling and stabilize the surface structure of LRMO (Figure 3d).^[35]

Transition metal (TM) oxides are also extensively used as coating layers, including WO_3 ,^[42] ZnO ,^[43] CeO_2 ,^[44] Pr_6O_{11} ,^[45] ZrO_2 ,^[46] Sm_2O_3 ,^[47] Fe_2O_3 ,^[48] TiO_2 ,^[49] Er_2O_3 ,^[50] Y_2O_3 ,^[51] RuO_2 ,^[52] La_2O_3 ,^[53] MoO_3 ,^[54] Co_3O_4 ,^[55] MnO_2 ,^[56] V_2O_5 ,^[57] and so on. The working mechanisms of TM oxide coatings are different from those of the above-mentioned non-transition metal oxide coatings. As is known, the decreased capacity of LRMO electrode can be attributed to the annihilation of the temporary oxygen vacancies generated the initial activation of Li_2MnO_3 . Therefore, fixing the lattice oxygen or isolated Li^+ are also

effective ways to improve cycling performance. WO_3 and CeO_2 with unique structure were applied as intercalation host, which can "catch" isolated Li^+ for reinsertion back into the layered lattice after the initial charge. The corresponding coating can suppress the initial activation of Li_2MnO_3 and improve the stability of the surface structure by protecting the LRMO from HF and other side reactions (Figure 3e).^[42,44b,d,58] Similarly, the ZrO_2 ,^[46] TiO_2 ,^[49] and Nb_2O_5 ,^[59] coatings can inhibit the release of oxygen, reduce the excessive anions involved in the redox reaction, and accelerate the diffusion of Li-ions. The ZnO coating or MoO_x coating containing oxygen vacancies can effectively accommodate the oxygen from the Li_2MnO_3 during the first cycle of activation and promote oxygen reversible redox process,^[43,60] accompanied by higher Li^+ conductivity and excellent electronic conductivity. In consideration of the cations with larger radius are tend to precipitate on the surface of the cathode rather than substitute the sites of Ni, Co, Mn, and Li. Zhang et al. coated a uniform, complete, and robust layer of Er_2O_3 with a thickness of ≈ 10 nm on the surface of LRMO cathode material by *in-situ* precipitation and encapsulation (Figure 3f),^[50] which can effectively stabilize the crystal structure of LRMO during cycling. The Er_2O_3 -coated LRMO cathode exhibited excellent capacity retentions of 99 % after 300 cycles at 200 mA g^{-1} and a high ICE of 87.8 %. A similar effect was also achieved by coating with V_2O_5 ,^[57] Co_3O_4 ,^[55] and $\text{Co}_x\text{O}_y/\text{C}$.^[61] These coating materials can be integrated into the LRMO material structure to enhance structural stability and protect the material against electrolyte erosion.

Binary oxide coated LRMO materials are expected to play dual roles. Duan et al. combined active coating (CeO_2) and inert coating (Al_2O_3) as a newly surface coating material (CeAlO_3).^[62] Such binary oxide coating provided many oxygen vacancies for LRMO as well as inhibited the side reaction between the electrode and electrolyte. Zhang et al. designed Mg_2TiO_4 coating on LRMO, Mg and Ti with high oxygen-affinity enhance the energy barrier for oxygen release reaction and stabilize the surface oxygen of LRMO. The modified LRMO electrode exhibits a high capacity retention of 81 % after 700 cycles at 2 C.^[63] Peng et al. developed a facile strategy to form a heterostructural NiFe_2O_4 coating through M–O–N bonding, reconstructed by the M–O bonds (M=Mn, Ni, Co) on the surface of LRMO and the N–O bonds (N=Ni, Fe) on the surface of NiFe_2O_4 .^[64] This NiFe_2O_4

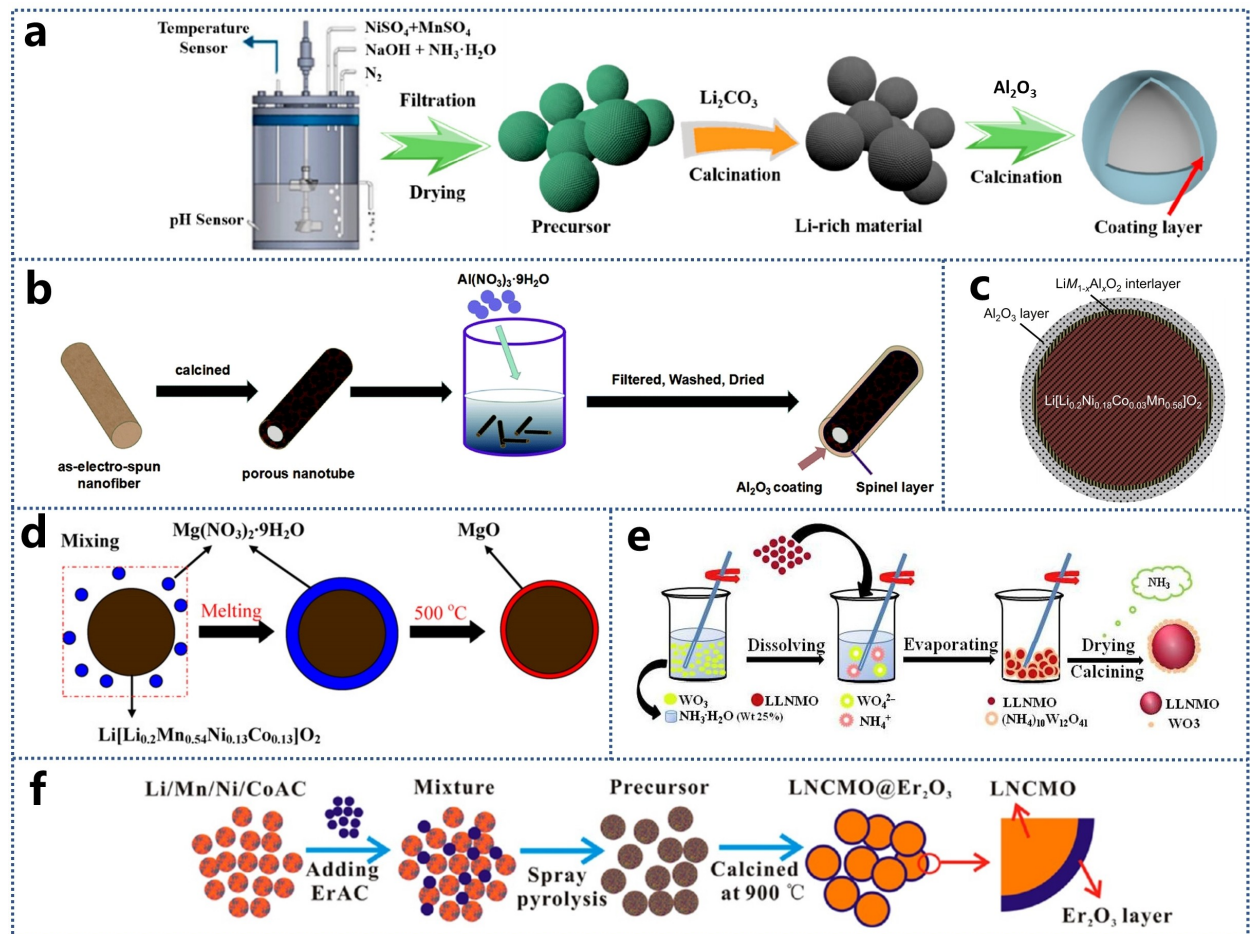


Figure 3. Schematic diagram of the synthetic process for the metal oxide coating on the LRMOs, which include, (a) DPC method. Reproduced with permission.^[34a] Copyright 2020, The Royal Society of Chemistry. (b and c) wet chemical synthesis. Reproduced with permission.^[34b,c] Copyright 2019, The Royal Society of Chemistry. Reproduced with permission.^[34c] Copyright 2015, Elsevier. (d) melting impregnation method. Reproduced with permission.^[35] Copyright 2012, Elsevier. (e) liquid-evaporation coating process. Reproduced with permission.^[42] Copyright 2018, Elsevier. (f) *in-situ* precipitation approach. Reproduced with permission.^[50] Copyright 2017, American Chemical Society.

coating trapped surface lattice oxygen to inhibit the irreversible oxygen-anion redox reaction and restrain cation migration, as well as blocked the HF produced by the decomposition of the electrolyte to reduce the dissolution of Mn. SrTiO₃, Ca_{0.95}Bi_{0.05}MnO₃, La₂CuO₄, and La–Co–O compound have similar effects of high oxygen-affinity, resulting in higher stability of the surface structure of coated-LRMO materials, as well as excellent electronic conductivity to improve the cycle performance of LRMO electrodes.^[65]

Ternary metal oxides coating, such as La₂Li_{0.5}Co_{0.5}O₄,^[66] La_{0.8}Sr_{0.2}MnO_{3-y},^[67] La_{0.9}Sr_{0.1}CoO₃,^[68] Gd_{0.1}Ce_{0.9}O_{2-δ},^[69] Ce_{0.8}Sn_{0.2}O_{2-α},^[70] etc., is also an effective strategy to improve the electrochemical performance of LRMO electrodes. Under the action of multiple elements, the coatings usually have high electronic/ionic conductivity, which can not only inhibit oxygen evolution but also improve the structural stability of LRMO materials.

The monometallic oxide coatings, such as Al₂O₃, MgO, and TiO₂, are primarily utilized to prevent HF erosion and structural degradation in the electrolyte of the LRMO cathode. However,

the main issue that needs to be addressed in LRMO is the release of oxygen during charging. Oxygen, with insufficient surface coordination, tends to decompose by breaking the Li–O and TM–O bonds and forming new O–O bonds. To address this, anti-spinel NiFe₂O₄ binary oxide, ternary oxide, and other coatings have been applied to the surface of LRMO. The multi-element oxide coating on the LRMO surface forms a continuous and stable interface through strong M–O–N bond cooperation (M=Ni, Co, Mn, N=Ni, Fe from binary/ternary oxides). This coating serves two functions: (1) It inhibits the collapse of the material structure during Li⁺ deintercalation process. (2) It prevents the adjacent surface lattice oxygen from participating in anionic redox and from penetrating from the surface into the matrix, effectively inhibiting the voltage attenuation of the battery and the release of oxygen.^[63–64] As a result, the electrochemical performance and capacity retention rate of LRMO materials are improved.

3.2. Metal Phosphates

Phosphates, one of the typical polyanionic compounds, such as AlPO₄, MnPO₄, FePO₄, CePO₄, LaPO₄,^[71] etc., are widely used as coating materials due to the stable tetrahedral polyanionic structural units. The metal phosphate tends to be transformed into amorphous state near the LRMO interface. This process can inhibit the occurrence of phase transition, make the structure inside and at the interface of the cathode material more stable, and improve the cycle stability of the material. The formed amorphous phosphates coating on the surface of LRMO can inhibit phase transition from a layered structure to a spinel structure to stabilize the structure.^[72] Wang et al. designed double-layer coating with 2 wt.% AlPO₄ and 3 wt% Al₂O₃ outer layer on the surface of LRMO. The double-layer coated LRMO electrodes delivered discharge capacities of 215 mAh g⁻¹ at 2 C, which were greatly improved compared with those of single-coated AlPO₄, CoPO₄, and Al₂O₃.^[73] This is mainly because of the increased retention of oxygen vacancies in the layered lattice of the double-coated LRMO sample during the initial charging process, suppressing the undesired SEI layers. In addition, SmPO₄, PrPO₄, and Mg₃(PO₄)₂ coatings have also been reported to stabilize the LRMO structure by mitigating the release of oxygen, while also protecting the LRMO material from side reactions with the electrolyte and increasing the migration rate of Li⁺ at the interface.^[74]

3.3. Metal Fluorides

The most commonly used lithium salt LiPF₆ in the electrolyte of lithium-ion battery readily reacts with trace water to form highly corrosive HF (LiPF₆ → LiF + PF₅, PF₅ + H₂O → 2HF + POF₃), which will further cause the dissolution of the transition metal ions in active material and deterioration of the electrochemical performances of the cathode. As fluorides don't react with HF, fluorides coating can be used to hinder the contact of HF and cathode material. Metal fluoride coatings can effectively alleviate the occurrence of interfacial side reactions between the electrode material and the electrolyte. F⁻ can also reduce the charge transfer resistance, improve the conductivity and crystal structure stability of the cathode material, and thus improve the rate performance and cycle stability of the cathode material. Furthermore, part of F ions of fluorides coating can bond with TM in LRMO to alleviate the migration of TM ions and inhibit phase transition. The reported fluorides coating including LiF,^[75] AlF₃,^[76] MgF₂,^[77] CaF₂,^[78] CoF₂,^[79] CeF₃,^[80] LaF₃,^[81] ZrF₄,^[82] SmF₃,^[83] FeF₃,^[84] and YF₃.^[85] Ultrathin AlF₃ coating on LRMO effectively protected the spinel like phase from attack by the acidic species in the electrolyte, prevented direct contact between the active material and the electrolyte and enhanced structural stability of LRMO.^[76] The MgF₂ coating induced the transformation of layered Li₂MnO₃ to spinel phase, which can reduce the irreversible capacity in the initial cycle, improve the coulombic efficiency and enhance cycle stability of the battery.^[77] Chong et al. developed a facial wet chemistry method to prepare CoF₂ protective layer on the surface of

LRMO.^[79] The coated LRMO electrodes exhibited the excellent rate capability of 167.5 mAh g⁻¹ at 5 C, and the capacity retention rate can reach 93.0% after 100 cycles at 0.1 C.

3.4. Carbon and Conductive Polymers Coatings

The above-mentioned metal oxides, phosphates, and fluorides coatings mainly improve the electrochemical performance of LRMO cathodes by reducing the side reactions at the interface between the active materials and the electrolyte. However, it cannot be ignored that the inactive electrochemical nature and low electronic conductivity of these coatings, which are not conducive to the improvement of the rate performance of active materials. By coating with electronic conductors, such as carbon materials or conductive polymers, LRMO with a highly conductive network can better avoid the above shortcomings.

3.4.1. Carbon Coating

During the process of the coating of carbon material onto the LRMO surface, oxidation of carbon at high temperatures leads to the transformation of the Li₂MnO₃ layered phase into the spinel phase, thereby enhancing its electrochemical performance (Li₂MnO₃ + C + O₂ → LiMn₂O₄ + CO₂, Mn⁴⁺ → Mn⁴⁺/Mn³⁺).^[86] Carbon-coated materials encompass carbon nanotubes, graphene quantum dots, and graphene, all of which possess high electronic conductivity and a large specific surface area.^[87]

Song et al. applied a graphene oxide (GO) coating layer to the surface of LRMO cathode material.^[88] Following annealing treatment, the surface layer transformed from a layered structure to a spinel phase, which facilitated rapid Li⁺ diffusion and enhanced the rate performance of the LRMO material. The GO-coated LRMO cathode exhibited an impressive initial discharge capacity of 313 mAh g⁻¹ at 0.05 C, with a discharge capacity of 201 mAh g⁻¹ at 10 C. However, its cycle performance remains suboptimal. To enhance the cycle performance of LRMO, utilizing N-doped graphene as a coating layer can effectively mitigate the rapid capacity and voltage decay.^[89] The modified electrode exhibited a capacity of 286.4 mAh g⁻¹ at 0.2 C, with a capacity retention rate of 86% after 200 cycles. The enhanced electrochemical performance can be attributed to the ability of the functional groups in N-doped graphene to effectively capture reactive oxygen species and mitigate the continuous decomposition of the electrolyte. Consequently, the LRMO electrode maintains better layered structure stability after long-term cycling. Furthermore, graphene quantum dots (GQDs) and carbon spheres, owing to their high electronic conductivity, can also effectively enhance the cycle and rate performance of the LRMO electrode.^[87b]

The carbon coating achieved via *ex-situ* methods poses challenges in achieving a uniform and dense coating, whereas *in-situ* coating facilitates the formation of a strong bond with the matrix. Shanmugam et al. conducted *in-situ* carbon coating on the surface of LRMO, the uniform and dense coating layer enhanced the electronic conductivity of the material, while

simultaneously inducing the formation of oxygen vacancies during the charging process.^[90] The coating layer is uniform and dense, which can not only improve the electronic conductivity of the material but also induce Mn⁴⁺ to be reduced to Mn³⁺ by the formed oxygen vacancies in the charging process, thereby improving the structural stability and cycle performance of the LRMO electrodes.^[86e,91]

3.4.2. Conductive Polymers Coating

Many conductive polymers exhibit superior electronic conductivity compared to carbon, coupled with high thermal stability. These polymers can be utilized as a coating layer to create a uniform and highly conductive film, thereby enhancing the charge transfer efficiency at the electrode/electrolyte interface and improving the thermal stability of the coated material. Some common examples of such conductive polymer coatings include polyaniline (PANI), polypyrrole (PPy), PEDOT:PSS, polyimide (PI), polyacrylonitrile (PAN), polyurethane (PU), etc.^[8,92] For example, PANI possesses a high charge storage capacity, excellent electrochemical performance, and reversible oxidation/reduction properties. It can be used as both a conductive matrix and an active material in the composite electrode. Wang et al. successfully achieved a uniform coating of PANI on the surface of LRMO cathode material with a layered/spinel hybrid structure through *in-situ* polymerization.^[92a] The modified LRMO electrodes exhibited excellent rate performance due to the synergistic effect of PANI coating and layered/spinel composite structure. Xue et al. proposed an *in-situ* chemical oxidation polymerization process to coat PANI on the surface of LRMO.^[92b] The LRMO electrode modified with 10 wt% PANI showed an initial discharge capacity of 313.5 mAh g⁻¹ at 0.05 C with ICE of 89.01%. It also demonstrated excellent cycling stability with a retained capacity of 282.1 mAh g⁻¹ after 80 cycles at 0.1 C, the impressive rate performance with a capacity of 198.6 mAh g⁻¹ even at 10 C.

While the improvement of the conductive polymer coating layer at the interface is evident, using a high molecular weight conductive polymer for the coating of the LRMO material would decrease the energy density and limit its practical application.

3.5. Lithium Compound Coatings

3.5.1. Lithium-Ion Conductive Coating

Lithium-ion conductive coatings are a viable approach to enhance the diffusion rate of lithium ions and the structural stability of the material. Generally, lithium-ion conductive materials can be categorized into low lithium-ion conductive materials (such as lithiated metal oxides) and fast lithium-ion conductive materials (such as solid electrolyte materials).

Typical low lithium-ion conductive materials include Li₂SnO₃,^[93] LiAlO₂,^[94] Li₂SiO₃,^[95] Li₂ZrO₃,^[96] Li₂WO₄,^[97] Li₂TiO₃,^[98] LiErO₂,^[99] etc. For example, Liu et al. developed a nano Li₂SnO₃ coating to protect the LRMO lattice oxygen from exposure to

the surface and prevent irreversible oxidation.^[93] Liu et al. reported an ultra-thin and uniform amorphous lithium-ion conductive Li₂TiO₃ (LTO) coating through molten LiCl-assisted solid-liquid reaction. In this process, the dissolved TiO₂ penetrated along the grain boundary and reacted with the primary particles of the LRMO.^[98b] The LTO coating inhibited the dissolution and oxygen release of TM and prevented the TM crossover effect of the lithium anode.^[98c] Additionally, the LTO coating exhibited rapid lithium-ion diffusion kinetics, acting as a "lithium-ion pump" to enhance the rate performance of the LRMO electrode.

The commonly used fast lithium-ion conductive materials are mainly solid electrolytes, such as LiAlF₄,^[100] Li₇La₃Zr₂O₁₂,^[101] Li_{6.25}La₃Zr₂Al_{0.25}O₁₂,^[102] LiAlO₂,^[94] Li-La-Ti-O,^[103] LiCeO₂,^[104] LiTaO₃,^[105] LiV₃O₈,^[106] Li_{0.5}Mn_{0.5}O,^[107] Li_{0.75}La_{0.42}TiO₃,^[108] etc. Gao et al. successfully modified superionic conductor Li_{1+x}Al_xTi_{2-x}(PO₄)₃ and conductor carbon nanotubes (CNTs) on the surface of LRMO materials. The electronic conductivity and ionic conductivity of LRMO composites can reach 8.91×10⁻⁸ S cm⁻¹ and 1.93×10⁻⁶ S cm⁻¹, respectively.^[109] Fast lithium-ion conductive Li₃PO₄ coating possesses several advantages: (1) the PO₄³⁻ polyanion has strong covalent bonds with the lattice of the LRMO, suppressing the release of surface oxygen;^[110] (2) the Li₃PO₄ coating blocks direct contact of the organic electrolyte with the cathode to reduce the dissolution of TM ions;^[111] (3) Li₃PO₄ can compensate for the loss of lithium ions during cycling and increase the initial discharge specific capacity and ICE.^[112] Zhang et al. proposed a wet chemical method to prepare Li₃PO₄ coated LRMO with layered/spinel heterostructures on the surface.^[113] The coating effectively suppressed the side reaction and maintained the structural stability of the LRMO.

3.5.2. Lithium Active Material Coating

Some researchers have proposed using electrochemically lithium active materials as a coating layer. This coating layer can enhance the interfacial reaction between the active material and electrolyte, as well as provide a rapid pathway for lithium ions diffusion on the surface of the material. The reported Lithium active material coatings include LiFePO₄, LiCoPO₄, LiMnPO₄, Li₄V₂Mn(PO₄)₄, and Li₃V₂(PO₄)₃, not only possess high lithium-ion conductivity, but also good structural stability.^[114] The unique surface charge compensation mechanism also regulates the surface and bulk lattice oxygen redox activity of LRMO materials during long-term cycling.^[114f] Zheng et al. proposed the sol-gel method to obtain nano-sized LiFePO₄ coated LRMO,^[114a] which facilitated the fast lithium-ion transport in the coating layer and improved the electrochemical performances of the electrode. The discharge capacity of the 5 wt% LiFePO₄ modified LRMO cathode is 282.8 mAh g⁻¹ at 0.1 C, with a high-capacity retention rate of 98.1% after 120 cycles and minimal potential decay. However, while the lithium cathode material coating layer can prevent direct contact between active materials and the electrolyte, it still reacts with LiPF₆ in the electrolyte during the electrochemical reaction. This reac-

tion consumes part of the active Li^+ in the system, resulting in a decrease in the cycle stability of the LRMO electrodes. Additionally, the SEI film of LRMO electrodes with electrochemically active coating is less stable than that with inert coatings and thickens with cycling, increasing the charge transfer resistance.^[115]

The spinel cathode materials, which has a 3D structure, provides increased lithium-ion diffusion channels on the material surface, maintains good structural stability, and suppresses structural degradation. As a result, the design of LRMO materials with layered-spinel composite heterostructures has emerged as prominent research in recent years.^[6g] The spinel phase is mainly composed of $\text{LiMn}_{1.5}\text{Ni}_{0.5}\text{O}_4$, LiMn_2O_4 , and $\text{Li}_4\text{Mn}_5\text{O}_{12}$.^[116] As shown in Figure 4a, in the LiMn_2O_4 structure, Li^+ is located at the center of the LiO_4 tetrahedron (8a site), $\text{Mn}^{3+}/\text{Mn}^{4+}$ is located inside the MnO_6 octahedron (16d site), and the 16c octahedron site remains vacant. Li^+ diffuses from one 8a site to another 8a site using the 16c site vacancy. The shared surface of the 8a site and the 16c site forms a 3D lithium diffusion path, allowing Li^+ ions to be transported quickly. As shown in Figure 4b, for the $\text{Li}_4\text{Mn}_5\text{O}_{12}$ spinel phase, all the manganese ions are in the Mn^{4+} valence state, and the excess lithium occupies part of the manganese sites, resulting in the

smallest Jahn-Teller effect and less Mn^{2+} dissolution. The spinel phase with $\text{Fd}\bar{3}m$ space group has the same empty 16c site, which ensures the 3D diffusion path and is conducive to the efficient diffusion of lithium, thereby improving the rate capability (Figure 4c). Zhang et al. successfully synthesized spinel $\text{Li}_4\text{Mn}_5\text{O}_{12}$ -coated LRMO by controlled KMnO_4 oxidation on the oxide precursor. The uniform epitaxial spinel $\text{Li}_4\text{Mn}_5\text{O}_{12}$ coating was intrinsically stable in lattice oxygen, providing the heterostructured material with favorable properties to prevent the escape of lattice oxygen from the fragile layered framework during charging voltage exceeding 4.5 V. The $\text{Li}_4\text{Mn}_5\text{O}_{12}$ -coated LRMO electrode exhibited significantly improved electrochemical performance with an initial discharge capacity of 276 mAh g^{-1} at 0.05 C, good capacity retention of 83.1% over 300 cycles, and greatly mitigated voltage decay.^[117] Upon integration with LRMOs, the material can leverage its inherent strengths while facilitating the creation of additional substructures like lithium vacancies and oxygen vacancies. This ensures a high Li^+ diffusion coefficient and suppresses oxygen release, leading to outstanding electrochemical performance that compensates for the shortcomings of the LRMO. Hence, the spinel phase is widely employed to enhance the electrochemical performances of the LRMO cathodes.

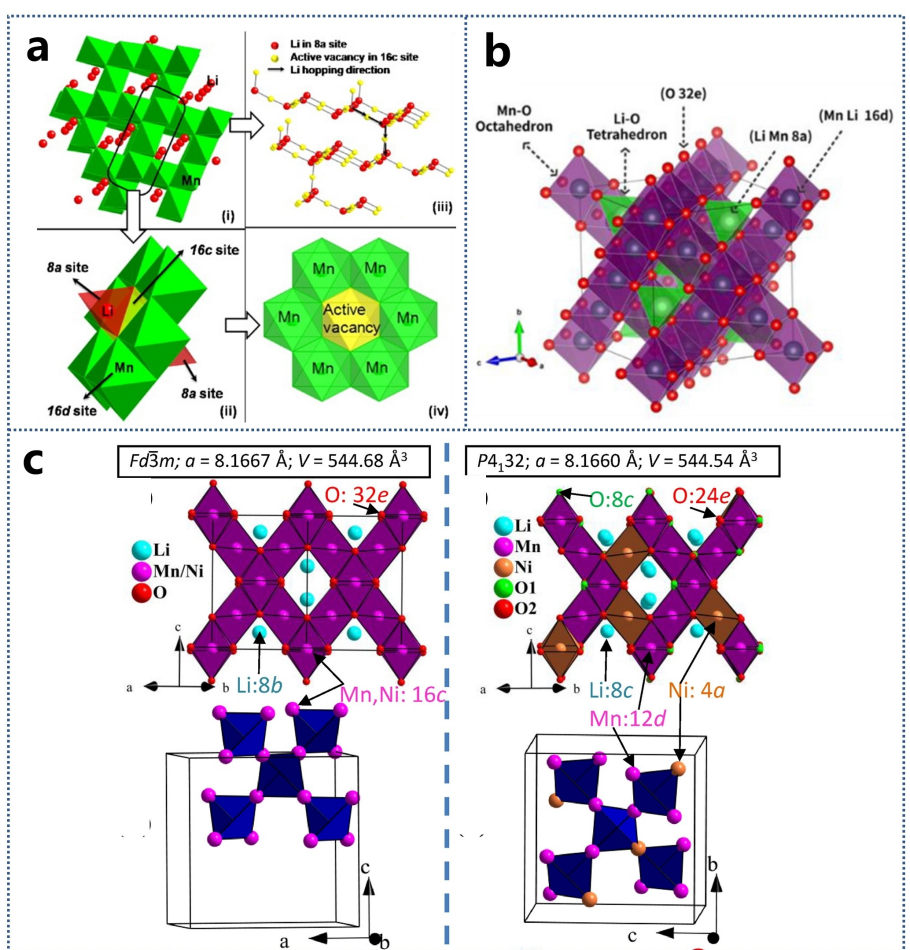


Figure 4. The crystal structure of (a) LiMn_2O_4 . Reproduced with permission.^[118] Copyright 2019, The Elsevier. (b) $\text{Li}_4\text{Mn}_5\text{O}_{12}$. Reproduced with permission.^[119] Copyright 2020, Wiley-VCH. and (c) $\text{LiMn}_{1.5}\text{Ni}_{0.5}\text{O}_4$. Reproduced with permission.^[120] Copyright 2019, The Author(s).

As far as we know, the surface structure of LRMO is typically transformed from a layered structure to a spinel structure and then to a rock salt structure by reducing the amount of lithium source during the synthesis process. The spinel-like phase can effectively utilize the delithiated oxygen vacancies, mitigate the cell volume change during cycling, and inhibit the irreversible oxygen evolution caused by the excessive oxidation of lattice oxygen atoms.^[6g] Wu et al. found that the types of lithium source will affect the synthesis of low-temperature mesophase in the synthesis process of LRMO and thus affect the structural evolution of the high-temperature section.^[121] LiOH reacts with the precursor at room temperature, and the carbonate precursor decomposes. Some LiOH reacts with $\text{Ni}_{0.25}\text{Mn}_{0.75}\text{CO}_3$ and transforms the structure of Li_2CO_3 . This low temperature reaction accelerates the nucleation process of the rock salt structure and establishes a foundation for the subsequent reaction path. When Li_2CO_3 is used as the lithium source, the precursor and Li_2CO_3 begin to decompose above 300°C, and the structure is more easily converted into a spinel phase structure. This stable spinel phase structure is more difficult to transform into an ordered layered structure, resulting in a small amount of spinel phase retained in the final formed LRMO layered material, forming a layered-spinel composite structure. Cao et al. also observed that the calcination temperature affects the proportion of layered-spinel components on the surface of LRMO materials, rather than the internal structure of the materials. When the spinel content is about 5.8%, the LRMO material exhibits excellent rate performance.^[6g]

Some researchers have also found that acid treatment can reduce the lithium content on the surface of LRMO materials

and generate a spinel phase on the surface of LRMO, such as NH_4F ,^[122] NH_4HF_2 ,^[123] $(\text{NH}_4)_2\text{SO}_4$,^[124] $(\text{NH}_4)_2\text{SiF}_6$,^[125] formic acid,^[126] citric acid,^[127] $\text{NH}_4\text{H}_2\text{PO}_4$,^[7,128] boric acid,^[116,129] $(\text{NH}_4)_2\text{S}_2\text{O}_8$,^[130] and oleic acid^[131] are exchanged with lithium ions in LRMO to construct lithium defects. Guo et al. used hydrogen ions in oleic acid (OA) to exchange with Li^+ in LRMO for constructing lithium defects. In the subsequent calcination process, TM ions occupied the lithium site, resulting in the formation of TM defects (Mn vacancies and TM doping) and the introduction of oxygen vacancies on the LRMO surface. The introduction of cation/anion double defects can enhance the Li^+ diffusion coefficient. Additionally, the *in-situ* surface reconstruction layer can improve the electronic conductivity and lead to the formation of SEI to stabilize the surface lattice oxygen (Figure 5a). Our group has used 4-(2-Hydroxyethyl)piperazine-1-ethanesulfonic acid (HEPES) aqueous solution to treat LRMO materials.^[132] Corrosion pits have been observed on the surface of LRMO material after heat treatment, and spinel phase was formed on the surface. This effectively improves the Li^+ conduction ability of the material, reduces the electrochemical impedance, and improves the cycle stability and rate discharge performance of the electrode. Materials with abundant oxygen vacancies can effectively suppress the Jahn-Teller distortion effect, thereby effectively improving the structural stability (Figure 5b).

Li et al. utilized phosphorus pentasulfide to conduct surface treatment on LRMO materials, resulting in the formation of spinel/rock salt phase *in-situ* and the creation of various amorphous layers that act as lithium ion conductors. The reconstruction of this active crystal plane greatly inhibits the

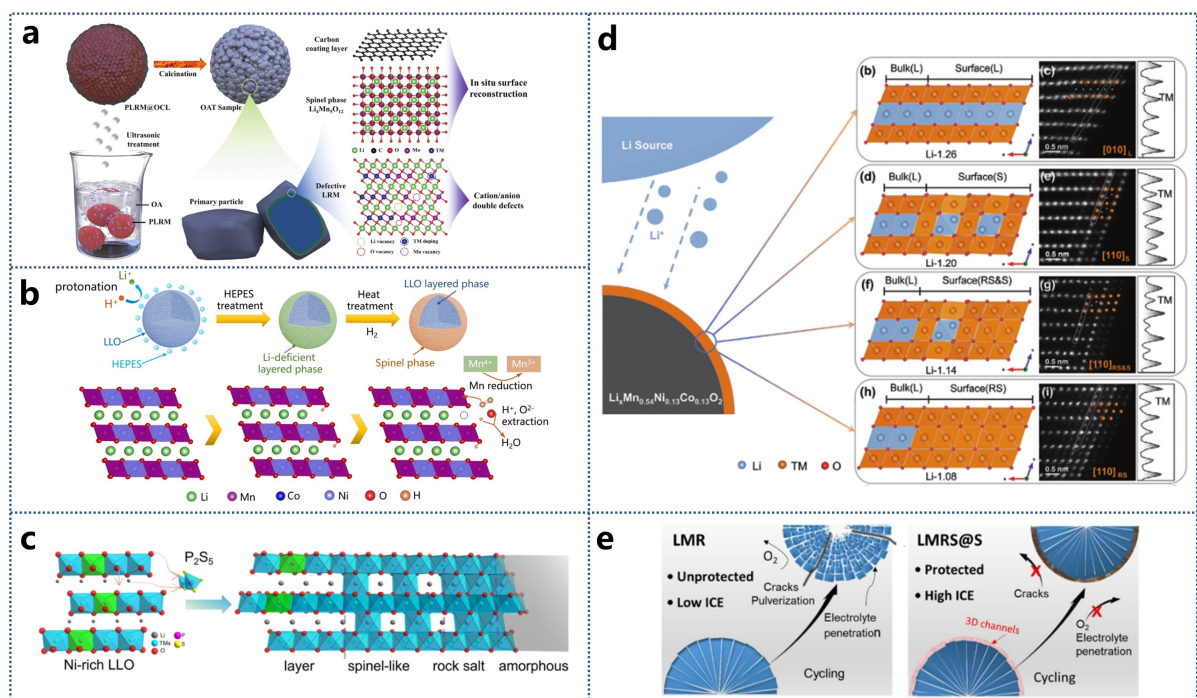


Figure 5. Schematic diagram of (a) OA. Reproduced with permission.^[131b] Copyright 2021, Wiley-VCH. (b) HEPES. Reproduced with permission.^[132] Copyright 2022, American Chemical Society. (c) P_2S_5 .^[133] Copyright 2022, Elsevier. (d) the Li source concentration. Reproduced with permission.^[134] Copyright 2023, Wiley-VCH. (e) S-assisted interface engineering. Reproduced with permission.^[135] Copyright 2022, Elsevier.

precipitation of oxygen during the charging process, thereby enhancing the stability of the material's surface structure. The formation and coating of an amorphous fast ion conductor layer on the surface of the material during surface modification further mitigates the occurrence of side reactions between the active material and the electrolyte. In the long cycle, PS-1% still retained its modified surface structure and layered bulk structure, with the outermost surface layer showing rock salt phase (Figure 5c).^[133] Hao et al. inhibited the volume strain and surface O₂ release by adjusting the amount of lithium source only during the synthesis process (Figure 5d). The spinel-like phase hinders the release of surface O₂ by accommodating O₂ in the surface layer. Compared with the unmodified LRMO cathode, the O₂ trapped in the bulk lattice hinders the strain evolution by about 70% at high voltage. Therefore, after 100 cycles at a rate of 0.1 C, the enhanced stability of the bulk and surface structure can significantly improve the capacity retention rate of 97.6% and the high coulombic efficiency of about 99.5%.^[134] An epitaxial spinel phase stabilized material (LMRS@S) has been developed for LRMO with proper S doping. The unique structure of LMRS@S effectively suppresses the percolating migration of oxygen from the bulk LRMO, phase transition, and collapse. It also provides more paths for Li ion insertion/deinsertion and reduces electrochemical polarization during the cycling process, as depicted in Figure 5e. This schematic diagram illustrates the degradation and *in-situ* stabilizer mechanisms. As a result, the LMRS@S cathode demonstrates excellent electrochemical performance, with a capacity retention of 82.1% over 600 cycles at 1 C. Additionally, it exhibits superior performance in a pouch-type full cell, with 81.7% capacity retention after 140 cycles at 1 C.^[135]

Combined with the advantages of coating modified LRMO, acidic inorganic salts are also used to modify LRMO cathode materials, and the spinel/layered heterostructures could be constructed on the surface of LRMO. For example, the layered@spinel@Li₂WO₄ structure is prepared by *in-situ* induction on the surface of LRMO treated with weakly acidic Li₂WO₄. The 3D structure of the spinel interlayer and the cubic tunnel structure of Li₂WO₄ coating layer are beneficial for improving the diffusion rate of Li⁺ and the rate performance. The formation of the spinel phase helps to inhibit the phase transition from the layered phase to the spinel phase.^[97b] With the help of Zr(HPO₄)₂·H₂O, the spinel phase containing O vacancies was *in-situ* induced on the surface of LRMO material. After Zr(HPO₄)₂ modification, the low O 2p non-bonding energy band and electron-rich layer at the interface inhibit the irreversible loss of lattice O and avoid the decomposition of the electrolyte surface. The outermost zirconium phosphate inert layer can prevent the highly active Oⁿ⁻ from corrosion by the electrolyte, thereby improving the stability of the surface structure.^[136]

4. Ionic Doping

Another effective modification method for LRMO materials is ion doping, which can improve the structural stability of

cathode materials for LIBs, increase conductivity, alleviate voltage attenuation, and improve the Li⁺ diffusion rate.^[139] The introduction of a certain amount of inert elements to replace the transition metal (TM) elements in the LRMO cathode has been shown to suppress voltage decay and capacity loss, resulting in better electrochemical performance. The basic principle of element substitution is similar ionic radius or the same valence state.^[140] Different from the surface coating, the introduction of doped ions will cause changes in the local environment of electrons and ions in the material, which can alleviate the cation disorder and structural changes during the cycle to a certain extent. At the same time, the doping ions can expand the interplanar spacing of the LRMO material lattice without destroying the structure and strengthen the structural integrity, so that the rate performance of the material is significantly improved.^[2b,12] According to the different types of doping elements, it can be divided into cation single, anion single, and multi-ion co-doping.^[6e,141]

Among them, cation doping is divided into Li layer doping (Na⁺, K⁺, Mg²⁺, Ti³⁺ substitution), TM layer doping (Al³⁺, La³⁺, Zr⁴⁺, Nb⁵⁺ substitution), and mixed doping according to the different doping sites. Anion doping can be divided into low valence anion doping (F⁻, Cl⁻, S²⁻, etc.) and polyanion doping (XO₄)⁻ (X=P, B, S, W, etc.). Doping these anions can enhance the TM–O bond energy, resulting in improved cycle stability and higher thermal stability.^[142] In addition, compared with the single doping strategy, the multi-ion doping combination can make full use of the common advantages of anions and cations, and synergistically improve the electrochemical performance of the material. Table 2 lists the representative examples of doping modified LRMO materials.

4.1. Cation Single Doping

4.1.1. Li Layer Doping

The most commonly used doping elements to replace Li⁺ sites are alkali metal ions that are in the same main group as Li, such as Na⁺ and K⁺. Because they are in the same main group, their electronic structures and electrochemical properties are similar. When these doping elements enter the lithium site, the structure of the material can be more stable, and the transmission energy barriers of ions and electrons can be reduced. Doping alkali metal ions with a larger radius can increase the migration barrier and reduce the kinetic migration rate of transition metal ions. For example, many studies have reported Na⁺ is doped into LRMO materials, including polymer-pyrolysis,^[143] solid-state method,^[144] solvothermal method,^[145] Li⁺/Na⁺ exchange reaction.^[146]

Ma et al. synthesized a series of Li_{1.2-2x}Na_xMn_{0.56}Ni_{0.16}Co_{0.08}O₂ (x=0,0.05, 0.1 and 0.2) cathode materials by high-temperature calcination technique.^[147] With the increase of Na doping amount, the proportion of Mn³⁺ in Na-doped samples gradually increased (Figure 6a). The peak area of the Na-doped sample at 531.4 eV is larger than that of the undoped sample, indicating more oxygen vacancies on the surface (Figure 6b). The HRTEM

Table 2. Effects of different elemental doping on the electrochemical performance of LRMO (1 C = 250 mA g⁻¹).

Dopant	Cathode materials	Initial discharge capacity/(mAh g ⁻¹)	Initial coulombic efficiency (%)	Capacity retention	Rate capacity/(mAh g ⁻¹)	Ref.
Li Layer	Na ⁺	Li _{1.17} Na _{0.02} Mn _{0.54} Ni _{0.13} Co _{0.13} O ₂	280 (0.08 C)	91.2	94.7%, 200 cycles, 0.8 C	214 (4 C) [146c]
	Na ⁺	Li _{1.17} Na _{0.03} Mn _{0.54} Ni _{0.13} Co _{0.13} O ₂	307 (0.12 C)	87.5	89%, 100 cycles, 0.4 C	139 (9.6 C) [143]
	K ⁺	Li _{1.151} K _{0.013} Mn _{0.552} Ni _{0.145} Co _{0.146} O ₂	315 (0.08 C)	75	85%, 110 cycles, 0.08 C	215 (1.6 C) [149]
	Mg ²⁺	Li [Li _{0.12} Mg _{0.04} Co _{0.13} Ni _{0.13} Mn _{0.54}]O ₂	272 (0.12 C)	78	93.3%, 300 cycles, 0.4 C	112 (9.6 C) [154]
	Mg ²⁺	Li _{1.18} Mg _{0.01} Mn _{0.54} Co _{0.13} Ni _{0.13} O ₂	305.3 (0.1 C)	89.0	76.1%, 100 cycles, 0.2 C	146.5 (3 C) [156]
TM Layer	Al ³⁺	Li _{1.2} Ni _{0.16} Mn _{0.51} Al _{0.03} Co _{0.08} O ₂	323.7 (0.1 C)	81.2	98%, 100 cycles, 0.08 C	≈ 100 (3.2 C) [159f]
	Fe ³⁺	Li _{1.2} Ni _{0.13} Co _{0.13} Mn _{0.54} O ₂	285.32 (0.1 C)	79.31	81.8%, 300 cycles, 1 C	117.4 (10 C) [162e]
	Cr ³⁺	Li _{1.2} [Mn _{0.54} Ni _{0.13} Co _{0.13}] _{0.095} Cr _{0.005} O ₂	270.7 (0.05 C)	81.8	90.98%, 200 cycles, 1 C	119.3 (10 C) [161a]
	Co ³⁺	Li _{1.231} Mn _{0.525} Ni _{0.154} Co _{0.12} O ₂	280.05 (0.1 C)	85.9	94.56%, 200 cycles, 0.5 C	127.06 (10 C) [163a]
	Y ³⁺	Li[Li _{0.2} Ni _{0.183} Mn _{0.585} Y _{0.03}]O ₂	253.9 (0.1 C)	77.6	92.7%, 50 cycles, 0.1 C	107 (2 C) [169b]
	V ⁵⁺	Li _{1.2} Mn _{0.515} Co _{0.075} Ni _{0.115} V _{0.015} O ₂	253 (0.1 C)	70.7	90.2%, 50 cycles, 1 C	99 (5 C) [176b]
	Sn ⁴⁺	Li(Li _{0.17} Ni _{0.25} Mn _{0.58})O ₂	250.2 (0.048 C)	70.9	93.17%, 120 cycles, 0.32 C	112 (5 C) [172a]
	Ti ⁴⁺	Li _{1.2} Mn _{0.6} Ni _{0.2} O ₂	276.9 (0.1 C)	—	85%, 500 cycles, 1 C	— [160]
	Zr ⁴⁺	Li _{1.2} Mn _{0.54} Ni _{0.13} Co _{0.13} O ₂	283.8 (0.2 C)	77.38	88%, 300 cycles, 1 C	157.7, (5 C) [166]
	Ru ⁴⁺	Li _{1.2} Ni _{0.2} Mn _{0.57} Ru _{0.03} O ₂	≈ 280 (0.1 C)	≈ 83	90%, 300 cycles, 1 C	162, (5 C) [171a]
	Nb ⁵⁺	Li _{1.2} Mn _{0.54} Ni _{0.13} Co _{0.13} O ₂	320 (0.1 C)	87	94.5%, 100 cycles, 0.1 C	≈ 200, (2 C) [167]
	W ⁶⁺	Li _{1.17} Mn _{0.5} Ni _{0.15} Co _{0.15} Al _{0.025} W _{0.01} O ₂	301.1 (0.1 C)	76.5	92.9%, 100 cycles, 0.5 C	150 (1 C) [175c]
	Mo ⁶⁺	Li _{1.2} Mn _{0.59} Ni _{0.1} Co _{0.1} Mo _{0.01} O ₂	193.9 (0.08 C)	81.4	92.5%, 250 cycles, 0.1 C	— [177c]
	Ta ⁵⁺	Li _{1.2099} Mn _{0.5374} Co _{0.1268} Ni _{0.1257} Ta _{0.0036} O ₂	262 (0.2 C)	81	93%, 200 cycles, 1 C	155, (5 C) [10]
	Te ⁶⁺	Li[Li _{0.2} Mn _{0.56} Ni _{0.16} Co _{0.08}] _{0.95} Te _{0.05} O ₂	271.6 (0.1 C)	88.2	84.3%, 100 cycles, 0.5 C	156.1, (5 C) [178]
	PO ₄ ³⁻	Li _{1.17} Mn _{0.5} Ni _{0.17} Co _{0.16} (PO ₄) _{0.05} O _{1.8}	300 (0.1 C)	86	95%, 100 cycles, 1 C	121 (6 C) [202]
Anion	SO ₄ ²⁻	Li(Li _{0.17} Ni _{0.20} Co _{0.05} Mn _{0.58})O _{1.97} (SO ₄) _{0.03}	261.2 (0.1 C)	83.5	≈ 80%, 400 cycles, 0.12 C	160 (6 C) [203]
	SiO ₄ ⁴⁻	Li(Li _{0.17} Ni _{0.20} Co _{0.05} Mn _{0.58})O _{1.95} (SiO ₄) _{0.05}	282.2 (0.1 C)	83.2	≈ 71%, 400 cycles, 0.12 C	150 (6 C) [203]
	F ⁻	Li _{1.2} Mn _{0.54} Ni _{0.13} Co _{0.13} O _{2-x} F _x	275.3 (0.2 C)	—	81.9%, 100 cycles, 1 C	133 (5 C) [185a]
	S ²⁻	Li _{1.2} Ni _{0.13} Co _{0.13} Mn _{0.54} O _{2-x} S _x	270.5 (0.04 C)	—	81.10%, 600 cycles, 0.4 C	174.8 (8 C) [188]
	Se ²⁻	Li _{1.2} Mn _{0.54} Ni _{0.13} Co _{0.13} O ₂	293.5 (0.08 C)	94.3	88.4%, 400 cycles, 0.8 C	≈ 150 (4 C) [190a]
	B ³⁺	Li _{1.144} Ni _{0.134} Co _{0.1344} Mn _{0.54} O ₂	275 (0.1 C)	87	93.2%, 80 cycles, 0.2 C	— [194]
	B ³⁺	Li _{1.15} Mn _{0.53} Ni _{0.22} Co _{0.1} O ₂	253 (0.1 C)	77.4	80.1%, 1200 cycles, 1 C	162 (5 C) [195b]
Multi-ion	Na ⁺ , F ⁻	Li _(1.2-y) Na _y Mn _{0.56} Ni _{0.16} Co _{0.08} O _(2-z/2) F _z	298 (0.1 C)	89.8	85.7%, 500 cycles, 5 C	174 10 C [215a]
	Al ³⁺ , F ⁻	Li _{1.2} Ni _{0.13} Co _{0.13-x} Mn _{0.54} Al _{0.01} O _{1.94} F _{0.06}	287 (0.1 C)	—	88.21%, 150 cycles, 0.5 C	157 (10 C) [214]
	Fe ³⁺ , Cl ⁻	Li _{1.2} Mn _{0.585} Ni _{0.185} Fe _{0.03} O _{1.98} Cl _{0.02}	232.4 (0.1 C)	73.1	86.4%, 500 cycles, 1 C	145.6, (5 C) [217]
	Al ³⁺ , BO ₃ ³⁻ /BO ₄ ⁵⁻	Li _{1.18} Mn _{0.52} Co _{0.13} Ni _{0.13} La _{0.02} Mg _{0.02} O ₂	250 (0.1 C)	71.6	92.0%, 100 cycles, 0.1 C	134, (5 C) [218]
	Mg ²⁺ , Al ³⁺	Li _{1.2} Mn _{0.52} Ni _{0.13} Co _{0.13} Mn _{0.01} Al _{0.01} O ₂	271.9 (0.05 C)	—	81.61%, 100 cycles, 0.1 C	119.8 (5 C) [205a]
	Na ⁺ , W ⁶⁺	Li _{1.16} Na _{0.01} Mn _{0.5} Ni _{0.15} Co _{0.15} Al _{0.025} W _{0.01} O ₂	326 (0.1 C)	78.6	93.4%, 100 cycles, 0.5 C	167.3 (5 C) [206]
	Nd ³⁺ , Al ³⁺	Li _{1.2} Mn _{0.53} Ni _{0.267} O ₂	247.4 (0.1 C)	80.5	82%, 200 cycles, 1 C	150 (10 C) [208]
	Ta ⁵⁺ , Mo ⁶⁺	Li _{1.168} Ta _{0.002} (Ni _{0.139} Co _{0.139} Mn _{0.552}) _{0.998} Mo _{0.002} O ₂	282.1 (0.1 C)	90.7	80%, 220 cycles, 1 C	157.8 (5 C) [210]
	Zn ²⁺ , Ti ⁴⁺	Li _{1.2} Mn _{0.6} Ni _{0.2} O ₂	245.2 (0.08 C)	75.9	87%, 150 cycles, 0.4 C	≈ 80 (8 C) [211a]

images of the original LRMO and Na-doped LRMO show lattice fringe spacing of ≈ 0.472 and 0.475–0.520 nm, respectively (Figure 6h–j). Compared to the pristine LRMO material (Figure 6c,e), the interlayer spacing of Na-doped LRMO is slightly enlarged, resulting in obvious stacking faults (Figure 6d,f). DFT calculations show that the surface oxygen vacancy-induced

structure affects the local environment of Mn coordination and enhances the stability of the structure. The ICE of the optimized LRMO cathode is 84.2%, and it has cycle stability, average voltage retention and rate performance.

He et al. used Na⁺ to replace part of Li in the Li layer of the LRMO material, stabilized the layered structure and inhibited

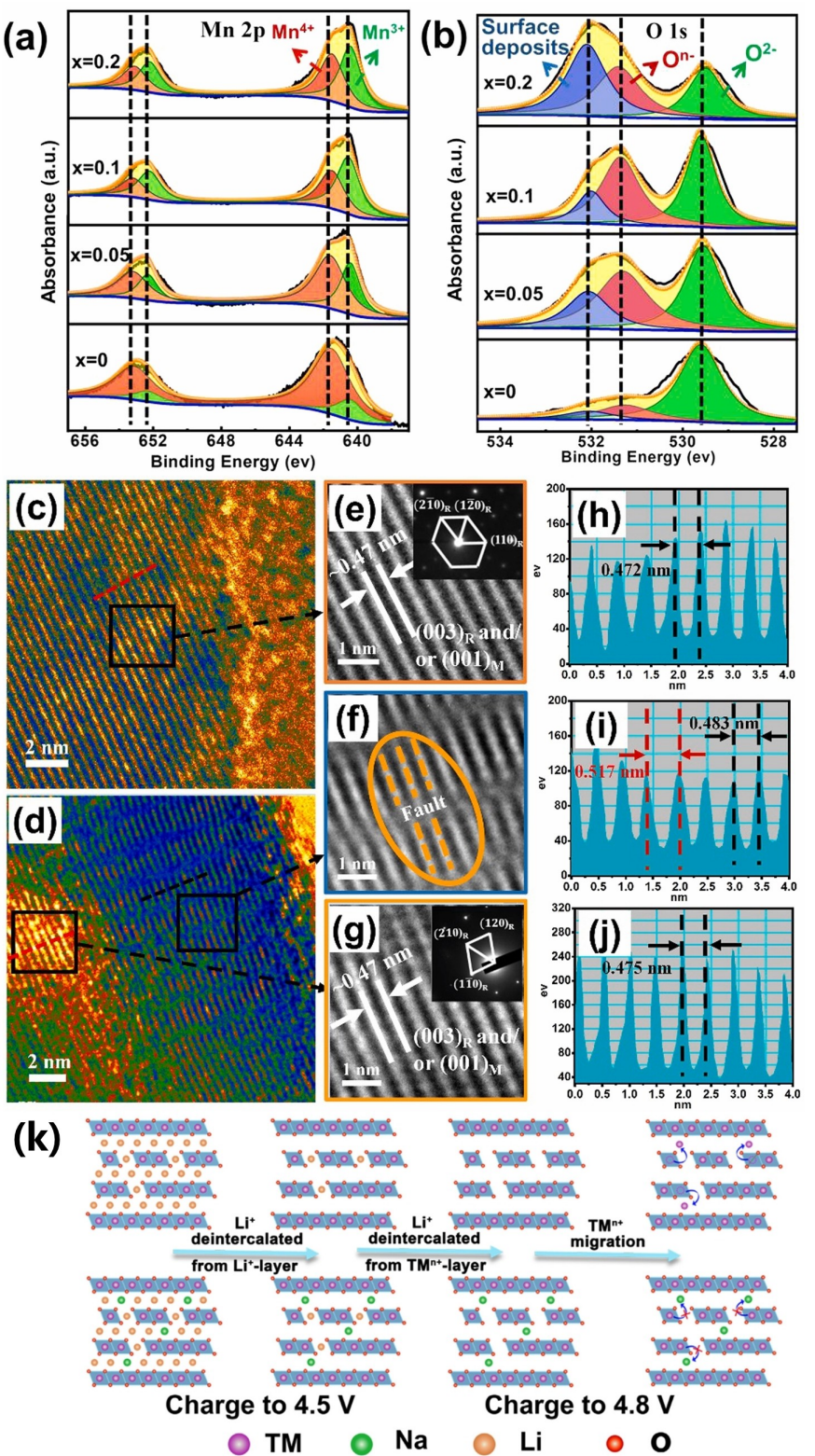


Figure 6. XPS spectra of (a) Mn 2p and (b) O 1s for the $\text{Li}_{1.2-x}\text{Na}_x\text{Mn}_{0.56}\text{Ni}_{0.16}\text{Co}_{0.08}\text{O}_2$ ($x = 0, 0.05, 0.1$ and 0.2) samples. Reproduced with permission.^[147] Copyright 2020, Elsevier. Morphology and lattice structure of (c, e, h) LLMO and (d, f, g, i, j) Na0.1-LLMO. (c, d) HRTEM and SAED images, (e-g) fast Fourier transform (FFT) and (h-j) corresponding line profiles of the Z-contrast information with the measured spacing of TM layers. Reproduced with permission.^[147] Copyright 2020, Elsevier. (k) The schematic diagram of the structure evolution during the delithiation process. Reproduced with permission.^[148] Copyright 2020, Elsevier.

the dissolution and phase transition of TM^{n+} (Figure 6k). Na^+ doping also promotes the diffusion of Li^+ and improves the electronic and ionic conductivity of the material to produce "pinning effect" and "pillar effect". DFT calculations show that the migration barrier of surface Li^+ in Na^+ doped material was 500 meV, which is 70.5 meV lower than that of the original material. The decrease of the energy barrier is due to the incorporation of Na^+ with a larger radius into the lithium layer, which increases the interlayer spacing and promotes the migration of Li^+ during the cycle.^[148]

Like Na^+ , K^+ doping with larger ion radius can enlarge the Li layer spacing, which promotes the diffusion of Li^+ ions, and inhibits the transformation of the layered structure to spinel structure. Li et al. used $\alpha\text{-MnO}_2$ doped with K^+ ions as a raw material and doped K^+ in the tetrahedral gap of the lithium layer of the LRMO material.^[149] The initial specific capacity of K-doped LRMO material was up to 315 mAh g^{-1} , and the capacity retention rate was 89% after 100 cycles. Cheng et al. used the combination of polyvinyl alcohol (PVA) pyrolysis surface treatment and K^+ doping to prepare amorphous nano carbon coated and K^+ doped LRMO materials. The amorphous carbon nanolayer has good electrical conductivity.^[150] Ding et al. used Li^+/K^+ heat exchange reaction to construct K^+ doped and $\text{K}_{1-x}\text{Li}_x\text{F}$ coatings on LRMO surface. The 0.5 wt% KF modified LRMO material showed better cycle/rate performance and low voltage attenuation.^[151] Zheng et al. used KMnO_4 to replace part of Li_2CO_3 and the precursor to prepare K-doped LRMO cathodes by high temperature solid phase method. The ICE of the K-doped cathode is 87%, and after 100 cycles at 0.5 C, the capacity retention rate is 94%, the discharge capacity is 244 mAh g^{-1} , and the discharge capacity is 133 mAh g^{-1} at 10 C.^[152]

Mg^{2+} doping is also a good choice. Yi et al. utilized coprecipitation to synthesize a series of $\text{Li}_{1.17}\text{Ni}_{0.25-x}\text{Mn}_{0.58}\text{Mg}_x\text{O}_2$ ($x=0, 0.01, 0.02, 0.05$).^[153] It was observed that the majority of Mg^{2+} ions occupied the Li site (3a site), thereby stabilizing the crystal structure and inhibiting the migration of nickel ions to the lithium site. This resulted in a shorter Li^+ diffusion distance and improved the electrochemical activity of LRMO. Wang et al. used polymer pyrolysis to introduce Mg ions into the TM layer of LRMO crystals to replace Li ions. This inhibited the mixed arrangement of cations, thereby slowing the phase transition during the insertion and extraction of lithium ions, and stabilizing the crystal structure of the active material.^[154] In addition, the doping of Mg ions increases the lithium layer spacing, promotes the removal and insertion of Li^+ , and has better cycling performance at high current density.^[155] Choi et al. used an electrolyte containing the $\text{Mg}(\text{ClO}_4)_2$ additive to selectively insert Mg^{2+} into the Li site in LRMO by *in-situ* electrochemical method. The embedding amount of Mg^{2+} increased with the increase of Mn content in $\text{Li}[\text{Mn}_{1-x}\text{M}_x]\text{O}_2$ ($\text{M}=\text{Co}$ and Ni). The thermodynamic favorable conditions of Mg^{2+} doped LRMO are illustrated by DFT calculation. Mg^{2+} ions at the Li site inhibited the mixing of cations and improved the capacity retention rate.^[141] Huang et al. found that Mg^{2+} was doped into the Li site of the Li layer, replacing part of the $\text{Li}-\text{O}-\text{Li}$ structure with a strong $\text{Li}-\text{O}-\text{Mg}$ structure. Mg-doped

LRMO has stable lattice structure and high reversibility of anionic REDOX reaction. DFT calculations demonstrated that Mg-doped LRMO has a lower O2p band top of about 0.81 eV, indicating a more stable lattice oxygen structure.^[156]

The researchers found that high-priced elements can also be doped in the lithium layer, which can significantly improve the voltage drop and circulation problems. Feng et al. directly synthesized Ti^{4+} doped LRMO materials using the sol-gel method. Through DFT calculation, it was found that although Ti^{4+} doping could not inhibit the transition from layered structure to spinel phase, it could stabilize the spinel-like phase structure, improve the material's electronic conductivity, Li^+ diffusion rate, Mn migration activation energy and enhance Ti–O bond.^[157]

4.1.2. TM Layer Doping

During the cycle, the TM in the Li_2MnO_3 phase undergoes a transition to the lithium layer. This transition causes a change in the material structure from layered to either a spinel or rock salt phase structure. This change in structure has a significant impact on the stability and electrochemical performance of the positive electrode material. Therefore, the research on cationic doping mainly focuses on the transition metal position doping to enhance the binding strength of TM and oxygen. When doped cations replace transition metal ions in the transition metal layer, it is particularly important to select metal elements with stronger bonds to oxygen than $\text{Ni}-\text{O}$, $\text{Co}-\text{O}$, or $\text{Mn}-\text{O}$ bonds.^[158] The common cations, such as Al ,^[159] Ti ,^[160] Cr ,^[161] Fe ,^[162] and Co ,^[163] ions tend to occupy the octahedral position of the TM site, thus forming a stronger TM–O bond, increasing the TM transition energy barrier, and inhibiting irreversible oxygen release (Figure 7a).

For example, Li et al. reported that Al doped in $\text{Li}[\text{Li}_{1/4}\text{Mn}_{1/2}\text{Ni}_{1/6}\text{Al}_{1/12}]\text{O}_2$ occupies the position of Mn in the $\text{Li}@\text{Mn}_6$ superstructure unit.^[159e] The partial transformation of the $\text{Li}@\text{Mn}_6$ superstructure in the transition metal layer to $(\text{Li}/\text{Ni})@(\text{Mn}/\text{Al}/\text{Li})_6$ leads to the antisite of Li/Ni in the transition metal layer. It inhibits the layered/spinel transition of the material during cycling, and these motifs can also partially destroy the polymerized $\text{Li}-\text{O}-\text{Li}$ structure and make the oxygen redox more reversible (Figure 7b). The capacity retention of the modified electrode was 91.4% after 500 cycles at 1 C. The Cr ion doped LRMO can reduce the oxygen release and limit the migration of TM into the Li layer, which reduces the discharge voltage attenuation in LRMO.^[161a] It also demonstrates reversible migration between octahedral and tetrahedral sites, indicating enhanced structural stability.^[164]

Fe doping can also play a similar role. Fe-doped LRMO has a stronger 3d Fe–O 2p covalent bond, which can alleviate oxygen release and improve the structural stability of LRMO. Currently, researchers have synthesized Fe-doped LRMOs such as $\text{Li}_{1.2}\text{Ni}_{0.13}\text{Mn}_{0.54}\text{Co}_{0.08}\text{Fe}_{0.05}\text{O}_2$,^[162a] $\text{Li}_{1.24}\text{Mn}_{0.60}\text{Ni}_{0.14}\text{Fe}_{0.02}\text{O}_2$,^[162b] $\text{Li}_{1.2}\text{Ni}_{0.13}\text{Co}_{0.13}\text{Mn}_{0.49}\text{Fe}_{0.05}\text{O}_2$,^[165] and $\text{Li}_{1.2}\text{Mn}_{0.54}\text{Ni}_{0.13}\text{Co}_{0.12}\text{Fe}_{0.01}\text{O}_2$.^[162d] For example, Hu et al. introduced Fe into the LRMO cathode material to induce a higher

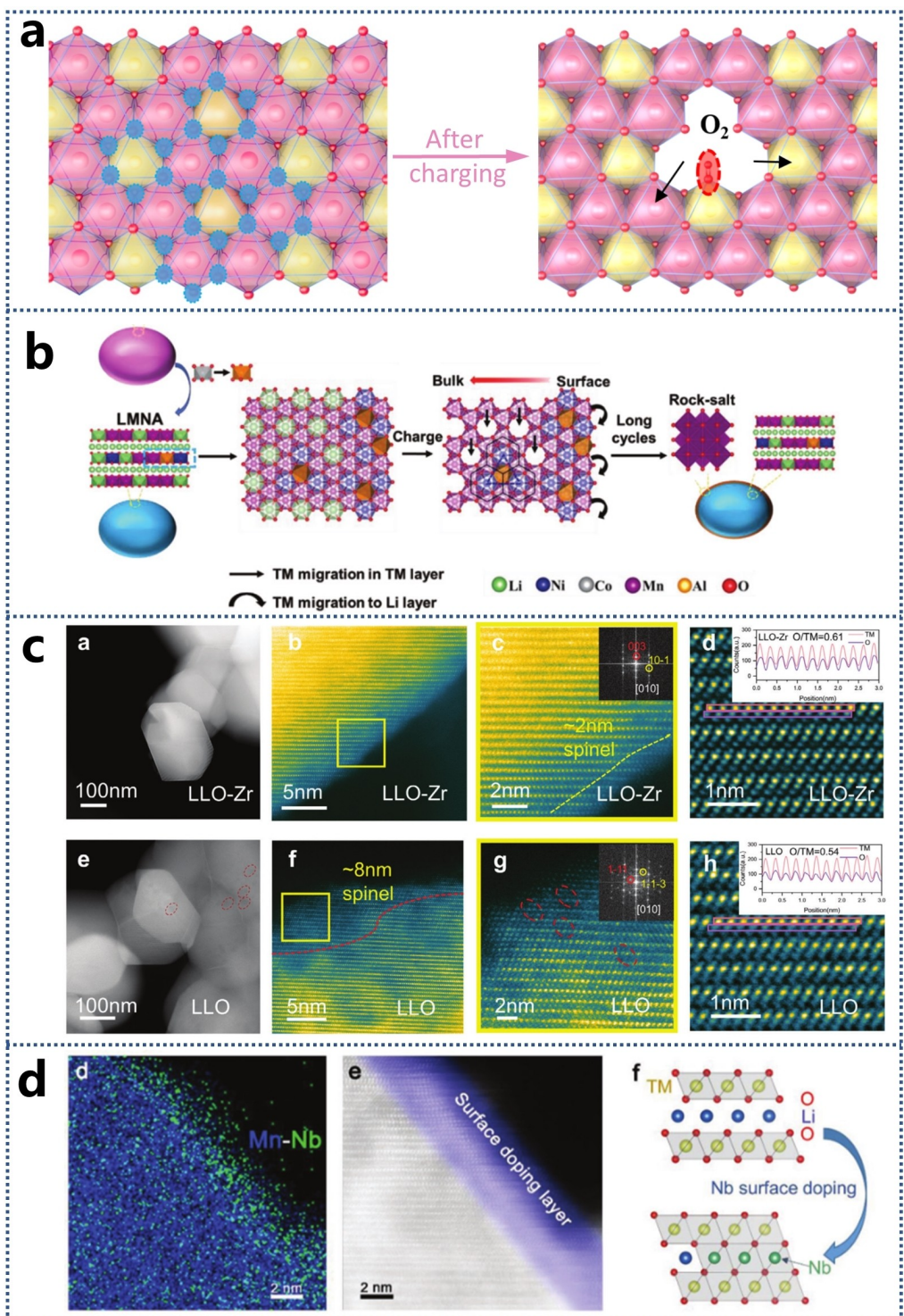


Figure 7. (a) Initial state and after charging state of the honeycomb superstructure within the transition metal layer. In this case, red represents O, pink represents Mn and yellow represents Li. Reproduced with permission.^[159] Copyright 2023, Elsevier. (b) The enhanced structural stability for LMNA by Al substitution. Reproduced with permission.^[159e] Copyright 2021, Wiley-VCH. (c) Structural degradation of the cycled Zr doped LRMO sample. HAADF-STEM, and iDPC images of LRMO being cycled for 100 cycles. Reproduced with permission.^[166] Copyright 2024, Wiley-VCH. (d) The EDS mapping and HAADF images of the LRMO–Nb sample, the schematic process of surface doping and the Nb-enhanced surface structure. Reproduced with permission.^[167] Copyright 2018, Wiley-VCH.

redox potential. Due to the 3d metal Fe-driven reduction coupling mechanism, the oxygen ions undergo reversible oxidation to peroxide-like transition, stabilizing oxygen holes

and inhibiting the release of oxygen.^[162c] In addition, the modified material exhibited a good discharge specific capacity of 307 mAh g^{-1} at 0.1 C ($1 \text{ C} = 250 \text{ mA g}^{-1}$), and the first charge-

discharge efficiency was 82.09%. The cobalt-containing spinel phase has a 3D lithium-ion diffusion channel, and metal Co doping can also improve the electronic conductivity of the material. Liu et al. constructed a spinel phase and surface cobalt gradient doping on the surface of $\text{Li}_{1.2}\text{Ni}_{0.2}\text{Mn}_{0.6}\text{O}_2$ microspheres. The surface modification of $\text{Li}_{1.2}\text{Ni}_{0.2}\text{Mn}_{0.6}\text{O}_2$ inhibits the irreversible phase transition from layered to spinel or rock salt structure, promotes the diffusion of Li^+ , and improves the surface stability of the active material.^[163a]

Metal elements with 4d and 5d atomic orbitals pose challenges in terms of migration due to their large ionic radius. However, this characteristic can be utilized to enhance the structural stability of transition metal layers. Examples of such elements include Nb,^[168] Y,^[169] Zr,^[166,170] Ru,^[166,170–171] Sn,^[166,170–172] Sb,^[173] Ta,^[10,174] W,^[175] V,^[176] Mo,^[177] and Te.^[178] For example, the addition of an appropriate amount of Y element can inhibit the release of O_2 during the initial charge of LRMO. Y doping can also reduce the electrochemical polarization and charge transfer resistance of Li_2MnO_3 and $\text{LiNi}_{1/2}\text{Mn}_{1/2}\text{O}_2$ components, while enhancing the diffusion ability of Li^+ .^[169a] Wang et al. incorporated Zr⁴⁺ into LRMO to adjust the local electronic structure and inhibit the diffusion of oxygen anions to the surface during cycling.^[166] Theoretical calculations indicate that the formation energy of oxygen vacancies is increased due to the strong covalent bonding between Zr–O, thereby inhibiting the loss of lattice oxygen at high voltage. In the LRMO–Zr sample subjected to 100 cycles, the particles remained intact with minimal cracks or voids, and the layered structure remained stable, except for a thin spinel structure ($\approx 2 \text{ nm}$) on the surface (Figure 7c). Conversely, the LRMO sample exhibited a significant number of intragranular voids and a thick layer of spinel and rock salt structure ($\approx 8 \text{ nm}$). The iDPC comparison of LRMO–Zr and LRMO samples after cycling showed that many oxygen vacancies were formed in pure LRMO, and the O/TM intensity ratio decreased from ≈ 0.64 to ≈ 0.54 , indicating that a large amount of oxygen was lost during the cycling process. For LRMO–Zr, the strength ratio changes little after cycling, indicating that Zr doping greatly enhances the stability of lattice oxygen.

Liu et al. reported that Nb⁵⁺ is doped in the lithium layer on the surface of the LRMO material, and the generated Nb–O bond energy is strong, which makes the surface oxygen of the material partially “inactivated” and improves the structural stability of the material (Figure 7d).^[167, 168d, e] The redox reaction of oxygen ions inside the material is reversible. The doped material exhibits a high initial capacity (320 mAh g^{-1}), and the capacity retention rate is still 94.5% after 100 cycles, with an average discharge voltage drop is only 136 mV .^[167] Dong et al. synthesized the original and Nb-doped LRMO cathode materials by solvothermal and high-temperature solid-state methods.^[168a] DFT calculations show that the strong Nb–O bond and the small Li-ion migration barrier can effectively stabilize the structure of the material and promote the diffusion of Li^+ after Nb doping. Fan et al. simultaneously doped Ru at the octahedral sites of the hexagonal and monoclinic phases of the LRMO material, realizing the regulation of the lattice oxygen of the cobalt-free LRMOs, improving the stability of the structure, and

obtaining a very low voltage decay ($< 0.45 \text{ mV cycle}^{-1}$). The doped LRMO material has a median voltage retention rate of 93.9% after 500 cycles at 1 C.^[171a] Qiao et al. reported the substitution of Sn⁴⁺ for Mn⁴⁺ in LRMO materials.^[179] The appropriate amount of Sn⁴⁺ inhibits cation mixing and enhances the ordered layer structure. As the amount of Sn⁴⁺ increases, the covalent of metal oxygen (M–O) decreases gradually. Sn⁴⁺ also inhibits the oxidation of O^{2-} ions to O_2 , resulting in minimal changes to the crystal structure.

The structure of the Li_2MnO_3 -like phase in the LRMO material was modified by trace Sb doping, which accelerated the diffusion kinetics of Li^+ and enhanced the stability of lattice oxygen.^[173b] DFT calculations indicate that trace Sb will preferentially and mainly enter the Li_2MnO_3 -like phase for doping modification. The Li–O bond in the Li_2MnO_3 phase is increased by about 0.0101 \AA , while the Mn–O bond is shortened by about 0.0033 \AA . Sb doping reduces the band gap between the valence band top and the conduction band bottom in the Li_2MnO_3 phase, and reduces the band top of its non-bonding orbital O 2p, thereby improving the electronic conductivity of the LRMO cathode material and the reversibility of the anionic oxygen redox reaction, which helps to improve the rate performance and cycle stability of the material. A gradient Ta⁵⁺ doped $\text{Li}_{1.2099}\text{Mn}_{0.5374}\text{Co}_{0.1268}\text{Ni}_{0.1257}\text{Ta}_{0.0036}\text{O}_2$ cathode with tunable electron and crystal surface structure was prepared.^[10] DFT calculations confirm that Ta⁵⁺ doping at transition metal sites increases the formation energy of oxygen vacancies on the surface of LRMOs, and the band gap in the density of states becomes narrower with better electronic conductivity. Therefore, the capacity retention rate of $\text{Li}_{1.2099}\text{Mn}_{0.5374}\text{Co}_{0.1268}\text{Ni}_{0.1257}\text{Ta}_{0.0036}\text{O}_2$ cathode material is 95% after 200 cycles at 1 C, and the discharge specific capacity is 155 mAh g^{-1} at 5 C. Meng et al. synthesized LRMO doped with W surface.^[175b] The introduction of high valence W reduced the valence state of TM, reduced the activity of surface lattice oxygen, shortened the length of the 4.5 V platform, and inhibited oxygen release. In addition, the strong bonding caused by the hybridization of W(f) and O(p) leads to the change of local electronic structure and stabilizes the LRMO lattice. Ion bulk doping can effectively inhibit the irreversible oxygen redox reaction on the surface of the material by changing the binding ability between transition metal cations and oxygen anions, and reduce the occurrence of phase transition induced by transition metal ion migration.

4.2. Anion Single Doping

In the case of high voltage, the oxygen ions in the LRMO material undergo oxidation and provide electrons to balance the imbalance of charge. It is difficult for oxygen ions to return to the lattice, resulting in the loss of discharge specific capacity and interfacial oxygen evolution, which will affect the safety performance, cycle stability and coulombic efficiency of the cathode material. Therefore, researchers have proposed anion doping strategies. Replacing the oxygen ions in the cathode material with anions can effectively inhibit the formation of

surface oxygen vacancies, improve the stability of the crystal structure, and improve its electrochemical performance. Among the anion doping experiments reported, the most common method is to replace oxygen with elements such as F, Cl, or S. F doping is currently the most effective among these elements due to the greater electronegativity and smaller ion size of F ions, which improves battery performance.^[180] F ions have a lower highest occupied molecular orbital than O²⁻, resulting in stronger ionicity between the transition metal and F ions. This inhibits the release of oxygen and improves the structural stability of the material.^[181]

Seaby et al. conducted a review on the effects of F doping on the activation, initial capacity, cycle stability, and rate performance of LRMO materials in recent years.^[182] It was found that F doping has a positive effect on cycle stability and rate

performance, but has both positive and negative effects on capacity. A very small amount of F (0.0050–0.0125 mol %) can simultaneously improve the capacity of 10%, cycle stability of 40–60% and rate performance of 10–20%. Song et al. found that the doping of F ions in LRMO promoted the reduction of Co³⁺ and Mn⁴⁺ ions in the cathode material.^[183] Zhang et al. reported that the substitution of F⁻ for O²⁻ causes a charge change, leading to the reduction of Mn⁴⁺ to Mn³⁺. This reduction is beneficial for the construction of 3D Li⁺ diffusion channels and the reduction of lattice stress.^[184] In addition, Li⁺ is coupled with doped F atoms at the lattice interface, and migrates to the Ni-rich R̄3m lattice site with lower migration energy, which improves the diffusion rate of Li⁺ (Figure 8a). F doping can form a more stable CEI layer on the surface of the LRMO electrode to increase the Li⁺ diffusion rate, reduce the

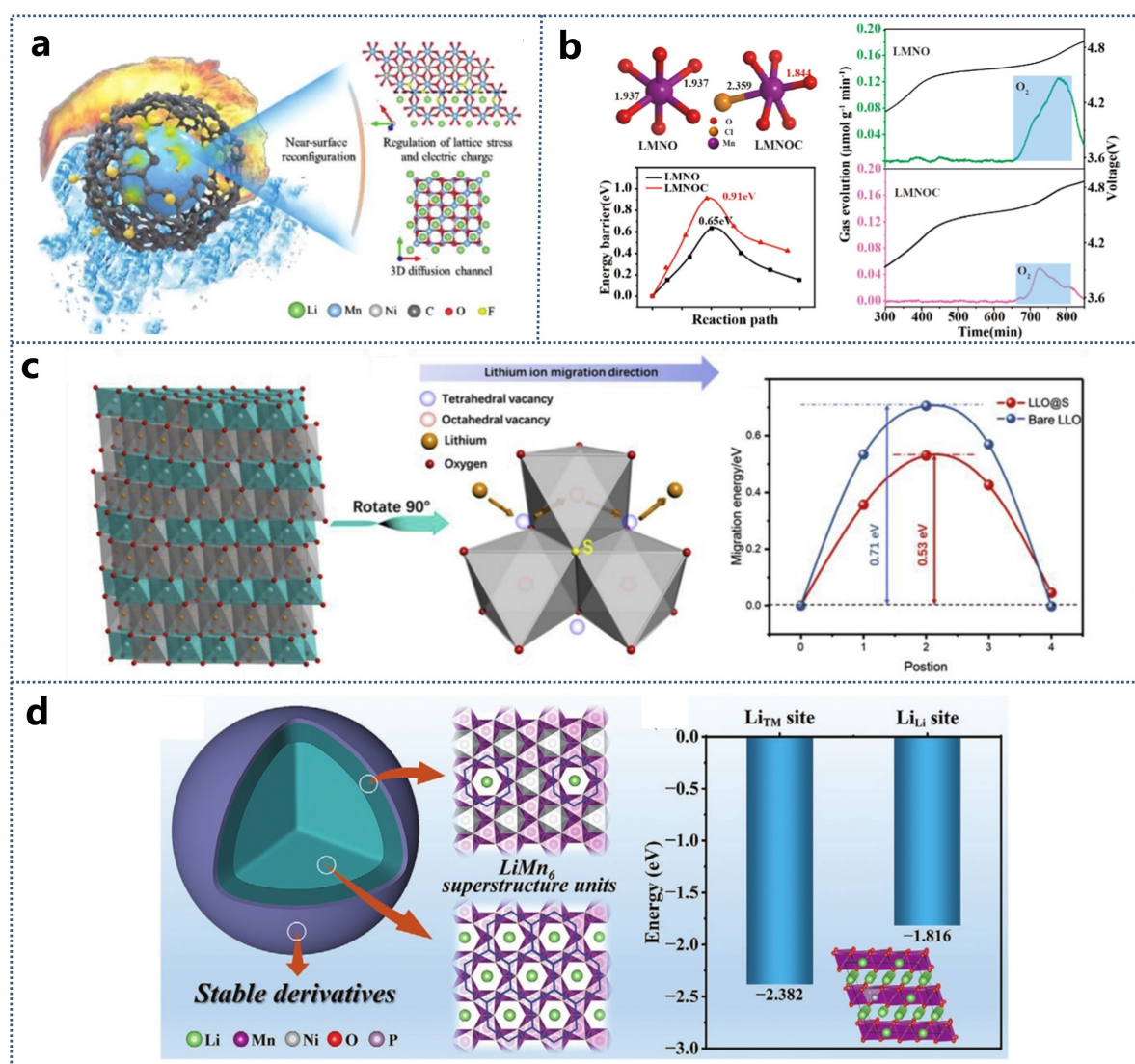


Figure 8. (a) Schematic of the near-surface reconfiguration by fluorinating graphene. Reproduced with permission.^[184] Copyright 2023, Wiley-VCH. (b) In Cl-doped LRMO ($\text{Li}_{1.2}\text{Mn}_{0.53}\text{Ni}_{0.27}\text{O}_{1.976}\text{Cl}_{0.024}$), Cl doping can suppress oxygen release and increase the TM-ion migration energy in the lattice of layered oxides. Reproduced with permission.^[186] Copyright 2021, American Chemical Society. (c) The schematic diagram of the lithium-ion migration path in the lattice of LRMOs and the migration energy barrier from the octahedral site to another one based on the first principle calculations. Reproduced with permission.^[188] Copyright 2019, Elsevier. (d) Schematic diagram of the LRMOs with a surface of diluted LiMn₆ superstructure units and the occupation energy of doped Ni at different Li vacancies. Reproduced with permission.^[191] Copyright 2023, Wiley-VCH.

dissolution of transition metals and stabilize the interface resistance. The CEI layer can also inhibit oxygen evolution, alleviate the transformation of the layered structure to the spinel structure, reduce the voltage drop during the cycle, and improve the cycle performance.^[185]

In the Cl-doped LRMO material structure, Cl ions not only enhance the redox reversibility of oxygen, but also inhibit the migration of transition metals during the cycle (Figure 8b).^[186] DFT calculations have demonstrated that the regulation mechanism of Cl-doping on the redox potential and redox process in LRMOs. The doping of Cl increases the TM–O bond spacing, reduces the band gap of the cathode material, effectively reduces the charging potential, and improves the stability of the structure and cycle.^[187] Sun et al. also used the gaseous sulfur treatment method to replace part of the O on the surface of the LRMO lattice with S. S ions reduce the oxygen partial pressure of LRMO and increase the lithium-ion conductivity, which is beneficial to stabilize the crystal structure of the material (Figure 8c).^[188] Theoretical calculations have shown that the energy required for the S-doped LRMO material to deintercalate and embed Li⁺ is –1132.14 and –1122.78 eV, respectively, and the energy is almost the same. Li⁺ shuttles reversibly in the S-doped LRMO material, so it has an ultra-high ICE.^[189] In the Se-doped LRMO cathode material, the presence of Se induces the electron localization effect, effectively reducing the energy of the O2p state, increasing the formation energy of oxygen vacancies, and consequently significantly reducing the loss of lattice oxygen.^[190]

Watanabe et al. found that the charge compensation in N-doped LRMO materials occurs through Mn oxidation and hole formation on the O 2p orbital.^[192] The introduction of P⁵⁺ doping increases the plane spacing of the LRMO material (003) crystal to 0.488 nm, which has resulting in higher Li⁺ conductivity. DFT calculations show that P ions make it easier for excited electrons to transfer from the valence band to the conduction band, and P can form strong covalent bonds, which helps to stabilize the structure of LRMO materials.^[193] Yin et al. doped B in H₃BO₃ on the surface of LRMO material by molten salt method, and formed a thin and stable B–O bond enhancement layer on the surface,^[194] which reduced oxygen release and did not affect the oxidation and reduction of oxygen in the bulk phase, and enhanced structural stability. The modified cathode materials have excellent electrochemical performance.^[195] Li et al. introduced the non-metallic element B into the bulk phase of the LRMO material, so that the material formed a defective electronic structure, dispersed the electrons of oxygen, and reduced the covalent bond of TM–O.^[196] Due to the stronger B–O bond energy, the combined effect of the two inhibits oxygen loss and TM migration.^[197] B ion doping can change the electronic structure and crystal structure stability of the material by adjusting the TM–O bond, but it is difficult to control and achieve uniformity, and the resulting local ligands are difficult to comprehensively improve the material properties.^[198]

In addition to the single-element anion doping described above, the polyanion group has a strong covalent bond with TM to form a polyhedral structure, so it is often used to stabilize

the layered structure and prevent the migration of TM during the cycle, making the layered structure more stable.^[199] At present, the reported polyanions include BO₃^{3–}, PO₄^{3–} and SiO₄^{3–}. Li et al. successfully doped boron polyanion into the cathode material. Due to the doping of boron polyanion, the TM–O covalent bond energy and O2p bond energy in the material change, and the stability of the material is improved. Due to the strong polarization effect of oxygen atoms on boron polyanion, the redox potential increased significantly.^[200] Ma et al. found that the doping of boron polyanion inhibits the attenuation of cyclic voltage, and it is easy to form an antistatic nanolayer on the surface, which hinders the formation of lithium-ion vacancies, protects the lithium-ion diffusion channel during the cycle, improves the capacity and rate performance of the cathode material, and inhibits the phase transition of layered spinel and eliminates the amorphous phase.^[201]

The large tetrahedral PO₄^{3–} ions with high electronegativity were doped into LRMO to moderately change its local environment. Due to the strong combination of PO₄^{3–} polyanion and transition metal cations (especially Ni), the Ni content in the Li layer decreased significantly from 14.4% to 1.2%.^[199] By using the strong interaction between PO₄^{3–} and Ni, Ni is confined in the Li vacancy of the super-structural unit LiMn₆, and the LRMO cathode material with a diluted super-structural unit surface and a derived interfacial protective layer is obtained (Figure 8d).^[191] The doping of polyanion PO₄^{3–} on the surface of LRMO cathode material was realized by adding NH₄H₂PO₄ and LiOH to the LRMO precursor at the same time. The doping of PO₄^{3–} polyanion stabilizes the surrounding reactive oxygen species and protects the LRMO electrode from electrolyte corrosion during the cycle.^[202] SiO₄^{4–} and SO₄^{2–} can increase the binding energy of transition metal cations and hydrogen ions, and stabilize the crystal structure of LRMO.^[203]

4.3. Multi-Ion Doping

Compared with single doping in which only cations or anions are doped, multi-element co-doping can combine the advantages of different anions and cations to better improve the electrochemical properties of LRMO. Multi-ion doping can be divided into multi-cation doping and anion-cation co-doping.

4.3.1. Multiple Cations Co-Doping

There are many researchers who focus on multiple cation co-doping. In Al/Ti co-doped LRMO materials, the strong Al–O bond plays a role in stabilizing the structure and improving the cyclic properties of LRMO, and the layer expansion effect caused by Ti doping can compensate for the rate performance attenuation caused by Al doping. Al/Ti co-doping inhibited the irreversible evolution of LRMOs and oxygen loss and promoted the diffusion rate of Li⁺. The capacity retention rate of the co-doped LRMO material was 89.7% after 500 cycles at 1 C, and the voltage attenuation per cycle was only 0.34 mV.^[204]

The co-doping of Mg/Al and Na/Mg ions into the TM layer of the LRMO material helps to expand the lithium layer spacing, reduce the potential barrier of Li^+ during the insertion and extraction process, and improve the rate capability.^[205] At the same time, the co-doped elements not only inhibit the formation of oxygen vacancies but also reduce the mixing of cations, thus hindering the transformation of the layered phase to the spinel phase during the cycle. Both Na^+ and W^{6+} cations are introduced into the LRMO lattice. Na^+ occupies the original Li site, and W^{6+} replaces some transition metal ions.^[206] DFT calculations show that the incorporation of W^{6+} reduces the energy band gap of LRMO and improves the electronic conductivity of the cathode powder. The introduction of Na^+ increases the interlayer spacing of Li, which promotes the diffusion of Li^+ in the interlayer. The use of Na^+ and Mo^{6+} to replace part of Li^+ and TM ions in the LRMO cathode also has similar electrochemical performance results.^[207]

It is found that Nd/Al ions selectively replace the Ni/Mn atoms in LRMO and pre-constructed heteroepitaxial interfaces, thereby regulating the activity of Ni ions and inhibiting the phase transition and dissolution of Mn ions.^[208] In Sn and Na ions co-doped LRMO cathode materials, Na^+ prevents the formation of impurity Li_2SnO_3 , the steric effect of Sn enhances the electrochemical stability, inhibits the voltage decay, and increases the energy barrier of Mn migration.^[209] Yang et al. found that Ta^{5+} and Mo^{6+} occupied Li sites and transition metal sites in LRMO materials, respectively, which helped to increase the concentration of Mn^{3+} and inhibit Li/Ni mixing and oxygen production. The strong bond energy of Ta–O and Mo–O can help to maintain the crystal structure and inhibit the erosion of the electrolyte during the cycle.^[10,210] In the Zn/Ti co-doped LMT material, the Ti content gradually increases from the surface to the bulk phase, while the Zn content gradually decreases. Ti doping forms a strong Ti–O bond, inhibits oxygen release, and ensures structural stability. The Zn in the Li layer acts as a pillar and blocks the migration path of TM, thereby inhibiting the migration and dissolution of TM. The enrichment of Zn/Ti on the surface leads to the site of the Li layer being occupied by doping elements, which makes the surface of Zn/Ti co-doped LRMO material form a cationic disordered interface layer, inhibits the migration of TM, and stabilizes the crystal structure. The stronger TM–O binding energy can inhibit the release of oxygen.^[211]

4.3.2. Anion-Cation Co-Doping

Cationic and anion doping involve the use of metal cations and anions for doping, using metal cations to improve the electronic conductance of materials, and using anion doping to improve the structural stability of materials. For example, Lee et al. used Nb^{5+} and F^- to replace Mn^{4+} and O^{2-} in the LRMO structure, respectively.^[212] It was found that Nb^{5+} and F^- inhibited TM migration and oxygen release induced structural transformation, respectively. Doped ions with larger radii increase the transfer rate of ions and electrons.^[213] Guo et al. obtained Al/F co-doped $\text{Li}_{1.2}\text{Ni}_{0.13}\text{Co}_{0.13-x}\text{Mn}_{0.54}\text{Al}_x\text{O}_{2(1-y)}\text{F}_{2y}$ cathode material. Al

and F doping can effectively alleviate the phase transition from LRMO to spinel and inhibit the capacity decay and voltage decay of the electrode material.^[214]

Zheng et al. introduced additional Ni–O, Na–O, and TM–F bonds through Na^+/F^- ion co-doping and appropriate increase of $\text{Li}^+/\text{Ni}^{2+}$ mixing, which can effectively adjust the TM 3d-O 2p band and non-bonded O-2p band to move toward the low energy level. This energy band shift increases the formation energy of oxygen vacancies in the material, stabilizes the lattice oxygen, and inhibits the phase transition of layered spinel.^[215] The increase of Li–O bond in LRMO crystal by Fe and F co-doping is much greater than the sum of Li–O bond increments by their respective doping, which is very beneficial to the performance. The incorporation of Fe ions effectively activates the redox reaction of TM and improves their electron and ion conduction. F ions effectively inhibit the escape of lattice oxygen, thereby improving the cycle stability.^[216] The doping of Fe and Cl enlarges the lithium layer spacing in the LRMO lattice, promotes the diffusion of lithium ions, enhances the binding energy between anions and cations, and reduces the irreversible oxygen release, which is beneficial to improving the first coulombic efficiency of the material, slowing down the voltage decay, and enhancing the cycle stability of the electrode.^[217]

If the anions in the mixed doping are replaced by polyanion groups, the stability of the structure can be further improved. For example, the introduction of Al^{3+} and $\text{BO}_3^{3-}/\text{BO}_4^{5-}$ into the LRMO positive electrode material enables two-bit occupancy and charge regulation of the structure. Al^{3+} and $\text{BO}_3^{3-}/\text{BO}_4^{5-}$ can not only effectively inhibit the loss of oxygen but also stabilize the layered structure. DFT calculations suggest adding a strong electron-withdrawing group ($\text{BO}_3^{3-}/(\text{BO}_4)^{5-}$) and Al^{3+} electron hole can not only improve the problem of poor Li_2MnO_3 electronic conductivity, but also can reduce the REDOX potential of Mn and O.^[218] In the co-doped LRMO cathode materials of K^+ and PO_4^{3-} , the doping of K^+ stabilizes the lithium layer spacing and facilitates the diffusion of Li^+ , thereby improving the cycling and rate performance. The doping of PO_4^{3-} changes the electronic structure of the material, weakens the covalency of TM–O, and reduces the irreversible loss of lattice oxygen, and stabilizes the structure.^[219] A stable oxygen-filled framework was constructed inside the LRMO crystal under the coordination of Fe^{3+} and PO_4^{3-} , which reduced the lattice distortion and cation mixing.^[220]

5. Coating and Doping

Previously, we have introduced various methods of surface coating and bulk ion doping. They have their own advantages and disadvantages. In theory, if surface coating and ion doping can be used for LRMO material modification at the same time, dual effects can be achieved. Many researchers have used the synergistic effect of doping and surface coating to not only inhibit the phase transition of the structure, but also reduce unnecessary side reactions on the electrode surface. For example, to obtain LRMO cathode materials with excellent electrochemical properties, the researchers combined Li_2ZrO_3

coating and Zr⁴⁺ doping to synergistically modify LRMO. The Li₂ZrO₃ coating can protect the LRMO material from hydrogen fluoride corrosion, and Zr⁴⁺ is doped into the structure of LRMO to form a highly stable structure at high temperature. The formation of Li₂ZrO₃ captures the inactive residual lithium on the surface, thereby reducing the electrochemically inactive residual lithium content and Li/TM ratio on the surface of the matrix material, and promoting the first cycle coulombic efficiency. The Li⁺ conductive Li₂ZrO₃ coating reduces the surface side reactions, inhibits the dissolution of transition metals, and improves the conductivity of lithium ions.^[221] Zr⁴⁺ doping into the LRMO structure enlarges the interplanar spacing and reduces the mixing of Li/Ni, which is beneficial to the diffusion of Li⁺. The synergistic effect of Li₂ZrO₃ coating and Zr⁴⁺ doping improves the stability of the layered structure. The co-modified LRMO cathode has higher rate performance and cycle stability.^[96c,d]

In Cr-doped and Li₃PO₄-coated LRMO, the doping of Cr stabilizes the layered structure and inhibits its transition to the spinel phase. The Li₃PO₄ coating limits the interfacial side reactions between the electrode and the electrolyte.^[222] In La-doped and CaF₂-coated LRMO materials, the CaF₂ coating inhibits the protection of the active material from electrolyte erosion. La—O has a higher binding energy than M—O, which is beneficial to stabilize the crystal structure of the LMRO material and inhibit the precipitation of oxygen in the lattice.^[223] Yu et al. found that doping Te⁶⁺ ions can induce partial Ni³⁺ ions in LRMO crystals to be reduced to Ni²⁺ ions, thereby improving the redox ability of TM ions and promoting the diffusion of Li⁺ ions. The Mg₃(PO₄)₂ component with a stable P=O bond can resist the erosion of acidic substances and inhibit the dissolution of TM ions into the electrolyte.^[224]

Wu et al. improved the electrochemical performance of LRMO materials by the synergistic effect of Cd doping and CdO coating. Doping Cd improves the electronic conductivity of LRMO and enhances the effect of the electrochemical potential. The nano-CdO particles prevent the active material from being corroded by the electrolyte, which is beneficial for improving the stability of LRMO during the cycle. Under the synergistic effect of these two modification strategies, the internal structure of LRMO crystal is changed, its surface and internal dynamics are enhanced, and the rate performance and cycle stability are improved. DFT calculation results show that Cd ions can inhibit the structural changes of LRMO cathode materials during charging and have a lower formation energy.^[225] Similar metal-doped, metal oxide-coated LRMO also has Ce doping and generates a LiCeO₂ coating with oxygen vacancies.^[226] Some researchers have also adopted the triple modification strategy of double cation doping and coating. For example, Qu et al. adopted LiVO₃ surface coating and Na, V double cation doping to improve the electrochemical performance of LRMO.^[106b] The surface coating of LiVO₃ prevents the occurrence of interfacial side reactions, promotes the diffusion kinetics of lithium ions between phases, and inhibits the irreversible O₂ release. In addition, Na and V double cation doping also helps to promote Li ion transfer and inhibit irreversible O₂ precipitation. Na ion doping with pillar effect expands the lattice space for faster Li

ion intercalation/deintercalation, and V ion doping further enhances the structural stability by forming stronger V—O bonds.

6. Single Crystallization

The most reported LRMO materials are polycrystalline (PC), which are formed by the agglomeration of primary particles. During charge and discharge cycling, the lattice constant of PC-LRMO undergoes significant changes, accompanied by the generation of stress and strain, resulting in the desorption of primary particles and the fragmentation of secondary spherical particles. The penetration of electrolyte along the crack will further cause severe activation and the accumulation of various side reactions, accelerating the degradation of the structure and electrochemical performance. The preparation of micron-sized "single crystal" LRMO (SC-LRMO) particles is one of the most effective strategies to solve the above problems. Due to its good integrity, less internal interface, good mechanical stability, and small specific surface area, SC-LRMO materials can inhibit the generation of cracks and the transformation from layered to spinel phase during long cycles, which is conducive to improving structural stability and capacity retention. It has been found that the single crystal morphology can inhibit the generation of microcracks and reduce the occurrence of side reactions due to its high mechanical strength and stable structure, thereby reducing the formation of new impedance layers, and the volume change of the material during the cycle is small (Figure 9b).^[227] It is expected to be used to solve the problems of oxygen loss and cycle performance of traditional polycrystalline LRMO materials.

Currently, there are three main methods for preparing single crystal materials, namely solid phase method, additive-assisted solid phase method and molten salt method. The solid phase method uses too high a temperature to disperse the aggregates, but this high temperature will cause serious loss of lithium. If the amount of lithium source is insufficient, lithium-rich materials cannot be formed. This method is difficult to control the amount of lithium source added. The molten salt method is a molten phase roasting method, which requires a large amount of molten salt compounds to form a molten phase during the roasting process to accelerate diffusion and mass transfer, and promote grain growth. The process flow is complex and must be washed and dried. The additive-assisted solid-phase method is to accelerate the diffusion of metal ions by adding additives after the lithium mixture is mixed, so that the particles grow to a certain extent and break the limitation of precursor agglomeration and disperse into a single particle, which effectively prevents the particles from agglomeration during the growth process. It is beneficial to the uniform growth of particles and obtain large particle materials with good dispersion and uniform size. This method can not only improve the dispersion of particles, but also adjust their crystal plane and morphology. At the same time, some additives can also be used as doping sources into the structure of LRMO

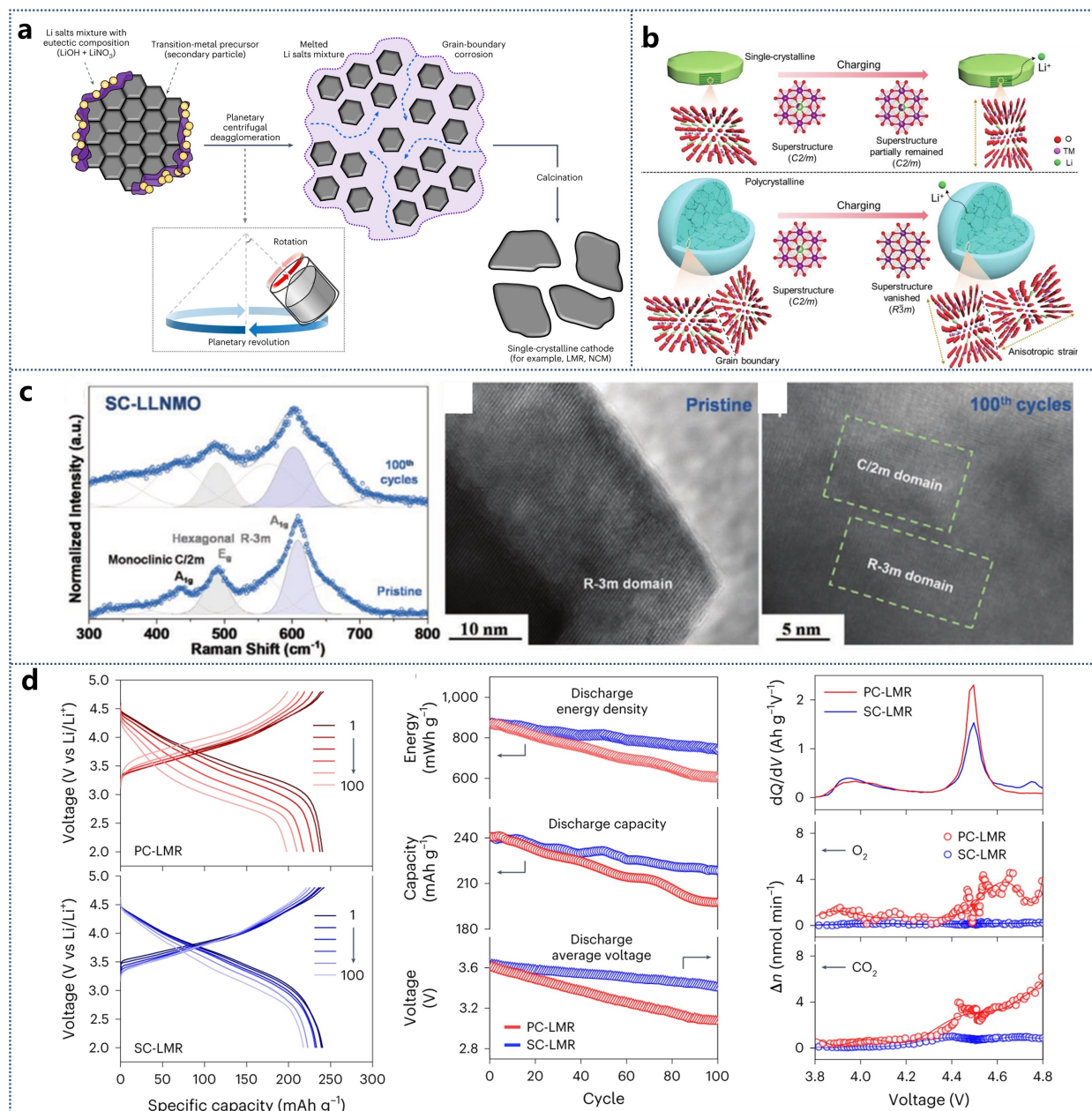


Figure 9. (a) Planetary centrifugal deagglomeration for single-crystalline cathode synthesis. Reproduced with permission.^[228] Copyright 2023, The Author(s). (b) Schematic diagram of the microstructural evolution of SC-LRMO and PC-LRMO cathodes during charging, showing a relatively low microstrain in the SC-LRMO cathode. Reproduced with permission.^[227] Copyright 2022, The Author(s). (c) The ex-situ Raman spectra and HR-TEM images of SC-LRMO electrode at the pristine state and after 100 cycles. Reproduced with permission.^[231] Copyright 2021, Wiley-VCH. (d) Voltage-capacity curves and cycling performance of PC-LRMO and SC-LRMO at 0.3 C. DEMS result of PC-LRMO and SC-LRMO during 1st cycle at 0.05 C. Reproduced with permission.^[228] Copyright 2023, The Author(s).

materials to improve the electrochemical performance of materials.

Yoon et al. proposed a new planetary centrifugal depolymerization process to prepare a micron-sized SC-LRMO cathode with excellent electrochemical performance and stability through a mechanochemical process under mild conditions (Figure 9a).^[228] The synthesized SC-LRMO can inhibit oxygen evolution, transition metal dissolution and voltage decay, showing excellent electrochemical performance. The initial discharge capacity of PC-LRMO is 254 mAh g^{-1} and the first cycle coulombic efficiency is 76.2% when cycled at 2.0–4.8 V

and 0.1 C. In contrast, the initial discharge capacity of SC-LRMO is 259 mAh g^{-1} , and the ICE is increased to 82.4%. After 100 cycles at 0.3 C, SC-LRMO has a more stable charge-discharge curve, higher capacity retention (90.6% for SC-LRMO and 82.1% for PC-LRMO), slower voltage decay ($2.28 \text{ mV cycle}^{-1}$ for SC-LRMO and $5.35 \text{ mV cycle}^{-1}$ for PC-LRMO) and higher discharge energy density retention (84.9% for SC-LRMO and 69.9% for PC-LRMO at 100 cycles) than PC-LRMO. GITT test showed that the voltage curve of SC-LRMO changed little before and after the cycle, indicating that the structure of SC-LRMO changed little. In-situ differential electrochemical mass spectrometry

(DEMS) showed that the amount of O₂ and CO₂ released from SC-LRMO was significantly inhibited compared to PC-LRMO. The decrease of gas precipitation is the result of the combined action of low specific surface area, single crystal lattice is not easy to break, and bulk oxygen loss is inhibited. Consistent with the DEMS results, the transition metal dissolution of SC-LRMO in high temperature cycles is also significantly lower than that of PC-LRMO (Figure 9d).

Liu et al. prepared micron-sized cobalt-free SC-LRMO cathode materials by molten salt method. The results show that the molten salts (LiNO₃ and H₃BO₃) with low melting point can be used as liquid phase medium at lower sintering temperature, which can improve the atomic mass transfer/heat transfer efficiency and single crystal nucleation/growth efficiency, and accelerate the formation of $\approx 1\text{ }\mu\text{m}$ SC-LRMOs with specific crystal orientation.^[229] Compared with PC-LRMO, SC-LRMO cathodes can effectively inhibit the structural degradation caused by lattice oxygen, alleviate the accumulation of anisotropic stress and strain during cycling, and reduce the interfacial side reactions, thereby obtaining excellent high-pressure stability and kinetic performance. It was found that SC-LRMO materials require a relatively strong electrochemical driving force to achieve oxygen activation. The SC-LRMO material can achieve a more stable oxygen redox reaction. The design of single crystal structure is beneficial to inhibit irreversible oxygen release and improve the structural stability and electrochemical performance during the cycle.^[230] Sun et al. found that SC-LRMO material can not only effectively inhibit oxygen evolution during the first cycle of oxygen activation, but also inhibit the layered/spinel phase transition during the cycle.^[231] The SC-LRMO cathode has a small volume change and a superlattice peak during the Li⁺ deintercalation process, which inhibits the generation of cracks and enhances the structural stability by using the oxygen redox reaction. The layered-spinel phase transition of SC-LRMO material during cycling can be effectively suppressed, and the spinel phase can hardly be observed after 100 charge-discharge cycles, which also proves that the single crystal morphology improves the structural stability and suppresses the voltage decay during long-term cycling (Figure 9c).

The obtained SC-LRMO nanosheets, with a thickness of $\approx 100\text{ nm}$, have a continuous internal lattice and no grain boundaries, which shortens the insertion/extraction path of Li⁺ and accelerates the electrode reaction kinetics process. The single crystal structure can also inhibit the irreversible phase transition from the layered phase to the spinel phase and the formation of internal cracks in the particles, and play a role in stabilising the layered structure.^[232] By comparing SC-LRMO materials with hexagonal flake, octahedral and long rod-like morphologies, it is found that Li⁺ prefers to migrate along the b-axis due to the lower activation barrier along the (010) plane. The large exposure of the (010) crystal plane is beneficial to the migration of Li⁺ and thus improves the rate performance of the material.^[233] Xie et al. found that the hexagonal SC-LRMO structure can improve the stability of surface oxidized oxygen ions and reduce the reduction of Mn⁴⁺ in single crystals.^[9]

The particle size and properties of SC-LRMO materials are also directly related. Compared with conventional polycrystalline secondary spherical particles, submicron-sized SC-LRMO materials and submicron-sized single crystal particles have excellent cycle performance, and there are no cracks on the surface of the particles after cycling.^[234] However, too large size will also affect the performance of the SC-LRMO materials. Recently, Zhang et al. synthesized an SC-LRMO cathode with a grain size of $\approx 3\text{ }\mu\text{m}$ by solid phase sintering. It is found that due to the increase of Li⁺ diffusion path and the aggravation of Li/Ni mixing, the Li⁺ diffusion efficiency of SC-LRMO cathode decreases, the structural stability deteriorates and the anion redox activity is inhibited, which eventually leads to the decrease of cycle performance and the aggravation of structural collapse.^[235] Surface coating and bulk doping are also effective for SC-LRMO materials. Liu et al. prepared SC-LRMO cathode materials by Na₂WO₄-assisted calcination and evaporation method. Na₂WO₄ promoted the growth of LRMO grains and uniformly wrapped on the surface of single crystal particles, protecting LRMOs from electrolyte corrosion. In addition, Na and W ions are doped into the lattice, which stabilizes the LRMO crystal structure and promotes the transport of Li⁺ ions. The obtained SC-LRMO has double modification effects of bulk doping and surface coating.^[236]

7. Summary and Outlook

Despite the LRMO cathodes exhibiting an actual capacity of $\approx 300\text{ mAh g}^{-1}$ and realizing various breakthroughs, their development status is still limited by some basic problems which are closely related to the activation of Li₂MnO₃ and the subsequent O release and evolution, as well as the corresponding atomic (TM/cation migration, mechanism evolution and valence reduction cation redox reaction) and macroscopic (pore formation behavior, surface cracking, and crushing) reactions. To solve these problems, this review summarizes the surface modification methods for LRMO cathode materials from the aspects of surface coating, ion doping, combined modification, and single crystal structure. At the same time, the mechanism of surface modifications on the improvement of electrochemical performance of LRMO cathodes is discussed and analyzed. The advantages and disadvantages of different modification methods of LRMO materials are summarized in Table 3.

- (1) Surface coating is the most widely used surface modification method for LRMO materials. It plays an important role in inhibiting the side reactions at the electrode/electrolyte interface, restraining the dissolution of TMs and the decomposition of the electrolyte. However, the coating layer formed on the surface of the LRMO cathode material by a solution chemical method combined with subsequent heat treatment often cannot fully guarantee the thickness, uniformity, and compactness, which affects the transfer of electrons/ions and the protective effect. Additionally, surface coating modification is hard to inhibit the phase transition of the LRMO cathode during cycling.

Table 3. Outline of various modified method for LRMO cathode materials with their advantages/disadvantages.

Modification method		Advantage	Disadvantage
Surface coating	Oxides	<ul style="list-style-type: none"> reduce the reactivity of the LRMO surface layer with HF. inhibit the side reactions. improve the cycle and thermal stability. 	<ul style="list-style-type: none"> hinder the charge transfer with excessive or dense coating. reduce the effective active mass.
	Metal phosphates	<ul style="list-style-type: none"> strong covalent interaction between metal ions and phosphate groups. effectively alleviates the interfacial reaction. stable SEI. improve the cycle stability. 	<ul style="list-style-type: none"> lacks electrochemical activity. reduces the capacity of the electrode.
	Metal fluorides	<ul style="list-style-type: none"> reduce the charge transfer resistance. improve the conductivity and crystal structure stability. improve the cycle stability. 	<ul style="list-style-type: none"> poor electronic conductivity instability at high temperature. high synthesis difficulty. poor reversibility of electrochemical reaction.
	Carbon	<ul style="list-style-type: none"> enhances the electronic conductivity. improves the rate performance. 	<ul style="list-style-type: none"> difficult to achieve uniform dispersion of carbon coating.
	Conductive polymers coating	<ul style="list-style-type: none"> block the cathode material and electrolyte. prevent the high valence metal cations and reactive oxygen species. inhibit the erosion of the cathode material by HF. improve the electronic conductivity. 	<ul style="list-style-type: none"> difficult to achieve uniform dispersion of conductive polymers coating. high cost.
	Lithium-ion conductive coating	<ul style="list-style-type: none"> provide a fast Li⁺ diffusion channel. reduce the polarization. improve the rate and cycle performance. 	<ul style="list-style-type: none"> difficult to achieve uniform dispersion of lithium-ion conductive coating.
	Lithium active material coating	<ul style="list-style-type: none"> alleviate the interfacial reaction. provide a fast Li⁺ diffusion channel. improve the rate and cycle performance. 	<ul style="list-style-type: none"> react with the electrolyte and consume part of Li⁺. low cycle retention rate.
Ionic doping	Cation single doping (Li Layer)	<ul style="list-style-type: none"> enlarges the interlayer spacing of the Li layer. faster Li⁺ transport speed. excellent rate performance. 	<ul style="list-style-type: none"> few available doped ions.
	Cation single doping (TM Layer)	<ul style="list-style-type: none"> reduce the polarization. reduce the charge transfer resistance. enhance the reversibility of lithium ion insertion and extraction. 	<ul style="list-style-type: none"> reduce the specific capacity. inhibitory effect on the corrosion of electrode.
	Anion single doping	<ul style="list-style-type: none"> inhibit the formation of surface oxygen vacancies. improve the stability of crystal structure. 	
	Multi-ion doping	<ul style="list-style-type: none"> expand the spacing of layered materials. inhibit Li/Ni mixing. increase Li⁺ diffusion rate. improve the rate performance. 	
Coating and doping		<ul style="list-style-type: none"> avoid the shortcomings of single surface modification method. 	<ul style="list-style-type: none"> complex process steps. unclear synergistic modification mechanism of more than two surface modification methods.
Single crystallization		<ul style="list-style-type: none"> inhibits the layered/spinel phase transition. inhibit oxygen release. 	<ul style="list-style-type: none"> high cost. complex process steps. low lithium ion diffusion rate.

(2) Ion doping can improve the structural stability and cycle stability of the cathode material of lithium ion battery, and increase the diffusion rate of Li⁺ ions, which is one of the effective ways to give the particles new physical and chemical properties. The mechanism of ion doping modification for cathode electrode materials is as follows: Ion doping can effectively inhibit the dissolution of Mn³⁺, prolong the life of cathode materials, and prevent transition metal elements from binding with oxygen ions. It improves the conductivity of the cathode material. Ion doping can

increase the diffusion channel of lithium ions, increase the diffusion rate of Li⁺ ions, and improve the conductivity of the material. It prevents the negative effects caused by the transition metal embedded in the lithium layer when it is difficult to escape.

Currently, cation doping is the main research direction, while research on anion doping is relatively limited. The structural stability and cycle stability of LRMO cathode materials are significantly improved by anions, especially polyanions with a polyhedral structure, which can restrain

the migration of transition metals, suppress the formation of Li vacancies, and inhibit the phase transition of the layered structure, thereby greatly affecting the capacity and cycle performance of cathode materials. Ionic doping includes single-element doping and multi-element doping. Single doping with lithium can increase the spacing of lithium layers, improve the diffusion coefficient of lithium ions, and enhance cycle and rate performance. Incorporating other metal ions or non-metal ions into the TM layer can improve the conductivity of the material and inhibit the migration of transition metal ions. Single doping with highly electronegative elements can inhibit the migration of transition metal ions and increase the operating voltage, thereby addressing the voltage attenuation problem. Single ion doped LRMO materials can only show excellent performance in one aspect. Multi-ion co-doping can enlarge the spacing of layered materials, inhibit the mixing of lithium nickel, increase the diffusion rate of lithium ions, and improve the magnification capacity of cathode materials, so it has become a widely used doping method at present. On this basis, the main research direction to optimize the electrochemical performances of LRMO is to exert the synergistic effect of multiple ions.

- (3) The single crystal LRMO material features a continuous lattice with no grain boundaries inside, which alleviates surface side reactions, such as CEI formation, transition metal dissolution, oxygen loss, and surface structure transformation. The single crystal LRMO material has high mechanical strength, allowing for high compacted density during compaction and can make better contact with the conductive agent to accelerate the transmission of Li^+ . However, the long-range diffusion pathway in SC-LRMO material not only limits the effective Li^+ transfer but also significantly weakens the kinetics of anionic redox. Therefore, the preparation of SC-LRMO material with a reasonable particle size can provide a faster Li^+ migration rate and reduce the highly active interface problem that is difficult to avoid for small single crystals.
- (4) Neither surface coating nor elemental doping alone can fully address all issues in LRMO materials. Hence, a combination of different modification methods and novel structures should be developed. It is of great significance for the future development of high-performance LRMO materials to stabilize the surface structure of the material, inhibit surface oxygen release, improve the kinetics of lithium-ion transport, and inhibit electrode polarization through *in-situ* reconstruction of the surface structure and induction of oxygen vacancies, surface spinel formation, and layered rock salt heterostructure.
- (5) The commercialization of LRMO materials is also important. To promote the practical application of LRMO materials, further efforts should be made to develop cost-effective techniques, as well as the design of optimal electrolytes, which can facilitate the formation of a stable CEI film, mitigate side reactions, and prevent capacity fade.

Acknowledgements

This work was financially supported by the National Natural Science Foundation of China (No. 22309138), the Natural Science Foundation of Hubei Province (2024AFB815) and Hubei Key Laboratory of Low Dimensional Optoelectronic Material and Devices (HLOM242006).

Conflict of Interests

The authors declare no conflict of interest.

Keywords: Ion doping · Lithium-ion batteries · Lithium-rich manganese oxide · Surface coating · Single crystal structures

- [1] a) X. Ou, T. Liu, W. Zhong, X. Fan, X. Guo, X. Huang, L. Cao, J. Hu, B. Zhang, Y. S. Chu, G. Hu, Z. Lin, M. Dahbi, J. Alami, K. Amine, C. Yang, J. Lu, *Nat. Commun.* **2022**, *13*, 2319; b) X. Zhu, T. U. Schulli, X. Yang, T. Lin, Y. Hu, N. Cheng, H. Fujii, K. Ozawa, B. Cowie, Q. Gu, S. Zhou, Z. Cheng, Y. Du, L. Wang, *Nat. Commun.* **2022**, *13*, 1565; c) G. George, A. Poater, M. Solà, S. Posada-Pérez, *Batteries Supercaps* **2024**, *7*, e202300452; d) T. A. Hendriks, M. A. Lange, E. M. Kiens, C. Baeumer, W. G. Zeier, *Batteries Supercaps* **2023**, *6*, e202200544; e) S. Künnle, J. M. Hesper, T. Lein, K. Voigt, D. Mikhailova, A. Michaelis, M. Winter, T. Placke, C. Heubner, *Batteries Supercaps* **2023**, *6*, e202300284; f) Y. Levartovsky, X. Wu, C. Erk, S. Maiti, J. Grinblat, M. Talianker, D. Aurbach, *Batteries Supercaps* **2021**, *4*, 221–231; g) S. Schweißler, M. Bianchini, P. Hartmann, T. Brezesinski, J. Janek, *Batteries Supercaps* **2020**, *3*, 1021–1027; h) A. Zülke, Y. Li, P. Keil, R. Burrell, S. Belaisch, M. Nagarathinam, M. P. Mercer, H. E. Hoster, *Batteries Supercaps* **2021**, *4*, 934–947; i) S. Kim, W. Cho, X. Zhang, Y. Oshima, J. W. Choi, *Nat. Commun.* **2016**, *7*, 13598.
- [2] a) B. Wang, J. Cui, Z. Li, H. Wang, D. Zhang, Q. Wang, H. Sun, Y. A. Wu, *Mater. Chem. Front.* **2023**, *7*, 2570–2594; b) C. Shen, L. Hu, Q. Duan, X. Liu, S. Huang, Y. Jiang, W. Li, B. Zhao, X. Sun, J. Zhang, *Adv. Energy Mater.* **2023**, *13*, 2302957.
- [3] J. Zheng, S. Myeong, W. Cho, P. Yan, J. Xiao, C. Wang, J. Cho, J. G. Zhang, *Adv. Energy Mater.* **2016**, *7*, 1601284.
- [4] J. J. Marie, R. A. House, G. J. Rees, A. W. Robertson, M. Jenkins, J. Chen, S. Agrestini, M. Garcia-Fernandez, K. J. Zhou, P. G. Bruce, *Nat. Mater.* **2024**, *23*, 818–825.
- [5] a) T. Liu, J. Liu, L. Li, L. Yu, J. Diao, T. Zhou, S. Li, A. Dai, W. Zhao, S. Xu, Y. Ren, L. Wang, T. Wu, R. Qi, Y. Xiao, J. Zheng, W. Cha, R. Harder, I. L. Robinson, J. Wen, J. Lu, F. Pan, K. Amine, *Nature* **2022**, *606*, 305–312; b) L. Wang, A. Dai, W. Xu, S. Lee, W. Cha, R. Harder, T. Liu, Y. Ren, G. Yin, P. Zuo, J. Wang, J. Lu, J. Wang, *J. Am. Chem. Soc.* **2020**, *142*, 14966–14973.
- [6] a) L. Zeng, H. Liang, B. Qiu, Z. Shi, S. Cheng, K. Shi, Q. Liu, Z. Liu, *Adv. Funct. Mater.* **2023**, *33*, 2213260; b) P. Kou, Z. Zhang, Z. Wang, R. Zheng, Y. Liu, F. Lv, N. Xu, *Energy Fuels* **2023**, *37*, 18243–18265; c) S. Kang, D. Choi, H. Lee, B. Choi, Y. M. Kang, *Adv. Mater.* **2023**, *35*, 2211965; d) Z. Deng, Y. Liu, L. Wang, N. Fu, Y. Li, Y. Luo, J. Wang, X. Xiao, X. Wang, X. Yang, X. He, H. Zhang, *Mater. Today* **2023**, *69*, 236–261; e) H. Chen, C. Sun, *Chem. Commun.* **2023**, *59*, 9029–9055; f) Z. Yin, H. Zhu, Y. Huang, D. Luo, Y. Ren, S. Lan, Q. Liu, *J. Mater. Chem. A* **2022**, *10*, 19387–19411; g) H. Xie, J. Cui, Z. Yao, X. Ding, Z. Zhang, D. Luo, Z. Lin, *Chem. Eng. J.* **2022**, *427*, 131978; h) L. Nie, S. Chen, W. Liu, *Nano Res.* **2022**, *16*, 391–402; i) X. Gou, Z. Hao, Z. Hao, G. Yang, Z. Yang, X. Zhang, Z. Yan, Q. Zhao, J. Chen, *Adv. Funct. Mater.* **2022**, *32*, 2112088.
- [7] W. Zeng, F. Liu, J. Yang, B. Zhang, F. Cao, W. Tian, J. Wang, R. Yu, F. Xia, H. Peng, J. Ma, Z. Wang, S. Mu, J. Wu, *Energy Storage Mater.* **2023**, *54*, 651–660.
- [8] T. Zeng, M. Yang, F. Sun, Z. Huang, W. Zhao, Z. Chen, D. Zou, J. Qiu, L. Wang, R. Wang, C. Zhang, T. Yang, W. Ji, J. Xu, W. Yin, R. Li, H. Meng, Y. Xiao, *Adv. Funct. Mater.* **2024**, *34*, 2314528.
- [9] Y. Xie, S. Meng, X. Chen, X. Liang, Y. Jin, L. Xiang, *J. Colloid Interface Sci.* **2021**, *594*, 485–492.

- [10] P. Yang, S. Zhang, Z. Wei, X. Guan, J. Xia, D. Huang, Y. Xing, J. He, B. Wen, B. Liu, H. Xu, *Small* **2023**, *19*, 2207797.
- [11] J. Wang, X. He, E. Paillard, N. Laszcynski, J. Li, S. Passerini, *Adv. Energy Mater.* **2016**, *6*, 1600906.
- [12] W. He, W. Guo, H. Wu, L. Lin, Q. Liu, X. Han, Q. Xie, P. Liu, H. Zheng, L. Wang, X. Yu, D. L. Peng, *Adv. Mater.* **2021**, *33*, 2005937.
- [13] B. Xu, C. R. Fell, M. Chi, Y. S. Meng, *Energy Environ. Sci.* **2011**, *4*, 2223–2233.
- [14] X. Li, X. Sun, X. Hu, F. Fan, S. Cai, C. Zheng, G. D. Stucky, *Nano Energy* **2020**, *77*, 105143.
- [15] R. A. House, G. J. Rees, M. A. Pérez-Osorio, J.-J. Marie, E. Boivin, A. W. Robertson, A. Nag, M. García-Fernandez, K.-J. Zhou, P. G. Bruce, *Nat. Energy* **2020**, *5*, 777–785.
- [16] X. Yu, Y. Lyu, L. Gu, H. Wu, S. M. Bak, Y. Zhou, K. Amine, S. N. Ehrlich, H. Li, K. W. Nam, X. Q. Yang, *Adv. Energy Mater.* **2013**, *4*, 1300950.
- [17] Y. Gao, X. Wang, J. Ma, Z. Wang, L. Chen, *Chem. Mater.* **2015**, *27*, 3456–3461.
- [18] a) M. Gu, A. Genc, I. Belharouak, D. Wang, K. Amine, S. Thevuthasan, D. R. Baer, J.-G. Zhang, N. D. Browning, J. Liu, C. Wang, *Chem. Mater.* **2013**, *25*, 2319–2326; b) P. Yan, J. Zheng, J. Zheng, Z. Wang, G. Teng, S. Kuppan, J. Xiao, G. Chen, F. Pan, J. G. Zhang, C. M. Wang, *Adv. Energy Mater.* **2016**, *6*, 1502455.
- [19] S. H. Lee, J.-S. Moon, M.-S. Lee, T.-H. Yu, H. Kim, B. M. Park, *J. Power Sources* **2015**, *281*, 77–84.
- [20] X. Li, M. Tang, X. Feng, I. Hung, A. Rose, P.-H. Chien, Z. Gan, Y.-Y. Hu, *Chem. Mater.* **2017**, *29*, 8282–8291.
- [21] N. Leifer, T. Penki, R. Nanda, J. Grinblat, S. Luski, D. Aurbach, G. Goobes, *Phys. Chem. Chem. Phys.* **2020**, *22*, 9098–9109.
- [22] Z. Q. Deng, A. Manthiram, *J. Phys. Chem. C* **2011**, *115*, 7097–7103.
- [23] Y. Shin, H. Ding, K. A. Persson, *Chem. Mater.* **2016**, *28*, 2081–2088.
- [24] L. Chen, Y. Su, S. Chen, N. Li, L. Bao, W. Li, Z. Wang, M. Wang, F. Wu, *Adv. Mater.* **2014**, *26*, 6756–6760.
- [25] G. Z. Wei, X. Lu, F. S. Ke, L. Huang, J. T. Li, Z. X. Wang, Z. Y. Zhou, S. G. Sun, *Adv. Mater.* **2010**, *22*, 4364–4367.
- [26] a) E. Hu, Y. Lyu, H. L. Xin, J. Liu, L. Han, S. M. Bak, J. Bai, X. Yu, H. Li, X. Q. Yang, *Nano Lett.* **2016**, *16*, 5999–6007; b) M. Sathiya, A. M. Abakumov, D. Foix, G. Rousse, K. Ramesha, M. Saubanere, M. L. Doublet, H. Vezin, C. P. Laisa, A. S. Prakash, D. Gonbeau, G. VanTendeloo, J. M. Tarascon, *Nat. Mater.* **2015**, *14*, 230–238; c) S. Sharifi-Asl, J. Lu, K. Amine, R. Shahbazian-Yassar, *Adv. Energy Mater.* **2019**, *9*, 1900551.
- [27] X. Li, Y. Qiao, S. Guo, Z. Xu, H. Zhu, X. Zhang, Y. Yuan, P. He, M. Ishida, H. Zhou, *Adv. Mater.* **2018**, *30*, 1705197.
- [28] J. Zhang, F. Cheng, S. Chou, J. Wang, L. Gu, H. Wang, H. Yoshikawa, Y. Lu, J. Chen, *Adv. Mater.* **2019**, *31*, e1901808.
- [29] E. Hu, X. Yu, R. Lin, X. Bi, J. Lu, S. Bak, K.-W. Nam, H. L. Xin, C. Jaye, D. A. Fischer, K. Amine, X.-Q. Yang, *Nat. Energy* **2018**, *3*, 690–698.
- [30] H. Zheng, X. Han, W. Guo, L. Lin, Q. Xie, P. Liu, W. He, L. Wang, D.-L. Peng, *Mater. Today Energy* **2020**, *18*, 100518.
- [31] C. Zhang, Y. Li, Y. Liu, X. Shen, Z. Hu, J.-M. Chen, H.-J. Lin, C.-T. Chen, Q. Kong, Y.-s. Hu, Y. Gao, S.-C. Haw, X. Wang, R. Yu, Z. Wang, L. Chen, *Nano Energy* **2024**, *121*, 109254.
- [32] D. Mohanty, J. Li, D. P. Abraham, A. Huq, E. A. Payzant, D. L. Wood, C. Daniel, *Chem. Mater.* **2014**, *26*, 6272–6280.
- [33] J. Kim, H. Cha, H. Lee, P. Oh, J. Cho, *Batteries Supercaps* **2020**, *3*, 309–322.
- [34] a) X. Li, Z. Cao, H. Dong, Z. Shi, H. Zhang, J. Li, S. Yang, S. Yang, *RSC Adv.* **2020**, *10*, 3166–3174; b) Y. Chen, X. Wang, J. Zhang, B. Chen, J. Xu, S. Zhang, L. Zhang, *RSC Adv.* **2019**, *9*, 2172–2179; c) G. Kobayashi, Y. Irii, F. Matsumoto, A. Ito, Y. Ohsawa, S. Yamamoto, Y. Cui, J.-Y. Son, Y. Sato, *J. Power Sources* **2016**, *303*, 250–256.
- [35] S. J. Shi, J. P. Tu, Y. Y. Tang, X. Y. Liu, Y. Q. Zhang, X. L. Wang, C. D. Gu, *Electrochim. Acta* **2013**, *88*, 671–679.
- [36] a) J. James Abraham, U. Nisar, H. Monawwar, A. Abdul Quddus, R. A. Shakoor, M. I. Saleh, R. Kahraman, S. Al-Qaradawi, A. S. Aljaber, *J. Mater. Sci.: Mater. Electron.* **2020**, *31*, 19475–19486; b) Y. Zhao, Z. Lv, T. Xu, J. Li, *J. Alloys Compd.* **2017**, *715*, 105–111.
- [37] M. Yu, X. Wei, X. Min, A. Yuan, J. Xu, *Mater. Chem. Phys.* **2022**, *286*, 126228.
- [38] C. Chen, T. Geng, C. Du, P. Zuo, X. Cheng, Y. Ma, G. Yin, *J. Power Sources* **2016**, *331*, 91–99.
- [39] a) M. J. Herzog, D. Esken, J. Janek, *Batteries Supercaps* **2021**, *4*, 1003–1017; b) A. Javed, A. Makvandi, F. Demelash, E. Adhitama, B. Heidrich, M. Peterlechner, G. Wilde, M. Winter, M. Börner, *Batteries Supercaps* **2024**, *7*, e202300580.
- [40] X. Zhang, I. Belharouak, L. Li, Y. Lei, J. W. Elam, A. Nie, X. Chen, R. S. Yassar, R. L. Axelbaum, *Adv. Energy Mater.* **2013**, *3*, 1299–1307.
- [41] Y. Wu, J. Ming, L. Zhuo, Y. Yu, F. Zhao, *Electrochim. Acta* **2013**, *113*, 54–62.
- [42] K. Mu, Y. Cao, G. Hu, K. Du, H. Yang, Z. Gan, Z. Peng, *Electrochim. Acta* **2018**, *273*, 88–97.
- [43] R. Yu, Y. Lin, Z. Huang, *Electrochim. Acta* **2015**, *173*, 515–522.
- [44] a) Y. Gao, R. L. Patel, K. Y. Shen, X. Wang, R. L. Axelbaum, X. Liang, *ACS Omega* **2018**, *3*, 906–916; b) G. Hu, Z. Xue, Z. Luo, Z. Peng, Y. Cao, W. Wang, Y. Zeng, Y. Huang, Y. Tao, T. Li, Z. Zhang, K. Du, *Ceram. Int.* **2019**, *45*, 10633–10639; c) J. Mei, Y. Chen, W. Xu, W. He, L. Wang, Q. Xie, D.-L. Peng, *Chem. Eng. J.* **2022**, *431*, 133799; d) K. Yang, Y. Liu, B. Niu, Z. Yang, J. Li, *Ionics* **2018**, *25*, 2027–2034; e) W. Yuan, H. Z. Zhang, Q. Liu, G. R. Li, X. P. Gao, *Electrochim. Acta* **2014**, *135*, 199–207.
- [45] H. Meng, H. Jin, J. Gao, L. Zhang, Q. Xu, J. *Electrochim. Soc.* **2014**, *161*, A1564–A1571.
- [46] S. Dong, X. He, Q. Xu, L. Ma, C. Hai, Y. Zhou, *Langmuir* **2023**, *39*, 7723–7730.
- [47] S. J. Shi, J. P. Tu, Y. J. Zhang, Y. D. Zhang, X. Y. Zhao, X. L. Wang, C. D. Gu, *Electrochim. Acta* **2013**, *108*, 441–448.
- [48] X. Zhai, P. Zhang, H. Huang, J. Zhou, X. Li, B. Chen, Y. He, Z. Guo, *Solid State Ionics* **2021**, *366*–367, 115661.
- [49] X. Ran, J. Tao, Z. Chen, Z. Yan, Y. Yang, J. Li, Y. Lin, Z. Huang, *Electrochim. Acta* **2020**, *353*, 135959.
- [50] S. Zhang, H. Gu, T. Tang, W. Du, M. Gao, Y. Liu, D. Jian, H. Pan, *ACS Appl. Mater. Interfaces* **2017**, *9*, 33863–33875.
- [51] a) Q. Chen, L. Luo, L. Wang, T. Xie, S. Dai, Y. Yang, Y. Li, M. Yuan, *J. Alloys Compd.* **2018**, *735*, 1778–1786; b) X. Wan, W. Che, D. Zhang, C. Chang, *Mater. Charact.* **2020**, *169*, 110602.
- [52] Y. Zhao, X. Hu, C. Ji, Y. Sun, Y. Wang, Z. Zhao, Z. Lv, *J. Electrochim. Soc.* **2016**, *163*, A2040–A2046.
- [53] L. Zhou, M. Tian, Y. Deng, Q. Zheng, C. Xu, D. Lin, *Ceram. Int.* **2016**, *42*, 15623–15633.
- [54] F. Meng, H. Guo, Z. Wang, J. Wang, G. Yan, X. Wu, X. Li, L. Zhou, *Appl. Surf. Sci.* **2019**, *479*, 1277–1286.
- [55] a) Y. Li, H. Huang, J. Yu, Y. Xia, C. Liang, Y. Gan, J. Zhang, W. Zhang, *J. Alloys Compd.* **2019**, *783*, 349–356; b) H. Wang, F. Liu, R. Yu, Z. Xiao, Z. Zhu, L. Zhou, J. Wu, *Nano Energy* **2022**, *100*, 107439.
- [56] a) S. Guo, H. Yu, P. Liu, X. Liu, D. Li, M. Chen, M. Ishida, H. Zhou, *J. Mater. Chem. A* **2014**, *2*, 4422–4428; b) Y. Jin, Y. Xu, X. Sun, L. Xiong, S. Mao, *Appl. Surf. Sci.* **2016**, *384*, 125–134; c) Y. Liu, S. Liu, Y. Wang, L. Chen, X. Chen, *J. Power Sources* **2013**, *222*, 455–460.
- [57] H. He, L. Zan, Y. Zhang, *J. Alloys Compd.* **2016**, *680*, 95–104.
- [58] L.-J. Zhou, Z.-L. Yin, Z.-Y. Ding, X.-H. Li, Z.-X. Wang, H.-J. Guo, *Ionics* **2017**, *24*, 2533–2542.
- [59] A. Zhu, J. Wu, B. Wang, J. Zhou, Y. Zhang, Y. Guo, K. Wu, H. Wu, Q. Wang, Y. Zhang, *ACS Appl. Mater. Interfaces* **2021**, *13*, 61248–61257.
- [60] a) Z. Yang, J. Zhong, J. Li, Y. Liu, B. Niu, F. Kang, *Ceram. Int.* **2019**, *45*, 439–448; b) C. Wang, F. Zhou, K. Chen, J. Kong, Y. Jiang, G. Yan, J. Li, C. Yu, W.-P. Tang, *Electrochim. Acta* **2015**, *176*, 1171–1181.
- [61] C. Huang, Z. Wang, Z.-Q. Fang, S.-X. Zhao, L.-j. Ci, *J. Power Sources* **2021**, *499*, 229967.
- [62] J. Duan, W. Tang, R. Wang, X. Tang, J. Li, M. Tang, P. Li, *Appl. Surf. Sci.* **2020**, *521*, 146504.
- [63] W. Zhang, Y. Sun, H. Deng, J. Ma, Y. Zeng, Z. Zhu, Z. Lv, H. Xia, X. Ge, S. Cao, Y. Xiao, S. Xi, Y. Du, A. Cao, X. Chen, *Adv. Mater.* **2020**, *32*, 2000496.
- [64] J. Peng, Y. Li, Z. Chen, G. Liang, S. Hu, T. Zhou, F. Zheng, Q. Pan, H. Wang, Q. Li, J. Liu, Z. Guo, *ACS Nano* **2021**, *15*, 11607–11618.
- [65] a) Z. Zhou, D. Chu, B. Gao, T. Momma, Y. Tateyama, C. Cazorla, *ACS Appl. Mater. Interfaces* **2022**, *14*, 37009–37018; b) X. Ji, Y. Xu, Y. Zhou, J. Song, H. Feng, P. Wang, J. Yang, F. Zhuge, H. Xie, Q. Tan, *Electrochim. Acta* **2022**, *421*, 140465; c) F. Guo, J. Lu, M. Su, Y. Chen, J. Zheng, L. Yin, H. Li, *Chin. Phys. B* **2023**, *32*, 088201; d) Z. Luo, Z. Zhou, Z. He, Z. Sun, J. Zheng, Y. Li, *Ceram. Int.* **2021**, *47*, 2656–2664.
- [66] X. Deng, M. Li, Z. Ma, X. Wang, *Nano Res.* **2023**, *16*, 10634–10643.
- [67] S. Hu, Y. Li, Y. Chen, J. Peng, T. Zhou, W. K. Pang, C. Didier, V. K. Peterson, H. Wang, Q. Li, Z. Guo, *Adv. Energy Mater.* **2019**, *9*, 1901795.
- [68] Y. Lei, Y. Elias, Y. Han, D. Xiao, J. Lu, J. Ni, Y. Zhang, C. Zhang, D. Aurbach, Q. Xiao, *ACS Appl. Mater. Interfaces* **2022**, *14*, 49709–49718.
- [69] F. Zheng, X. Ou, Q. Pan, X. Xiong, C. Yang, Z. Fu, M. Liu, *Chem. Eng. J.* **2018**, *334*, 497–507.
- [70] Y. Liu, Z. Yang, J. Li, B. Niu, K. Yang, F. Kang, *J. Mater. Chem. A* **2018**, *6*, 13883–13893.

- [71] a) J. Ma, B. Li, L. An, H. Wei, X. Wang, P. Yu, D. Xia, *J. Power Sources* **2015**, *277*, 393–402; b) F. Wu, X. Zhang, T. Zhao, L. Li, M. Xie, R. Chen, *ACS Appl. Mater. Interfaces* **2015**, *7*, 3773–3781; c) Z. Wang, E. Liu, C. He, C. Shi, J. Li, N. Zhao, *J. Power Sources* **2013**, *236*, 25–32; d) J. J. Chen, Z. D. Li, H. F. Xiang, W. W. Wu, S. Cheng, L. J. Zhang, Q. S. Wang, Y. C. Wu, *RSC Adv.* **2015**, *5*, 3031–3038; e) X. Zhang, X. Xie, R. Yu, J. Zhou, Y. Huang, S. Cao, Y. Wang, K. Tang, C. Wu, X. Wang, *ACS Appl. Energy Mater.* **2019**, *2*, 3532–3541.
- [72] a) F. Meng, H. Guo, Z. Wang, X. Li, Y. Deng, *Ionics* **2019**, *26*, 2117–2127; b) L. Zhou, Z. Zheng, W. Xia, J. Sun, F. Bei, *Ionics* **2023**, *29*, 1311–1322.
- [73] Q. Y. Wang, J. Liu, A. V. Murugan, A. Manthiram, *J. Mater. Chem.* **2009**, *19*, 4965–4972.
- [74] a) L. He, J. Xu, T. Han, H. Han, Y. Wang, J. Yang, J. Wang, W. Zhu, C. Zhang, Y. Zhang, *Ceram. Int.* **2017**, *43*, 5267–5273; b) F. Ding, J. Li, F. Deng, G. Xu, Y. Liu, K. Yang, F. Kang, *ACS Appl. Mater. Interfaces* **2017**, *9*, 27936–27945; c) W. Liu, P. Oh, X. Liu, S. Myeong, W. Cho, J. Cho, *Adv. Energy Mater.* **2015**, *5*, 1500274.
- [75] Z. Du, W. Peng, Z. Wang, H. Guo, Q. Hu, X. Li, *Ionics* **2018**, *24*, 3717–3724.
- [76] a) G. R. Li, X. Feng, Y. Ding, S. H. Ye, X. P. Gao, *Electrochim. Acta* **2012**, *78*, 308–315; b) Y. Li, K.-y. Liu, M.-y. LÜ, L. Wei, J.-j. Zhong, *Trans. Nonferrous Met. Soc. China* **2014**, *24*, 3534–3540; c) Y. K. Sun, M. J. Lee, C. S. Yoon, J. Hassoun, K. Amine, B. Scrosati, *Adv. Mater.* **2012**, *24*, 1192–1196; d) J. Zhang, D. Zhang, Z. Wang, F. Zheng, R. Zhong, R. Hong, *J. Mater. Sci.* **2023**, *58*, 4525–4540; e) J. Zheng, M. Gu, J. Xiao, B. J. Polzin, P. Yan, X. Chen, C. Wang, J.-G. Zhang, *Chem. Mater.* **2014**, *26*, 6320–6327; f) Z. Zhu, F. Cai, J. Yu, *Ionics* **2016**, *22*, 1353–1359.
- [77] a) H. G. Kim, Y. J. Park, *ACS Appl. Energy Mater.* **2021**, *4*, 8220–8230; b) H. J. Lee, Y. J. Park, *Mater. Res. Bull.* **2014**, *58*, 169–173; c) S. Sun, N. Wan, Q. Wu, X. Zhang, D. Pan, Y. Bai, X. Lu, *Solid State Ionics* **2015**, *278*, 85–90; d) D.-d. Wang, F. Wang, H.-h. Zhai, Y.-p. Li, N.-c. Yang, K.-h. Chen, *J. Electrochem.* **2020**, *26*, 289–297.
- [78] X. Liu, T. Huang, A. Yu, *Electrochim. Acta* **2015**, *163*, 82–92.
- [79] S. Chong, Y. Chen, W. Yan, S. Guo, Q. Tan, Y. Wu, T. Jiang, Y. Liu, *J. Power Sources* **2016**, *332*, 230–239.
- [80] C. Lu, H. Wu, Y. Zhang, H. Liu, B. Chen, N. Wu, S. Wang, *J. Power Sources* **2014**, *267*, 682–691.
- [81] a) C.-D. Li, Z.-L. Yao, J. Xu, P. Tang, X. Xiong, *Ionics* **2016**, *23*, 549–558; b) J. Liu, F. Bei, L. Wen, Z. Zheng, B. Zhang, Q. Han, L. Wang, Y. Wu, X. He, *Electrochim. Acta* **2024**, *479*, 143882; c) Q. Xie, Z. Hu, C. Zhao, S. Zhang, K. Liu, *RSC Adv.* **2015**, *5*, 50859–50864.
- [82] X. Zhang, Y. Yang, S. Sun, Q. Wu, N. Wan, D. Pan, Y. Bai, *Solid State Ionics* **2016**, *284*, 7–13.
- [83] C. Lu, H. Wu, B. Chen, H. Liu, Y. Zhang, *J. Alloys Compd.* **2015**, *634*, 75–82.
- [84] T. Zhao, L. Li, R. Chen, H. Wu, X. Zhang, S. Chen, M. Xie, F. Wu, J. Lu, K. Amine, *Nano Energy* **2015**, *15*, 164–176.
- [85] B. Liu, Z. Zhang, J. Wan, S. Liu, *Ionics* **2017**, *23*, 1365–1374.
- [86] a) Q. Xia, X. Zhao, M. Xu, Z. Ding, J. Liu, L. Chen, D. G. Ivey, W. Wei, *J. Mater. Chem. A* **2015**, *3*, 3995–4003; b) S. Pang, K. Xu, Y. Wang, X. Shen, W. Wang, Y. Su, M. Zhu, X. Xi, *J. Power Sources* **2017**, *365*, 68–75; c) K. Park, J. Kim, J.-H. Park, Y. Hwang, D. Han, *J. Power Sources* **2018**, *408*, 105–110; d) Y. Ma, P. Liu, Q. Xie, G. Zhang, H. Zheng, Y. Cai, Z. Li, L. Wang, Z.-Z. Zhu, L. Mai, D.-L. Peng, *Nano Energy* **2019**, *59*, 184–196; e) B. Song, C. Zhou, Y. Chen, Z. Liu, M. O. Lai, J. Xue, L. Lu, *RSC Adv.* **2014**, *4*, 44244–44252.
- [87] a) K. C. Jiang, X. L. Wu, Y. X. Yin, J. S. Lee, J. Kim, Y. G. Guo, *ACS Appl. Mater. Interfaces* **2012**, *4*, 4858–4863; b) M. Yu, X. Wei, X. Min, A. Yuan, J. Xu, *Energy Fuels* **2022**, *36*, 5502–5512.
- [88] B. Song, M. O. Lai, Z. Liu, H. Liu, L. Lu, *J. Mater. Chem. A* **2013**, *1*, 9954–9965.
- [89] M. Chen, G. Zhang, B. Wu, M. Liu, J. Chen, W. Xiang, W. Li, *ACS Appl. Energy Mater.* **2022**, *5*, 4307–4317.
- [90] V. Shanmugam, S. Natarajan, L. S. Lobo, A. Mathur, M. B. Sahana, G. Sundararajan, R. Gopalan, *J. Power Sources* **2021**, *515*, 230623.
- [91] D. Lu, Y. Chen, C. Zheng, Y. Li, *Ionics* **2019**, *26*, 2177–2186.
- [92] a) D. Wang, X. Wang, X. Yang, R. Yu, L. Ge, H. Shu, *J. Power Sources* **2015**, *293*, 89–94; b) Q. Xue, J. Li, G. Xu, H. Zhou, X. Wang, F. Kang, *J. Mater. Chem. A* **2014**, *2*, 18613–18623; c) C. Wu, X. Fang, X. Guo, Y. Mao, J. Ma, C. Zhao, Z. Wang, L. Chen, *J. Power Sources* **2013**, *231*, 44–49; d) F. Wu, J. Liu, L. Li, X. Zhang, R. Luo, Y. Ye, R. Chen, *ACS Appl. Mater. Interfaces* **2016**, *8*, 23095–23104; e) J. Zhang, Q. Lu, J. Fang, J. Wang, J. Yang, Y. NuLi, *ACS Appl. Mater. Interfaces* **2014**, *6*, 17965–17973; f) C. Zheng, Z. Yang, J. Feng, J. Zhong, Z. Wei, J. Li, *J. Mater. Chem. A* **2022**, *10*, 16046–16060.
- [93] Q. Li, D. Zhou, L. Zhang, D. Ning, Z. Chen, Z. Xu, R. Gao, X. Liu, D. Xie, G. Schumacher, X. Liu, *Adv. Funct. Mater.* **2019**, *29*, 1806706.
- [94] W. He, C. Zhang, M. Wang, B. Wei, Y. Zhu, J. Wu, C. Liang, L. Chen, P. Wang, W. Wei, *Adv. Funct. Mater.* **2022**, *32*, 2200322.
- [95] a) D. Wang, X. Zhang, R. Xiao, X. Lu, Y. Li, T. Xu, D. Pan, Y.-S. Hu, Y. Bai, *Electrochim. Acta* **2018**, *265*, 244–253; b) M. Xu, Q. Lian, Y. Wu, C. Ma, P. Tan, Q. Xia, J. Zhang, D. G. Ivey, W. Wei, *RSC Adv.* **2016**, *6*, 34245–34253.
- [96] a) J. Chen, S. Cao, Z. Li, H. Li, C. Guo, R. Wang, L. Wu, Y. Zhang, Y. Bai, X. Wang, *ACS Appl. Mater. Interfaces* **2023**, *15*, 36394–36403; b) Z. He, J. Li, Z. Luo, Z. Zhou, X. Jiang, J. Zheng, Y. Li, J. Mao, K. Dai, C. Yan, Z. Sun, *ACS Appl. Mater. Interfaces* **2021**, *13*, 49390–49401; c) J. Zhang, H. Zhang, R. Gao, Z. Li, Z. Hu, X. Liu, *PCCP* **2016**, *18*, 13322–13331; d) J.-C. Zheng, Z. Yang, P.-b. Wang, L.-b. Tang, C.-s. An, Z.-j. He, *ACS Appl. Mater. Interfaces* **2018**, *10*, 31324–31329.
- [97] a) Y. Zhu, N. Zhang, L. Zhao, J. Xu, Z. Liu, Y. Liu, J. Wu, F. Ding, *J. Alloys Compd.* **2019**, *811*, 152023; b) S. Yuan, H. Zhang, D. Song, Y. Ma, X. Shi, C. Li, L. Zhang, *Chem. Eng. J.* **2022**, *439*, 135677.
- [98] a) N. Hu, Y. Yang, L. Li, Y. Zhang, Z. Hu, L. Zhang, J. Ma, G. Cui, *Energy Environ. Mater.* **2023**, *0*, e12610; b) J. Liu, Z. Wu, M. Yu, H. Hu, Y. Zhang, K. Zhang, Z. Du, F. Cheng, J. Chen, *Small* **2022**, *18*, 2106337; c) E. Zhao, X. Liu, Z. Hu, L. Sun, X. Xiao, *J. Power Sources* **2015**, *294*, 141–149; d) Y. Zhai, J. Zhang, H. Zhang, X. Liu, C.-W. Wang, L. Sun, X. Liu, *J. Electrochem. Soc.* **2019**, *166*, A1323–A1329.
- [99] Z. Wei, D. Zhang, J. Zhong, C. Zheng, J. Feng, J. Li, *Batteries Supercaps* **2023**, *6*, e202200568.
- [100] S. Zhao, B. Sun, K. Yan, J. Zhang, C. Wang, G. Wang, *ACS Appl. Mater. Interfaces* **2018**, *10*, 33260–33268.
- [101] W. Shu, Z. Jian, J. Zhou, Y. Zheng, W. Chen, *ACS Appl. Mater. Interfaces* **2021**, *13*, 54916–54923.
- [102] Y. Wei, J. Cheng, D. Li, Y. Li, Z. Zeng, H. Liu, H. Zhang, F. Ji, X. Geng, J. Lu, L. Ci, *Adv. Funct. Mater.* **2023**, *33*, 2214775.
- [103] H. Zhang, T. Yang, Y. Han, D. Song, X. Shi, L. Zhang, L. Bie, *J. Power Sources* **2017**, *364*, 272–279.
- [104] Y. Liu, Z. Yang, J. Zhong, J. Li, R. Li, Y. Yu, F. Kang, *ACS Nano* **2019**, *13*, 11891–11900.
- [105] M. Si, D. Wang, R. Zhao, D. Pan, C. Zhang, C. Yu, X. Lu, H. Zhao, Y. Bai, *Adv. Sci.* **2020**, *7*, 1902538.
- [106] a) X. Liu, Q. Su, C. Zhang, T. Huang, A. Yu, *ACS Sustainable Chem. Eng.* **2015**, *4*, 255–263; b) Y. Qu, W. Tang, H. Liu, C. Li, L. Zou, Z. Chen, Z. Yang, J. Su, W. Zhang, *Ind. Eng. Chem. Res.* **2023**, *62*, 10467–10476.
- [107] A. Zhu, Q. Wang, Y. Zhang, Y. Zhang, X. He, K. Wu, H. Wu, Q. Wang, W. Cai, Y. Zhang, *J. Energy Chem.* **2022**, *71*, 384–391.
- [108] C.-C. Yang, P.-C. Liao, Y.-S. Wu, S. J. Lue, *Appl. Surf. Sci.* **2017**, *399*, 670–681.
- [109] D. Gao, Z. Zeng, H. Mi, L. Sun, X. Ren, P. Zhang, Y. Li, *J. Mater. Chem. A* **2019**, *7*, 23964–23972.
- [110] Y. Su, F. Yuan, L. Chen, Y. Lu, J. Dong, Y. Fang, S. Chen, F. Wu, *J. Energy Chem.* **2020**, *51*, 39–47.
- [111] a) J. Cao, H. Huang, Y. Qu, W. Tang, Z. Yang, W. Zhang, *Nanoscale* **2021**, *13*, 20488–20497; b) D. Chen, F. Zheng, L. Li, M. Chen, X. Zhong, W. Li, L. Lu, *J. Power Sources* **2017**, *341*, 147–155; c) Y. Lee, J. Lee, K. Y. Lee, J. Mun, J. K. Lee, W. Choi, *J. Power Sources* **2016**, *315*, 284–293; d) J. Liu, Y. Zhang, J. Liu, J. Li, X. Qiu, F. Cheng, *Acta Chim. Sin.* **2020**, *78*, 1426–1433; e) X. Liu, Z. Wang, W. Zhuang, L. Ban, M. Gao, W. Li, Y. Yin, Z. Wang, S. Lu, *New J. Chem.* **2020**, *44*, 3584–3592; f) Z. Wang, S. Luo, J. Ren, D. Wang, X. Qi, *Appl. Surf. Sci.* **2016**, *370*, 437–444.
- [112] W. Feng, Z. Huang, W. Li, *J. Electroanal. Chem.* **2022**, *917*, 116250.
- [113] X. Zhang, R. Yu, Y. Huang, X. Wang, Y. Wang, B. Wu, Z. Liu, J. Chen, *ACS Sustainable Chem. Eng.* **2018**, *6*, 12969–12979.
- [114] a) F. Zheng, C. Yang, X. Xiong, J. Xiong, R. Hu, Y. Chen, M. Liu, *Angew. Chem. Int. Ed. Engl.* **2015**, *54*, 13058–13062; b) M.-J. Lee, E. Lho, P. Oh, Y. Son, J. Cho, *Nano Res.* **2017**, *10*, 4210–4220; c) B. Liu, Q. Zhang, S. He, Y. Sato, J. Zheng, D. Li, *Electrochim. Acta* **2011**, *56*, 6748–6751; d) Q. Q. Qiao, H. Z. Zhang, G. R. Li, S. H. Ye, C. W. Wang, X. P. Gao, *J. Mater. Chem. A* **2013**, *1*, 5262–5268; e) S.-q. Yang, P.-b. Wang, H.-x. Wei, L.-b. Tang, X.-h. Zhang, Z.-j. He, Y.-j. Li, H. Tong, J.-c. Zheng, *Nano Energy* **2019**, *63*, 103889; f) T. Jenkins, J. A. Alarco, B. Cowie, I. D. R. Mackinnon, *J. Mater. Chem. A* **2022**, *10*, 24487–24509.
- [115] U. Nisar, N. Muralidharan, R. Essehli, R. Amin, I. Belharouak, *Energy Storage Mater.* **2021**, *38*, 309–328.
- [116] a) Y. Ouyang, Y. Zhang, G. Wang, X. Wei, A. Zhang, J. Sun, S. Wei, L. Song, F. Dai, Z. S. Wu, *Adv. Funct. Mater.* **2024**, *34*, 2401249; b) L. Wang, L. Xu, W. Xue, Q. Fang, H. Liu, Y. Liu, K. Zhou, Y. Li, X. Wang, X. Wang, X. Yang, X. Yu, X. Wang, *Nano Energy* **2024**, *121*, 109241.

- [117] X. D. Zhang, J. L. Shi, J. Y. Liang, Y. X. Yin, J. N. Zhang, X. Q. Yu, Y. G. Guo, *Adv. Mater.* **2018**, *30*, 1801751.
- [118] B. Xu, S. Meng, *J. Power Sources* **2010**, *195*, 4971–4976.
- [119] Y. Cen, Y. Liu, Y. Zhou, L. Tang, P. Jiang, J. Hu, Q. Xiang, B. Hu, C. Xu, D. Yu, C. Chen, *ChemElectroChem* **2020**, *7*, 1115–1124.
- [120] X. Hou, X. Liu, H. Wang, X. Zhang, J. Zhou, M. Wang, *Energy Storage Mater.* **2023**, *57*, 577–606.
- [121] C. Wu, L. Qiu, D.-Q. Wang, T. Chen, J. Li, Z.-G. Wu, Y. Song, X.-D. Guo, *Ind. Eng. Chem. Res.* **2022**, *61*, 453–463.
- [122] a) L. Li, Y. L. Chang, H. Xia, B. H. Song, J. R. Yang, K. S. Lee, L. Lu, *Solid State Ionics* **2014**, *264*, 36–44; b) D. Luo, X. Ding, J. Fan, Z. Zhang, P. Liu, X. Yang, J. Guo, S. Sun, Z. Lin, *Angew. Chem. Int. Ed.* **2020**, *59*, 23061–23066.
- [123] H. Liu, C. Du, G. Yin, B. Song, P. Zuo, X. Cheng, Y. Ma, Y. Gao, *J. Mater. Chem. A* **2014**, *2*, 15640–15646.
- [124] Y. Liu, H. Zhuo, Y. Yin, S. Lu, Z. Wang, W. Zhuang, *ACS Appl. Mater. Interfaces* **2020**, *12*, 27226–27240.
- [125] Q. Luo, J. Kang, Z. Liao, X. Feng, H. Zou, W. Yang, C. Pai, R. Waiyin Sun, S. Chen, *ACS Appl. Energy Mater.* **2022**, *5*, 4641–4650.
- [126] P. Vanaphuti, L. Azhari, X. Ma, Y. Liu, J. Hou, G. A. Tompsett, Z. Yang, Y. Wang, *Batteries Supercaps* **2022**, *5*, e202100377.
- [127] F. Klein, C. Pfeifer, J. Bansmann, Z. Jusys, R. J. Behm, M. Wohlfahrt-Mehrens, M. Lindén, P. Axmann, *J. Electrochem. Soc.* **2022**, *169*, 120533.
- [128] a) Z. Chang, Y. Zhang, W. He, J. Wang, H. Zheng, B. Qu, X. Wang, Q. Xie, D.-L. Peng, *Ind. Eng. Chem. Res.* **2022**, *61*, 7464–7473; b) X. Li, K. Zhang, D. Mitlin, E. Paek, M. Wang, F. Jiang, Y. Huang, Z. Yang, Y. Gong, L. Gu, W. Zhao, Y. Du, J. Zheng, *Small* **2018**, *14*, 1802570.
- [129] L. Ku, Y. Cai, Y. Ma, H. Zheng, P. Liu, Z. Qiao, Q. Xie, L. Wang, D.-L. Peng, *Chem. Eng. J.* **2019**, *370*, 499–507.
- [130] J. Zheng, S. Deng, Z. Shi, H. Xu, H. Xu, Y. Deng, Z. Zhang, G. Chen, *J. Power Sources* **2013**, *221*, 108–113.
- [131] a) H. Dong, D. Jiang, S. Xing, L. Zhao, L. Hu, J. Mao, H. Zhang, *Small* **2023**, *20*, 2307156; b) W. Guo, C. Zhang, Y. Zhang, L. Lin, W. He, Q. Xie, B. Sa, L. Wang, D. L. Peng, *Adv. Mater.* **2021**, *33*, 2103173.
- [132] J. Wu, H. Li, Y. Liu, Y. Ye, Y. Yang, *ACS Sustainable Chem. Eng.* **2022**, *10*, 6165–6180.
- [133] G. Li, Z. Ren, A. Li, R. Yu, W. Quan, C. Wang, T. Lin, D. Yi, Y. Liu, Q. Zhang, J. Wang, H. Yu, X. Sun, *Nano Energy* **2022**, *98*, 107169.
- [134] Z. Hao, H. Sun, Y. Ni, G. Yang, Z. Yang, Z. Hao, R. Wang, P. Yang, Y. Lu, Q. Zhao, W. Xie, Z. Yan, W. Zhang, J. Chen, *Adv. Mater.* **2024**, *36*, 2307617.
- [135] W. Li, B. Zhao, J. Bai, H. Ma, P. Wang, Y. Mao, K. Xiao, X. Wang, P. Tong, X. Zhu, Y. Sun, *Chem. Eng. J.* **2023**, *454*, 140398.
- [136] H. X. Wei, Y. M. Liu, Y. H. Luo, Y. D. Huang, L. B. Tang, Z. Y. Wang, C. Yan, J. Mao, K. H. Dai, Q. Wu, X. H. Zhang, J. C. Zheng, *Adv. Funct. Mater.* **2023**, *34*, 2307583.
- [137] C. Song, W. Feng, Z. Shi, Z. Huang, *Ionics* **2020**, *27*, 457–468.
- [138] Z. Li, M. Yuan, H. Liu, J. Liu, S. Xie, T. Wang, J. Yan, *J. Mater. Res.* **2022**, *37*, 3831–3841.
- [139] a) G. Ko, S. Jeong, S. Park, J. Lee, S. Kim, Y. Shin, W. Kim, K. Kwon, *Energy Storage Mater.* **2023**, *60*, 102840; b) F. Maroni, S. Dongmo, C. Gauckler, M. Marinaro, M. Wohlfahrt-Mehrens, *Batteries Supercaps* **2021**, *4*, 1221–1251.
- [140] B. Zhang, Y. Zhang, X. Wang, H. Liu, Y. Yan, S. Zhou, Y. Tang, G. Zeng, X. Wu, H. G. Liao, Y. Qiu, H. Huang, L. Zheng, J. Xu, W. Yin, Z. Huang, Y. Xiao, Q. Xie, D. L. Peng, C. Li, Y. Qiao, S. G. Sun, *J. Am. Chem. Soc.* **2023**, *145*, 8700–8713.
- [141] A. Choi, J. Lim, H. J. Kim, S. C. Jung, H. W. Lim, H. Kim, M. S. Kwon, Y. K. Han, S. M. Oh, K. T. Lee, *Adv. Energy Mater.* **2017**, *8*, 1702514.
- [142] Y. Wang, L. Wang, X. Guo, T. Wu, Y. Yang, B. Wang, E. Wang, H. Yu, *ACS Appl. Mater. Interfaces* **2020**, *12*, 8306–8315.
- [143] W. He, D. Yuan, J. Qian, X. Ai, H. Yang, Y. Cao, *J. Mater. Chem. A* **2013**, *1*, 11397–11403.
- [144] a) H. Chen, W. Li, *Ionics* **2022**, *28*, 2083–2097; b) K. Zhang, H. Sheng, X. Wu, L. Fu, Z. Liu, C. Zhou, R. Holze, Y. Wu, *ACS Appl. Energy Mater.* **2020**, *3*, 8953–8959; c) H. Liu, L. Tao, W. Wang, B. Zhang, M. Su, *Ionics* **2018**, *25*, 959–968.
- [145] a) Q. Wang, W. He, L. Wang, S. Li, H. Zheng, Q. Liu, Y. Cai, J. Lin, Q. Xie, D.-L. Peng, *ACS Sustainable Chem. Eng.* **2020**, *9*, 197–206; b) D. Wang, M. Liu, X. Wang, R. Yu, G. Wang, Q. Ren, X. Yang, *RSC Adv.* **2016**, *6*, 57310–57319.
- [146] a) X. Ding, Y. X. Li, S. Wang, J. M. Dong, A. Yasmin, Q. Hu, Z. Y. Wen, C. H. Chen, *Nano Energy* **2019**, *61*, 411–419; b) R. P. Qing, J. L. Shi, D. D. Xiao, X. D. Zhang, Y. X. Yin, Y. B. Zhai, L. Gu, Y. G. Guo, *Adv. Energy Mater.* **2015**, *6*, 1501914; c) S. Cao, J. Chen, H. Li, Z. Li, C. Guo, G. Chen, X. Guo, X. Wang, *J. Power Sources* **2023**, *555*, 232398.
- [147] Q. Ma, Z. Chen, S. Zhong, J. Meng, F. Lai, Z. Li, C. Cheng, L. Zhang, T. Liu, *Nano Energy* **2021**, *81*, 105622.
- [148] W. He, P. Liu, Y. Zhou, H. Zheng, Z. Zheng, B. Liu, J. Yuan, Q. Zhang, L. Wang, Q. Luo, Q. Xie, B. Qu, D.-L. Peng, *Sustainable Mater. Technol.* **2020**, *25*, e00171.
- [149] Q. Li, G. Li, C. Fu, D. Luo, J. Fan, L. Li, *ACS Appl. Mater. Interfaces* **2014**, *6*, 10330–10341.
- [150] Y. Cheng, Z. Wu, X. Dai, J. Hu, Z. Tai, J. Sun, Y. Liu, Q. Tan, Y. Liu, *J. Colloid Interface Sci.* **2022**, *605*, 718–726.
- [151] X. Ding, Y. X. Li, X. D. He, J. Y. Liao, Q. Hu, F. Chen, X. Q. Zhang, Y. Zhao, C. H. Chen, *ACS Appl. Mater. Interfaces* **2019**, *11*, 31477–31483.
- [152] Z. Zheng, X.-D. Guo, Y.-J. Zhong, W.-B. Hua, C.-H. Shen, S.-L. Chou, X.-S. Yang, *Electrochim. Acta* **2016**, *188*, 336–343.
- [153] T.-F. Yi, Y.-M. Li, S.-Y. Yang, Y.-R. Zhu, Y. Xie, *ACS Appl. Mater. Interfaces* **2016**, *8*, 32349–32359.
- [154] Y. X. Wang, K. H. Shang, W. He, X. P. Ai, Y. L. Cao, H. X. Yang, *ACS Appl. Mater. Interfaces* **2015**, *7*, 13014–13021.
- [155] a) X. Jin, Q. Xu, H. Liu, X. Yuan, Y. Xia, *Electrochim. Acta* **2014**, *136*, 19–26; b) H. Xu, S. Deng, G. Chen, *J. Mater. Chem. A* **2014**, *2*, 15015–15021.
- [156] C. Huang, Z. Wang, H. Wang, D. Huang, Y.-b. He, S.-x. Zhao, *Mater. Today Energy* **2022**, *29*, 101116.
- [157] X. Feng, Y. Gao, L. Ben, Z. Yang, Z. Wang, L. Chen, *J. Power Sources* **2016**, *317*, 74–80.
- [158] H. Konishi, A. Gunji, X. Feng, S. Furutsuki, *J. Solid State Chem.* **2017**, *249*, 80–86.
- [159] a) S. Li, L. Yang, Z. Liu, C. Zhang, X. Shen, Y. Gao, Q. Kong, Z. Hu, C.-Y. Kuo, H.-J. Lin, C.-T. Chen, Y. Yang, J. Ma, Z. Hu, X. Wang, R. Yu, Z. Wang, L. Chen, *Energy Storage Mater.* **2023**, *55*, 356–363; b) A. Celeste, F. Girardi, L. Gigli, V. Pellegrini, L. Silvestri, S. Brutti, *Electrochim. Acta* **2022**, *428*, 140737; c) D. De Sloovere, S. K. Mylavarapu, J. D'Haen, T. Thersleff, A. Jaworski, J. Grins, G. Svensson, R. Stoyanova, L. O. Josang, K. R. Prakasha, M. Merlo, E. Martinez, M. Nel-Lo Pascual, J. Jacas Biendicho, M. K. Van Bael, A. Hardy, *Small* **2024**, *20*, 2400876; d) M. Ha, A. Hajibabaei, D. Y. Kim, A. N. Singh, J. Yun, C. W. Myung, K. S. Kim, *Adv. Energy Mater.* **2022**, *12*, 2201497; e) Z. Li, Y. Li, M. Zhang, Z. W. Yin, L. Yin, S. Xu, C. Zuo, R. Qi, H. Xue, J. Hu, B. Cao, M. Chu, W. Zhao, Y. Ren, L. Xie, G. Ren, F. Pan, *Adv. Energy Mater.* **2021**, *11*, 2101962; f) P. K. Nayak, J. Grinblat, M. Levi, E. Levi, S. Kim, J. W. Choi, D. Aurbach, *Adv. Energy Mater.* **2016**, *6*, 1502398; g) T. Tang, H.-L. Zhang, *Electrochim. Acta* **2016**, *191*, 263–269; h) W. Yan, Y. Xie, J. Jiang, D. Sun, X. Ma, Z. Lan, Y. Jin, *ACS Sustainable Chem. Eng.* **2018**, *6*, 4625–4632; i) T.-F. Yi, X. Han, S.-Y. Yang, Y.-R. Zhu, *Sci. China Mater.* **2016**, *59*, 618–628; j) Y. Jin, N. Wang, C. Lin, W. Liu, S.-T. Myung, Y. Jin, *Chem. Eng. J.* **2023**, *474*, 145552; k) X. Zhao, M. Yang, J. Wang, D. Wang, *Chem. Res. Chin. Univ.* **2023**, *39*, 630–635.
- [160] D. Luo, J. Cui, B. Zhang, J. Fan, P. Liu, X. Ding, H. Xie, Z. Zhang, J. Guo, F. Pan, Z. Lin, *Adv. Funct. Mater.* **2021**, *31*, 2009310.
- [161] a) H. Li, H. Guo, Z. Wang, J. Wang, X. Li, N. Chen, W. Gui, *Int. J. Hydrogen Energy* **2018**, *43*, 11109–11119; b) N. Phattharasupakun, C. Geng, M. B. Johnson, R. Väli, M. Sawangphruk, J. R. Dahn, *J. Electrochem. Soc.* **2020**, *167*, 160545; c) S. Sallard, J. Billaud, D. Sheptyakov, P. Novák, C. Villevieille, *ACS Appl. Energy Mater.* **2020**, *3*, 8646–8657; d) B. Song, C. Zhou, H. Wang, H. Liu, Z. Liu, M. O. Lai, L. Lu, *J. Electrochem. Soc.* **2014**, *161*, A1723–A1730.
- [162] a) D. Boopathi, D. Swain, P. K. Nayak, *Energy Fuels* **2023**, *37*, 19266–19277; b) A. Celeste, M. Paolacci, P. G. Schiavi, S. Brutti, M. A. Navarra, L. Silvestri, *ChemElectroChem* **2023**, *10*, e202201072; c) K. Hu, L. Ren, W. Fan, B. Zhang, M. Zuo, Y. Zhang, G. Lv, H. Xu, W. Xiang, X. Guo, *J. Energy Chem.* **2022**, *71*, 266–276; d) T. Liang, W. Zeng, L. Yang, S. Liu, Y. Huang, H. He, X. Chen, A. He, *J. Alloys Compd.* **2022**, *910*, 164862; e) Q. Lu, Y. Wang, K. Yu, G. Zhao, Y. Cheng, Z. Yu, *J. Alloys Compd.* **2023**, *937*, 168426.
- [163] a) H. Liu, W. Xiang, C. Bai, L. Qiu, C. Wu, G. Wang, Y. Liu, Y. Song, Z.-G. Wu, X. Guo, *Ind. Eng. Chem. Res.* **2020**, *59*, 19312–19321; b) B. Yuan, S.-X. Liao, Y. Xin, Y. Zhong, X. Shi, L. Li, X. Guo, *RSC Adv.* **2015**, *5*, 2947–2951.
- [164] Y. Fan, E. Olsson, B. Johannessen, A. M. D'Angelo, L. Thomsen, B. Cowie, L. Smillie, G. Liang, Y. Lei, G. Bo, Y. Zhao, W. K. Pang, Q. Cai, Z. Guo, *ACS Energy Lett.* **2024**, *9*, 487–496.
- [165] R. N. Ramesha, C. P. Laisa, K. Ramesha, *Electrochim. Acta* **2017**, *249*, 377–386.

- [166] G. Wang, C. Xie, H. Wang, Q. Li, F. Xia, W. Zeng, H. Peng, G. Van Tendeloo, G. Tan, J. Tian, J. Wu, *Adv. Funct. Mater.* **2024**, *34*, 2313672.
- [167] S. Liu, Z. Liu, X. Shen, W. Li, Y. Gao, M. N. Banis, M. Li, K. Chen, L. Zhu, R. Yu, Z. Wang, X. Sun, G. Lu, Q. Kong, X. Bai, L. Chen, *Adv. Energy Mater.* **2018**, *8*, 1802105.
- [168] a) S. Dong, Y. Zhou, C. Hai, J. Zeng, Y. Sun, Y. Shen, X. Li, X. Ren, C. Sun, G. Zhang, Z. Wu, *J. Power Sources* **2020**, *462*, 228185; b) C. Hou, Y.-R. Xing, L.-L. Yu, Y.-H. Si, H. Lu, Y.-J. Zhao, *Electrochim. Acta* **2022**, *404*, 139744; c) H. Li, Z. Li, J. Liu, S. Cao, J. Chen, H. Hu, C. Guo, X. Zhang, X. Wang, *ACS Appl. Energy Mater.* **2023**, *6*, 10773–10783; d) X. Liu, B. Yu, M. Wang, Y. Jin, Z. Fu, J. Chen, Z. Ma, B. Guo, Y. Huang, X. Li, *Mater. Today Commun.* **2022**, *32*, 104170; e) C. Zhang, B. Wei, W. Jiang, M. Wang, W. Hu, C. Liang, T. Wang, L. Chen, R. Zhang, P. Wang, W. Wei, *ACS Appl. Mater. Interfaces* **2021**, *13*, 45619–45629; f) M. Zubairi, G. Li, B. Wang, L. Wang, H. Yu, *ACS Appl. Energy Mater.* **2018**, *2*, 503–512.
- [169] a) S.-Y. Liu, Y.-H. Zhou, Y.-B. Zhang, S.-J. Xia, Y. Li, X. Zhou, B. Qiu, G.-J. Shao, Z.-P. Liu, *Tungsten* **2022**, *4*, 336–345; b) L. Sun, X. Yi, X. Ren, P. Zhang, J. Liu, *J. Electrochem. Soc.* **2016**, *163*, A766–A772.
- [170] a) P. P. Dahiya, C. Ghanty, K. Sahoo, S. Basu, S. B. Majumder, *J. Electrochem. Soc.* **2018**, *165*, A3114–A3124; b) Z. He, Z. Wang, H. Chen, Z. Huang, X. Li, H. Guo, R. Wang, *J. Power Sources* **2015**, *299*, 334–341.
- [171] a) Y. Fan, E. Olsson, G. Liang, Z. Wang, A. M. D'Angelo, B. Johannessen, L. Thomsen, B. Cowie, J. Li, F. Zhang, Y. Zhao, W. K. Pang, Q. Cai, Z. Guo, *Angew. Chem. Int. Ed. Engl.* **2023**, *62*, e202213806; b) B. Song, M. O. Lai, L. Lu, *Electrochim. Acta* **2012**, *80*, 187–195.
- [172] a) A. Yalçın, M. Demir, M. O. Güler, M. Gönen, M. Akgün, *Electrochim. Acta* **2023**, *440*, 141743; b) Y. Zhao, M. Xia, X. Hu, Z. Zhao, Y. Wang, Z. Lv, *Electrochim. Acta* **2015**, *174*, 1167–1174.
- [173] a) Z. Chen, Q. Liu, X. Yan, H. Zhu, J. Liu, J. Duan, Y. Wang, *J. Phys. Chem. Lett.* **2022**, *13*, 8214–8220; b) D. Mao, Z. Fan, L. Song, P. Zhang, J. Xie, S. Su, G. Liu, H. Wang, W. Chu, *Nano Energy* **2024**, *121*, 109231; c) R. Yu, Z. Zhang, S. Jamil, J. Chen, X. Zhang, X. Wang, Z. Yang, H. Shu, X. Yang, *ACS Appl. Mater. Interfaces* **2018**, *10*, 16561–16571.
- [174] E. Wang, D. Xiao, T. Wu, B. Wang, Y. Wang, L. Wu, X. Zhang, H. Yu, *Battery Energy* **2023**, *2*, 20220030.
- [175] a) L. Guo, X. Tan, D. Mao, T. Zhao, L. Song, Y. Liu, X. Kang, H. Wang, L. Sun, W. Chu, *Electrochim. Acta* **2021**, *370*, 137808; b) J. Meng, L. Xu, Q. Ma, M. Yang, Y. Fang, G. Wan, R. Li, J. Yuan, X. Zhang, H. Yu, L. Liu, T. Liu, *Adv. Funct. Mater.* **2022**, *32*, 2113013; c) X. Wan, D. Hang, X. Zhu, W. Che, D. Zhang, C. Chang, *ACS Sustainable Chem. Eng.* **2021**, *9*, 17221–17231.
- [176] a) D. Han, K. Park, J.-H. Park, D.-J. Yun, Y.-H. Son, *J. Ind. Eng. Chem.* **2018**, *68*, 180–186; b) C. Lu, S. Yang, H. Wu, Y. Zhang, X. Yang, T. Liang, *Electrochim. Acta* **2016**, *209*, 448–455.
- [177] a) K.-Q. Geng, M.-Q. Yang, J.-X. Meng, L.-F. Zhou, Y.-Q. Wang, S. Dmytro, Q. Zhang, S.-W. Zhong, Q.-X. Ma, *Tungsten* **2022**, *4*, 323–335; b) X. Ji, Y. Xu, H. Feng, P. Wang, Y. Zhou, J. Song, Q. Xia, Q. Tan, *ACS Appl. Mater. Interfaces* **2021**, *13*, 47659–47670; c) N. Srivastava, S. K. Singh, D. Meghnani, R. Mishra, R. K. Tiwari, A. Patel, A. Tiwari, R. K. Singh, *ACS Appl. Energy Mater.* **2022**, *5*, 12183–12195; d) Y. Zang, C.-X. Ding, X.-C. Wang, Z.-Y. Wen, C.-H. Chen, *Electrochim. Acta* **2015**, *168*, 234–239.
- [178] J. Meng, Z. Wang, L. Xu, H. Xu, S. Zhang, Q. Yan, *J. Electrochem. Soc.* **2017**, *164*, A2594–A2602.
- [179] Q.-Q. Qiao, L. Qin, G.-R. Li, Y.-L. Wang, X.-P. Gao, *J. Mater. Chem. A* **2015**, *3*, 17627–17634.
- [180] U. Breddemann, J. Sicklinger, F. Schipper, V. Davis, A. Fischer, K. Huber, E. M. Erickson, M. Daub, A. Hoffmann, C. Erk, B. Markovsky, D. Aurbach, H. A. Gasteiger, I. Krossing, *Batteries Supercaps* **2021**, *4*, 632–645.
- [181] a) B. Wang, J. Cui, Z. Li, H. Wang, D. Zhang, Q. Wang, H. Sun, Z. Hu, *J. Alloys Compd.* **2022**, *929*, 167304; b) Y. Wang, H.-T. Gu, J.-H. Song, Z.-H. Feng, X.-B. Zhou, Y.-N. Zhou, K. Wang, J.-Y. Xie, *J. Phys. Chem. C* **2018**, *122*, 27836–27842.
- [182] T. Liu, S.-X. Zhao, L.-L. Gou, X. Wu, C.-W. Nan, *Rare Met.* **2018**, *38*, 189–198.
- [183] J. H. Song, A. Kapyloou, H. S. Choi, B. Y. Yu, E. Matulevich, S. H. Kang, *J. Power Sources* **2016**, *313*, 65–72.
- [184] Y. Zhang, S. Zheng, C. Meng, H. Liu, C. Dong, X. Shi, P. Das, R. Huang, Y. Yu, Z. S. Wu, *Adv. Funct. Mater.* **2023**, *33*, 2300987.
- [185] a) L. Di, C. Yufang, S. Weiwei, X. Wei, Y. Shuaiyu, L. Shiqiang, Z. Lanlan, Z. Yanshuang, Y. Tianyan, X. Peitao, Z. Chunman, *Adv. Energy Mater.* **2023**, *13*, 2301765; b) L. Li, B. H. Song, Y. L. Chang, H. Xia, J. R. Yang, K. S. Lee, L. Lu, *J. Power Sources* **2015**, *283*, 162–170; c) C. Wu, S. Cao, X. Xie, C. Guo, H. Li, Z. Li, Z. Zang, B. Chang, G. Chen, X. Guo, T. Wu, X. Wang, *Chem. Eng. J.* **2022**, *429*, 132141.
- [186] T. Wang, C. Zhang, S. Li, X. Shen, L. Zhou, Q. Huang, C. Liang, Z. Wang, X. Wang, W. Wei, *ACS Appl. Mater. Interfaces* **2021**, *13*, 12159–12168.
- [187] H. Yan, B. Li, Z. Yu, W. Chu, D. Xia, *J. Phys. Chem. C* **2017**, *121*, 7155–7163.
- [188] Z. Sun, L. Xu, C. Dong, H. Zhang, M. Zhang, Y. Ma, Y. Liu, Z. Li, Y. Zhou, Y. Han, Y. Chen, *Nano Energy* **2019**, *63*, 103887.
- [189] J. An, L. Shi, G. Chen, M. Li, H. Liu, S. Yuan, S. Chen, D. Zhang, *J. Mater. Chem. A* **2017**, *5*, 19738–19744.
- [190] a) J. Chen, H. Chen, W. Deng, X. Gao, S. Yin, Y. Mei, S. Zhang, L. Ni, J. Gao, H. Liu, Y. Tian, L. Yang, X. Deng, G. Zou, H. Hou, J. Xie, X. Ji, *Energy Storage Mater.* **2022**, *51*, 671–682; b) Q. Ma, R. Li, R. Zheng, Y. Liu, H. Huo, C. Dai, *J. Power Sources* **2016**, *331*, 112–121.
- [191] W. Cheng, Q. Liu, J. Ding, X. Wang, L. Wang, J. Wang, W. Zhang, Y. Huang, *Small* **2023**, *19*, 2301564.
- [192] A. Watanabe, K. Yamamoto, T. Uchiyama, T. Matsunaga, A. Hayashi, K. Maeda, H. Kageyama, Y. Uchimoto, *ACS Appl. Energy Mater.* **2020**, *3*, 4162–4167.
- [193] Y. Kang, X. Guo, Z. Guo, J. Li, Y. Zhou, Z. Liang, C. Han, X. He, Y. Zhao, N. Tavajohi, B. Li, *J. Energy Chem.* **2021**, *62*, 538–545.
- [194] C. Yin, X. Wen, L. Wan, Z. Shi, Z. Wei, X. Li, Q. Gu, B. Qiu, Z. Liu, *J. Power Sources* **2021**, *503*, 230048.
- [195] a) J. Liu, S. Wang, Z. Ding, R. Zhou, Q. Xia, J. Zhang, L. Chen, W. Wei, P. Wang, *ACS Appl. Mater. Interfaces* **2016**, *8*, 18008–17; b) Z. Ren, G. Li, X. Bai, W. Hu, X. Li, H. He, Z. Chang, Y. Liu, Z. Wang, Z. Liang, L. Guo, Z. Gao, J. Wang, *Electrochim. Acta* **2023**, *461*, 142630.
- [196] S. Li, X. Fu, Y. Liang, S. Wang, X. a. Zhou, H. Dong, K. Tu, C. Gao, X. Cui, *ACS Sustainable Chem. Eng.* **2020**, *8*, 9311–9324.
- [197] Z. Sun, L. Xu, C. Dong, H. Zhang, M. Zhang, Y. Liu, Y. Zhou, Y. Han, Y. Chen, *J. Mater. Chem. A* **2019**, *7*, 3375–3383.
- [198] L. Pan, Y. Xia, B. Qiu, H. Zhao, H. Guo, K. Jia, Q. Gu, Z. Liu, *J. Power Sources* **2016**, *327*, 273–280.
- [199] H. Z. Zhang, Q. Q. Qiao, G. R. Li, X. P. Gao, *J. Mater. Chem. A* **2014**, *2*, 7454–7460.
- [200] B. Li, H. Yan, J. Ma, P. Yu, D. Xia, W. Huang, W. Chu, Z. Wu, *Adv. Funct. Mater.* **2014**, *24*, 5112–5118.
- [201] L. Ma, L. Mao, X. Zhao, J. Lu, F. Zhang, P. Ding, L. Chen, F. Lian, *ChemElectroChem* **2017**, *4*, 3068–3074.
- [202] Y. Zhao, J. Liu, S. Wang, R. Ji, Q. Xia, Z. Ding, W. Wei, Y. Liu, P. Wang, D. G. Ivey, *Adv. Funct. Mater.* **2016**, *26*, 4760–4767.
- [203] H.-Z. Zhang, F. Li, G.-L. Pan, G.-R. Li, X.-P. Gao, *J. Electrochem. Soc.* **2015**, *162*, A1899–A1904.
- [204] E. Wang, D. Xiao, T. Wu, X. Liu, Y. Zhou, B. Wang, T. Lin, X. Zhang, H. Yu, *Adv. Funct. Mater.* **2022**, *32*, 2201744.
- [205] a) Y. Liang, S. Li, J. Xie, L. Yang, W. Li, C. Li, L. Ai, X. Fu, X. Cui, X. Shangguan, *New J. Chem.* **2019**, *43*, 12004–12012; b) Y. Sun, L. Zhang, S. Dong, J. Zeng, Y. Shen, X. Li, X. Ren, L. Ma, C. Hai, Y. Zhou, *Electrochim. Acta* **2022**, *414*, 140169.
- [206] Y. Liu, X. Wan, J. Zheng, *Ceram. Int.* **2024**, *50*, 6289–6298.
- [207] L. Zhou, L. Qiao, X. Wu, H. Min, X. Liu, H. Yang, *J. Alloys Compd.* **2023**, *957*, 170423.
- [208] W. Jiang, C. Zhang, Y. Feng, B. Wei, L. Chen, R. Zhang, D. G. Ivey, P. Wang, W. Wei, *Energy Storage Mater.* **2020**, *32*, 37–45.
- [209] Y. Hu, Z. Qin, B. Cong, J. Pei, S. Sun, G. Chen, *ChemElectroChem* **2021**, *8*, 2315–2320.
- [210] J. Yang, Y. Chen, Y. Li, X. Xi, J. Zheng, Y. Zhu, Y. Xiong, S. Liu, *ACS Appl. Mater. Interfaces* **2021**, *13*, 25981–25992.
- [211] a) W. Cheng, J. Ding, Z. Liu, J. Zhang, Q. Liu, X. Wang, L. Wang, Z. Sun, Y. Cheng, Z. Xu, Y. Lei, J. Wang, Y. Huang, *Chem. Eng. J.* **2023**, *451*, 138678; b) H. Zhang, J. Jiao, A. Zen, E. Zhao, J. Zhao, X. Xiao, *Electrochim. Acta* **2023**, *468*, 143167.
- [212] J. Lee, D. A. Kitchae, D. H. Kwon, C. W. Lee, J. K. Papp, Y. S. Liu, Z. Lun, R. J. Clement, T. Shi, B. D. McCloskey, J. Guo, M. Balasubramanian, G. Ceder, *Nature* **2018**, *556*, 185–190.
- [213] S. Jiao, Y. Sun, J. Wang, D. Shi, Y. Li, X. Jiang, F. Wang, Y. Zhang, J. Liu, X. Wang, X. Yu, H. Li, L. Chen, X. Huang, *Adv. Energy Mater.* **2023**, *13*, 2301636.
- [214] B. Guo, J. Zhao, X. Fan, W. Zhang, S. Li, Z. Yang, Z. Chen, W. Zhang, *Electrochim. Acta* **2017**, *236*, 171–179.
- [215] a) H. Zheng, C. Zhang, Y. Zhang, L. Lin, P. Liu, L. Wang, Q. Wei, J. Lin, B. Sa, Q. Xie, D. L. Peng, *Adv. Funct. Mater.* **2021**, *31*, 2100783; b) P. Zhang, X. Zhai, H. Huang, J. Zhou, X. Li, Y. He, Z. Guo, *Ceram. Int.* **2020**, *46*, 24723–24736.

- [216] D. Mao, X. Tan, Z. Fan, L. Song, Y. Zhang, P. Zhang, S. Su, G. Liu, H. Wang, W. Chu, *ACS Appl Mater Interfaces* **2023**, *15*, 10774–10784.
- [217] L. Nie, Z. Wang, X. Zhao, S. Chen, Y. He, H. Zhao, T. Gao, Y. Zhang, L. Dong, F. Kim, Y. Yu, W. Liu, *Nano Lett.* **2021**, *21*, 8370–8377.
- [218] C. Li, X. Cai, X. Fu, N. Zhang, H. Ding, P. Wang, X. Zhou, L. Song, J. Huang, S. Li, *J. Alloys Compd.* **2022**, *924*, 166527.
- [219] a) H. Liu, B. He, W. Xiang, Y. C. Li, C. Bai, Y. P. Liu, W. Zhou, X. Chen, Y. Liu, S. Gao, X. Guo, *Nanotechnology* **2020**, *31*, 455704; b) Y. Liu, D. Ning, L. Zheng, Q. Zhang, L. Gu, R. Gao, J. Zhang, A. Franz, G. Schumacher, X. Liu, *J. Power Sources* **2018**, *375*, 1–10; c) Y. Peng, L. Wu, C.-F. Li, B.-C. Luo, X.-Y. Feng, Z.-Y. Hu, Y. Li, B.-L. Su, *Electrochim. Acta* **2023**, *454*, 142390; d) D. Mao, X. Tan, L. Guo, T. Zhao, Z. Fan, L. Song, Y. Zhang, G. Liu, H. Wang, W. Chu, *ACS Appl Mater Interfaces* **2022**, *14*, 19594–19603.
- [220] Y. Xu, M. Zhang, L. Yi, K. Liang, *J. Alloys Compd.* **2021**, *865*, 158899.
- [221] S. Cangaz, F. Hippauf, R. Takata, F. Schmidt, S. Dörfler, S. Kaskel, *Batteries Supercaps* **2022**, *5*, e202200100.
- [222] Z. Tai, W. Zhu, M. Shi, Y. Xin, S. Guo, Y. Wu, Y. Chen, Y. Liu, *J Colloid Interface Sci* **2020**, *576*, 468–475.
- [223] M. Li, Y. Zhou, X. Wu, L. Duan, C. Zhang, F. Zhang, D. He, *Electrochim. Acta* **2018**, *275*, 18–24.
- [224] R. Yu, M. N. Banis, C. Wang, B. Wu, Y. Huang, S. Cao, J. Li, S. Jamil, X. Lin, F. Zhao, W. Lin, B. Chang, X. Yang, H. Huang, X. Wang, X. Sun, *Energy Storage Mater.* **2021**, *37*, 509–520.
- [225] J. Wu, H. Li, Y. Liu, Y. Ye, Y. Yang, *J. Phys. Chem. C* **2022**, *126*, 2410–2423.
- [226] Z. Yu, K. Yu, F. Ji, Q. Lu, Y. Wang, Y. Cheng, H. Li, F. Xu, L. Sun, H. J. Seifert, Y. Du, J. Wang, *Inorg. Chem. Front.* **2023**, *10*, 682–691.
- [227] X. Yang, S. Wang, D. Han, K. Wang, A. Tayal, V. Baran, A. Missyul, Q. Fu, J. Song, H. Ehrenberg, S. Indris, W. Hua, *Small* **2022**, *18*, 2201522.
- [228] M. Yoon, Y. Dong, Y. Huang, B. Wang, J. Kim, J.-S. Park, J. Hwang, J. Park, S. J. Kang, J. Cho, J. Li, *Nat. Energy* **2023**, *8*, 482–491.
- [229] K. Liu, Q. Zhang, Z. Lu, H. Zhu, M. Song, L. Chen, C. Zhang, W. Wei, *ACS Appl Mater Interfaces* **2024**, *16*, 14902–14911.
- [230] a) T. Wu, X. Zhang, Y. Wang, N. Zhang, H. Li, Y. Guan, D. Xiao, S. Liu, H. Yu, *Adv. Funct. Mater.* **2022**, *33*, 2210154; b) J. Li, H. Lin, C. Tang, D. Yu, J. Sun, W. Zhang, Y. Wang, *Nanotechnology* **2021**, *33*, 065705.
- [231] J. Sun, C. Sheng, X. Cao, P. Wang, P. He, H. Yang, Z. Chang, X. Yue, H. Zhou, *Adv. Funct. Mater.* **2021**, *32*, 2110295.
- [232] Z. Hao, X. Gou, H. Ma, Z. Yang, Z. Hao, G. Yang, Y. Lu, Q. Zhao, H. Jin, Q. Zhang, Z. Yan, J. Chen, *Sci. China Mater.* **2023**, *66*, 3424–3432.
- [233] Y. Zhang, Q. Song, T. Wang, Q. Zhao, R. Zhang, J. Zhao, *J. Power Sources* **2019**, *413*, 425–431.
- [234] a) Y. Su, M. Wang, M. Zhang, L. Chen, N. Li, L. Chen, Y. Chen, J. Liu, Y. Li, *J. Alloys Compd.* **2022**, *905*, 164204; b) S. Lin, Z. Wang, T. Lu, H. Wang, P. Li, F. Yang, Z. Guo, *J. Alloys Compd.* **2020**, *822*, 153638.
- [235] B. Zhang, Y. Zhang, H. Wu, L. Zeng, X. Wang, H. Liu, X. Wu, J. Chen, H. Zhang, Y. Yan, Y. Tang, H. Huang, L. Zheng, Q. Zhang, Q. Xie, D.-L. Peng, C. Li, Y. Qiao, S.-G. Sun, *Energy Storage Mater.* **2023**, *62*, 102926.
- [236] J. Duan, F. Wang, M. Huang, M. Yang, S. Li, *Small* **2023**, *20*, 2307998.

Manuscript received: June 30, 2024

Revised manuscript received: August 21, 2024

Accepted manuscript online: August 23, 2024

Version of record online: October 22, 2024